UNIVERSITY OF TURKU
Faculty of Science

Correlation of bedrock outcrop structures with subsurface data – with emphasis on the needs of geoenergy research

Ella Virta

Bedrock geology

Master's thesis

Credits: 30 op

28.2.2023

Turku

Master's thesis

Subject: Bedrock geology
Author: Ella Virta
Title: Correlation of bedrock outcrop structures with subsurface data – with emphasis on the needs of geoenergy research
Supervisors: Pietari Skyttä & Teemu Lindqvist
Number of pages: 76 pages + 3 appendixes
Date: 28.2.2023

The demand of energy is constantly increasing in this rapidly developing world. At the same time, the transition of contaminant ways of energy production is more often replaced by production methods that are using renewable energy sources. One of these renewable sources is geothermal energy which inexhaustibly forms in the interior of the Earth. The use of geothermal energy is expanding year by year from the most suitable areas into such areas, where conditions are more challenging. The risk surveying and site selection related to the building of geothermal wells has mainly been utilizing subsurface methods that are certainly effective, however more expensive, and arduous to execute. This study compiles structural geological features made during comprehensive bedrock mapping on the area, where geothermal well, with target depth of 2,5 kilometers, was drilled by Helen Oy. The location of the geothermal well was selected before bedrock mapping of the area.

The main goal was to understand the variation of fractures within the diverse lithologies, the relationship, the relationship between faults and fractures and the control of ductile structures to fracturing. The characteristics of these features are crucial with respect to the proper functioning of the well. Later, this data was compared with subsurface data, which gave an estimation of reliability and usefulness of bedrock mapping in the geoenergy projects. Possible reliability would justify the use of cheaper and more easily executed surface methods which would be a great step of development to production of geothermal energy.

The study area in Ruskeasuo, Helsinki, consists of different types of gneisses and granites, where fracturing is widely observed. The main interest in the area is a prominent sub-vertical E-W trending fault, which is located on the northern side of the geothermal well. Multiple fracture measurements made in the field and by using 2D-and 3D-data indicates that the fault is dipping about 80^{o} towards the geothermal well, located in the south. The drilling process of the well was not easy. The drilling stopped at the depth of 865 meters, when crucial fractures were encountered. It is possible to assume, that these fractures are related to the aforementioned fault, that is assumed to intersect the well at this depth.

The studies made from the well indicated some temperature changes at the depth of about 800 meters that might be related to fractures. Geophysical measurements and visual imaging of the well failed completely and data from the orientations of the structures intersecting the well could not be collected. The E-W trending fault observed from surface was also detected from the reflection seismic data.

Since subsurface studies did not produce beneficial data from the well, the correlation to the surface data was not fully proven in this case. However, this kind of structural geological mapping can reveal features that need to be taken into a consideration when selecting the suitable drilling site.

Key words: geothermal energy, well, bedrock mapping, fracture, fault, photogrammetry

Pro gradu – tutkielma

Oppiaine: Kallioperägeologia
Tekijä: Ella Virta
Otsikko: Kallioperäpaljastuman rakenteiden korreloitavuus maanalaisen datan kanssa – painottuen geoenergiatutkimuksen tarpeisiin
Ohjaajat: Pietari Skyttä & Teemu Lindqvist
Sivumäärä: 76 sivua + 3 liitettä
Päivämäärä: 28.2.2023

Energian tarve kasvaa jatkuvasti nopeasti kehittyvässä maailmassamme. Samanaikaisesti käynnissä on siirtymä, jonka aikana saastuttavat energiantuotantomuodot korvataan yhä useammin uusiutuvia energialähteitä käyttävillä tuotantomuodoilla. Maan sisuksissa ehtymättömästi syntyvä geoterminen energia on yksi näistä energialähteistä. Geotermistä energiaa hyödynnetään tehokkaasti jo sille luonnollisesti suotuisilla alueilla, ja sen käyttöä pyritään laajentamaan myös alueille, joilla olosuhteet voivat olla haastavammat. Geotermisten kaivojen rakennukseen liittyvien riskien kartoituksessa ja paikan valinnassa on tähän asti hyödynnetty lähes ainoastaan tehokkaita, mutta usein kalliita ja työläitä maanalaisia menetelmiä. Tässä tutkimuksessa kaivonrakennukselle keskeistä rakennegeologista dataa kerättiin kallioperäkartoituksessa alueelta, jonne Helen Oy porasi geotermisen kaivon. Kaivon tavoitesyvyys oli 2,5 kilometriä, ja sen paikka valittiin ennen kartoitusta.

Tutkimuksen tavoite oli selvittää rakoilun vaihtelua eri litologioiden välillä, tutkia rakoilun luonnetta ja suhdetta siirroksiin sekä havainnoida duktiilien rakenteiden vaikutusta rakoiluun. Lopulta maanpäällistä dataa vertailtiin maanalaiseen dataan, jonka avulla saatiin arvio kallioperäkartoituksen tulosten käyttökelpoisuudesta geoenergiaprojekteissa. Tulosten hyödynnettävyys voisi lisätä edullisempien ja helpommin toteutettavien maanpäällisten tutkimusten käyttöä, joka olisi iso askel geotermisen energian tuotannon kehittämisessä.

Tutkimusalue sijaitsee Ruskeasuolla Helsingissä. Alueelle tyypillisiä kivilajeja ovat erilaiset gneissit ja graniitit, joissa voi havaita tiheää rakoilua. Alueen kiinnostavin geologinen rakenne on merkittävä itä-länsisuuntainen siirros, joka sijaitsee geotermisen kaivon pohjoispuolella. Useiden kenttämittausten ja 2D-ja 3D-materiaalin perusteella on mahdollista havaita siirroksen kaatuvan noin 80^{o} kohti etelässä sijaitsevaa geotermistä kaivoa. Kaivon porausprosessi oli vaikea. Poraus lopetettiin 865 metrin syvyydessä tiheän rakoilun takia. On mahdollista olettaa, että tämä rakoilu liittyy kaivon pohjoispuolella sijaitsevaan siirrokseen, joka läpäisee kaivon tällä syvyydellä.

Kaivosta saatujen mittaustentulosten mukaan lämpötilassa tapahtuu muutos noin 800 metrin syvyydessä. Tämä muutos voi liittyä rakoiluun. Kaivon geofysikaaliset mittaukset ja reikäkuvaukset epäonnistuivat täysin, jonka vuoksi rakosuuntadataa ei saatu kerättyä. Maan päällä vaivattomasti havaittava itä-länsisuuntainen siirros on myös näkyvissä seimisessä datassa. Maanpäällisten menetelmien luotettavuutta ja niiden korreloitavuutta maanalaiseen dataan ei tässä tutkimuksessa pystytä täysin todistamaan geofysikaalisten mittausten epäonnistumisen takia.

Tämän tutkimuksen mukaan geotermisten kaivojen sijainnin valitseminen ei voi täysin perustua rakennegeologiseen kartoitukseen. Kattava kallioperäkartoitus voi kuitenkin paljastaa oleellisia geologisia rakenteita, jotka tulee huomioida kaivon paikan valinnassa.

Avainsanat: geoterminen energia, kaivo, kallioperäkartoitus, rako, siirros, fotogrammetria

Table of contents

1. Introduction

Planning and drilling of a geothermal well is an expensive process. Successful results require careful planning, fitting drilling technique, right tools, professionals, and a lot of information about the area. Financial resources of the project are typically limited, which means that budget of the process can be exceeded if unexpected and unwanted surprises occur. For these reasons, is very important that these negative consequences could be avoided as far as possible. Limited budget also excludes more expensive studies, for example seismic studies. Therefore, it is important to develop less expensive ways to collect crucial information about these bedrock conditions that affect the drilling. The amount of the heat that can be collected from the well should also be sufficient.

One of the most inexpensive ways to gather important information is to execute careful bedrock mapping within the area of the planned geothermal well/wells. This kind of mapping of the area reveals the variation of rock types and structural geological features which may ultimately provide justifications for the site selection of the wells.

The nature of the fractures has a huge effect to the proper functioning of the well. For example, unfavorably oriented or sized fractures may affect the coherency of the bedrock and cause stability problems to the drilling process. These kinds of unfavorable features may complicate the drilling process for example in the areas where faults with abundant fractures are located. If these harmful features can be detected from the surface, and further extrapolated to depth, the process of planning and drilling of geothermal wells could be more cost-efficient and easier. This information is especially crucial to the drilling companies which typically have limited knowledge about the geology of the drilling site, even though they are experts on drilling. Drillers of the geothermal well are typically responsible for the possible failures which means that it is important that harmful features such as fractures will not remain uncertain or unknown. On the other hand, the fracturing of the rock might be necessary, or even compulsory, to maintain the proper functioning of the well since warm water/rock needs interact with the well. This interaction ensures that the heat production of the well is on sufficient level. Overall, this kind of information about the favorable and unfavorable features such as fractures and nature of the rock should be easily reachable and understood.

Since the demand of energy is rising in every part of the world, major cities such as city of Helsinki need constant development to response to the increasing demand. At the same time, it is important to prevent the development of climate change since permanent changes are getting more typical if estimated 1.5-2 ºC warming is occurring in the near future (Vähäaho 2021).

The area of this study is in Ruskeasuo, Helsinki, where Helen Oy started to drill a medium-deep geothermal well in 2021. The well was targeted to reach to 2,5 kilometers. The drilling site of the well was selected since Helen Oy's heating center was located on its side. Therefore, during the site selection of the well, the geological characteristics of the area were unknown.

In this study, I executed comprehensive bedrock mapping of the area within the immediate vicinity of the Ruskeasuo drilling site. Mapping data includes observations on lithology and structural geological features, such fractures, faults, foliations, and folds. The main goal was to gather data from the variation of fracturing between different rock types, how faults and fractures are related to each other, and how the ductile structure, especially foliation, is controlling the orientation of fracturing. I further compared this information with subsurface data which included for example reflection seismic and borehole data, that was gathered before and during this study by other operators. This comparison between surface and subsurface datasets gave an estimation of the reliability and usefulness of bedrock mapping in the projects that are related to production of geothermal energy. By observing possible harmful and continuous structural geological features from surface level that would harm the drilling process or proper functioning of the well, the location of the well can be selected better. This study started in the beginning of the summer of 2022.

2. Background of geothermal energy

Geothermal energy is constantly forming heat in the interior of the Earth, which is always available for usage (Boden 2017). It is therefore considered as an exhaustible energy source (Boden 2017). The sources of the heat energy can be divided into two sources; sources that have generated heat energy in the past such as decay of short-lived radioactive isotopes or differentiation of the planet, and sources, which that produce currently heat energy such as decay of long-lived radioactive isotopes or chemical reactions (Eppelbaum et al. 2014). The temperature difference of the hot inner part of the Earth and the cold surface is creating geothermal heat flux which flows from inner parts to towards the surface (Eppelbaum et al.

2014). This flux is in Finland about 42 milliwatts per square meter (City of Helsinki 2019). The phase of the rising is dependent on the thermal conductivity and geothermal heat flux of the crust (Eppelbaum et al. 2014).

Geothermal energy can be categorized into shallow, medium-deep and deep energy in low-enthalpy areas for example in Finland (Hakala et al. 2021). Shallow geothermal energy utilizes low-depth geological units that includes sources of low enthalpy (Arola et al. 2022). Thermal energy in these sources is a combination of energy that is produced in active processes that occur in the interior of Earth, radioactive reactions of different minerals in the upper crust and radiation of the Sun (Arola et al. 2022). The amount of short wavelength radiation from the Sun to the surface of the earth in Finland is about 800-1100 kWh/m^2, which is over 2000 times the amount of heat energy that geothermal flux transports to the surface level (City of Helsinki 2019). The exploitation of shallow geothermal energy typically includes a borehole heat exchanger (Arola et al. 2022). In the depths of 500 meters of bedrock in Finland, temperature is varying between 8 and 14°C which is not sufficient to heat buildings without ground-source heat pump (GSHP) (Arola et al. 2022). The utilization of geothermal energy from the bedrock is done by using systems that include ground-source heat pump, heat wells and the internal systems in buildings (City of Helsinki 2019).

Shallow geothermal energy has a low enthalpy source in the geological units that are located in low depths (Hakala et al. 2021). Shallow geothermal energy is produced by different processes such as radioactive reactions of minerals in upper crust of Earth or solar irradiance and typically borehole heat exchanger (BHE) is utilized. (Hakala et al. 2021). Temperature of the bedrock of Finland varies typically between 8-14°C when the depth is 500 meters which means that ground-source heat pump (GSHP) is required when buildings are heated (Hakala et al. 2021). Ideally BHEs are used with GSHP which means that thermal and physical factors such as thermal conductivity of subsurface, thermal resistance of BHE, undisturbed temperature of the bedrock and especially natural convection need to be carefully considered (Hakala et al. 2021). Special attention is needed when considering natural convection since groundwater is naturally filling the boreholes in the Fennoscandia (Hakala et al. 2021). These thermogeological parameters can be studied by using thermal response test (TRT) where elements are heated to produce thermal energy for heat exchanger fluid

The heat from the Earth's crust can be utilized as energy from the smallest hot springs to the larger and more complex power stations (Nadimi et al. 2018). The geothermal energy is an

economically sustainable and inexpensive way to produce electricity that is commonly utilized in e.g., Iceland (Nadimi et al. 2018). Utilization of the conventional hydrothermal resources require that all three main components, heat, fluid and permeability, are present in suitable proportions (Nadimi et al. 2018). In some cases, geothermal resources with low natural permeabilities can be transformed into an economically profitable resource by engineering the reservoir (Nadimi et al. 2018). Such an engineered thermal reservoir is called an enhanced geothermal system (EGS), and it uses mainly chemical enhancement along with hydraulic fracturing (Nadimi et al. 2018).

Geothermal wells can be separated into two categories. The first category includes wells that are based on a closed loop system which includes collector pipe inside the energy well (Vähäaho 2021). The energy is collected inside the pipe (Vähäaho 2021). The second category of wells is based on enhanced geothermal system (EGS), which require network of clefts that is inserted into the bedrock (figure 1). Injection of water in EGS with high pressure to the bedrock is called hydraulic stimulation (to c. 900 bars; Vähäaho 2021). This carefully controlled process causes re-opening of pre-existing fractures which creates permeability and makes water to circulate in fractured rock (Vähäaho 2021). Circulating water finally transports heat to the surface level through these fractures (Vähäaho 2021).

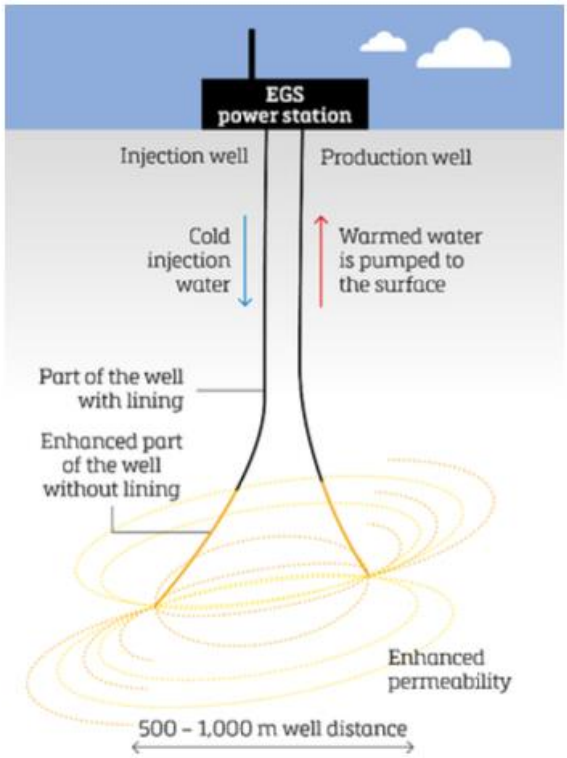

Figure 1: Concept of geothermal EGS power station (Vähäaho 2021).

2.1 Heat

Heat to the EGS is created in network of multiple simulated fractures and in crystalline bedrock rocks that have low permeability (Doe and McLaren 2016). Unlike permeable and porous hydrothermal system which produce hot water directly, EGS uses conductive transfer to create heat from rock which circulates in the fluid (Doe and McLaren 2016). The estimated amount of thermal energy in crystalline basement rocks is about 13,000,000 Exa-Joules whereas in hydrothermal systems the amount only varies between 2,400 and 9,600 Exa-Joules (Doe and McLaren 2016). This allows the minimum temperature to vary from 80ºC-180ºC when the lowest temperature is suitable for binary systems and highest to flash power systems (Finnila et al. 2015).

Geothermal energy can be considered as baseload energy that produces electrical or thermal energy constantly (Boden 2017). This energy can be used as power generation, geothermal heat pumps (geoexchange) and direct use (Boden 2017). Direct use is typically associated with in shallow depths and lower temperatures, and for example EGS is used in greater depths and in higher temperatures (figure 2). Direct use is typically associated with heating of buildings, aquaculture and to needs of households (Boden 2017). Higher temperatures (>100ºC) are required if generation of electrical power is considered. Geoexchange heat pumps which uses heat deposited to the ground in the summertime and withdrawn in the wintertime, can be used widely in the world (Boden 2017). Geothermally heated fluids are typically absent in most places in the world, which makes geoexchange systems the most efficient way for heating and cooling of buildings when transportation of heat is easier that creating heat (Boden 2017).

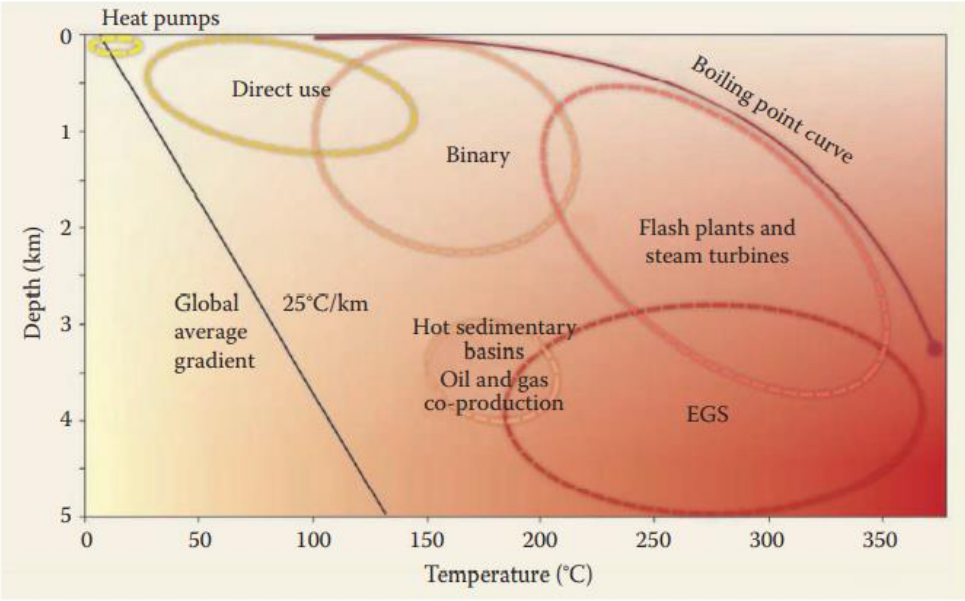

Figure 2: Temperature-depth graph showing different regions where different geothermal energy types can be utilized (Boden 2017).

Heat transfer from Earth's interior towards its surface occurs by conduction (Boden 2017). Transferred heat has an average gradient between 20-30ºC/kilometer in the upper crust, thus the temperature might be lower or higher which depends on the thermal conductivity of the rock and the geological setting of the area (Boden 2017). Geothermal gradient is typically determined when temperature variations in boreholes are being measured (Boden 2017). Convective geothermal systems include fluid circulation that is due buoyancy forces created by density differences between hot upwelling (low-density) and cool descending fluids (denser) (Boden 2017). This means that the bulk of heat is being transferred by movement of material (advection) and a smaller amount due conduction (Boden 2017). Convection includes conduction along advection which makes it the most effective way of heat transfer in the Earth (Boden 2017). Heat flow by solids is very slow or impossible which means that the sufficient heat cannot be transported from depths to the Earth's surface for utilization of geothermal power plants (Boden 2017). Thermal loss is related on the thermal and hydraulic properties of the subsurface, regional groundwater flow, shape of storage volume and heat loss to the surface (Heatstore 2019).

Thermogeological parameters are thermal and physical factors that affect heat exchange processes that occur in the interior of the Earth (Arola et al. 2022). The most important is to focus on thermogeological parameters that are defining effectivity of thermal conductivity in

subsurface, naturally occurring convection, thermal resistance of BHE (Borehole Heat Exchanger) and the temperature of undisturbed bedrock (Arola et al. 2022).

2.2 Fluid

One of the most important thermogeological parameters in shallow geothermal sources is natural convection (Arola et al. 2022). This natural convection may produce false information of thermal conductivity values in cylindrical drill hole, since groundwater temperature increases simultaneously with depth due geothermal gradient (Arola et al. 2022). For this reason, density of groundwater in the drill hole is nonlinearly dependent on temperature (Arola et al. 2022).

Water is a polar molecule that tends to stick to the other molecules by hydrogen bonds (Boden 2017). Hydraulic conductivity (K) measures how material permits fluid flow which can vary many magnitudes in several geological materials, and with direction and distance just like permeability (Boden 2017). Natural convection and hydraulic conductivity are in crucial part when geothermal reservoir is prospected (Boden 2017). Water has a high heat capacity which means that certain absorbed or released energy is required to make changes in water temperature (Boden 2017). Water has also a high specific heat, which means that it can be a great storage for heat (Boden 2017). From the geothermal perspective, water tends to stick into itself which is due the surface tension that is affecting to the weak hydrogen bonds that are located between water molecules (Boden 2017). Polar nature of water also dissolves ionic substances such as salt to itself which is typical in higher temperatures due rock alteration (Boden 2017). Water molecule has a bending nature, and since the hydrogen bonds are created between hydrogen and oxygen atoms, water will expand almost 10% while it is freezing (Boden 2017). This leads to the result where ice will melt, or water will remain in the liquid form, due increased pressure (Boden 2017). Constantly forming and breaking hydrogen bonds in liquid water molecules are helping to retain high specific heat of water (Boden 2017).

2.3 Permeability

Permeability means the ability of material to transmit fluid, and it is typically measured in darcys (d) or millidarcys (md) whereas porosity describes the ratio of volume of voids to solid rocks and it is measured typically in percentages (Boden 2017). Better connection between pores (figure 3B) makes fluid movement more effortless due better permeability in comparison with situation where pores are not fully connected (figure 3A) Geological materials are either

characterized by matrix porosity and permeability or by using fracture porosity and permeability (Boden 2017).

Matrix porosity and permeability of the rock are primary or essential qualities in the rock (Boden 2017). Small pores have higher surface area-to-volume in comparison with larger pores which means that water has larger area where it can be attached to (Boden 2017). If materials have small, connected pores, the permeability may be lower than in other material that has lower porosity connectivity where pore size is larger (Boden 2017). Porosity is in general decreasing with depth due lithostatic pressure that is increasing (Boden 2017). This higher pressure will squeeze or compress fracture grains and walls closer together which leads to reduction of primary matrix and secondary fracture porosity (Boden 2017). Like porosity, permeability will be decreased when going deeper in the crust (Boden 2017). Permeability is sensitive to gap size which means that even small reductions in fracture width or pore size created by compression affects the permeability (Boden 2017).

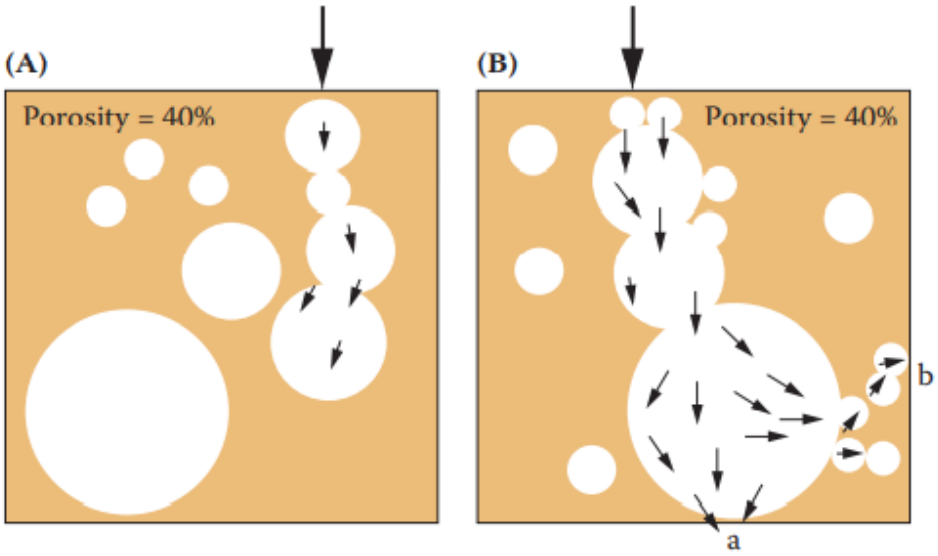

Figure 3: Presentation of contrasting permeabilities of two rocks with similar porosities (40%) but different connectivity between the pores, and finally, different permeability (Boden 2017).

Fracture porosity and permeability can be considered as secondary processes that break rocks due stresses acting within the Earth (Boden 2017). This breaking generates faults that are an indication of stress history of the rock, and joints which may additionally reflect unloading or heating and cooling of the rock (Boden 2017). Figure 4 shows three different fractures where the white area represents open or pore space (Boden 2017). Fractures A and B have a high matrix porosity with little matrix permeability. Fracture A has rougher edges with mineral

precipitates whereas walls of fracture B are smooth. Fracture C is porous, but permeability is absent as the fracture is isolated. The decrease of porosity is more or less linear in comparison with permeability, which shows decrease with exponential behavior (Boden 2017). Typically, geothermal reservoirs dominated by matrix porosity must have higher porosity level to reach given permeability than systems that are fracture-dominated (Boden 2017).

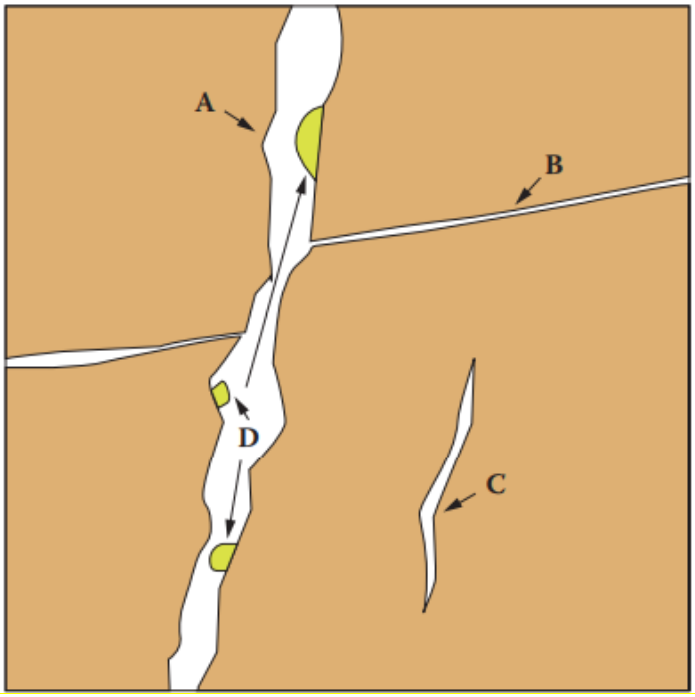

Figure 4: Three different fractures A-B that have different characteristics (Boden 2017).

2.4 Thermal conductivity

Thermal conductivity of the rock specifies the ability of the heat to transfer (Eppelbaum et al. 2014). Evaluation of absorption and conduction of heat of upper crust of the Earth is crucial when thermal properties of the rock are investigated (Roberstson 1988). Thermal conductivity depends on pressure, temperature, composition, porosity and properties of pore-filling gases and fluids (Eppelbaum et al. 2014). Thermal conductivity is sensitive to variation of temperature, and it typically decreases when temperature increases (Boden 2017). Thermal conductivity of different rock types is most dependent on the most typical minerals in continental crust, quartz (high thermal conductivity) and feldspar, which have significant difference on the values of thermal conductivity, and therefore it affects to the heat flow (Boden 2017). This means that that specific minerals can increase or decrease thermal conductivity of the whole rock (Boden 2017). Thermal conductivity is significantly different

in matrix minerals and pore-filling materials, which means that thermal conductivity decreases when porosity and fracturing is increasing (Schön 2011). Thermal conductivity is also typically higher in water-saturated rocks and lower in dry porous or gas-bearing rocks (Schön 2011). Thermal conductivity is dependent on the crack filling materials in fractured rocks (Schön 2011).

The overall thermal conductivity and transportation of energy in the bedrock are also affected by the amount and the movement of bedrock groundwater (City of Helsinki 2019). If the bedrock is used for cooling purposes, the groundwater will transfer heat energy to wider area in the bedrock which will enhance the cooling effect (City of Helsinki 2019). If the bedrock is used to collect heat energy, the groundwater will gather heat energy from the wider area which increases the amount of energy (City of Helsinki 2019).

2.5. Brittle structures and ductile structures

Brittle structures for example joints and faults are evidence of deformation that has occurred in the upper crust (Fossen 2016). Joints does not show relative movement across the fracture whereas faults require relative movement between rocks located on each side of fractures (Boden 2017). These structures can be found in almost every part of the world, where the surface of the Earth is in a solid phase (Fossen 2016). These structures are forming when exhumation and cooling is occurring in the rock or during earthquakes, when the atomic scale crystal lattices are breaking apart (Fossen 2016). Grains will be crushed and reorganized during brittle fracturing and strain will be more localized (Fossen 2016). The breaking point or fracturing is achieved when threshold level of stress is applied (Boden 2017). Brittle breaking occurs typically under low temperature and pressure conditions (Boden 2017).

Fracture can be considered as any kind of planar or subplanar discontinuity which can form due external or internal stress (Fossen 2016). Typically, in this kind of situation, reduction or loss of cohesion is present in fractures (Fossen 2016). These discontinuities are much narrower in one dimension in comparison with other two dimensions (Fossen 2016). Fractures are commonly described as surfaces although some sort of thickness is always present (Fossen 2016). There are two categories of fractures (figure 5): shear fractures (also known as slip surfaces) and extension or opening fractures that include joints, fissures, and veins (Fossen 2016: Peacock et al. 2016).

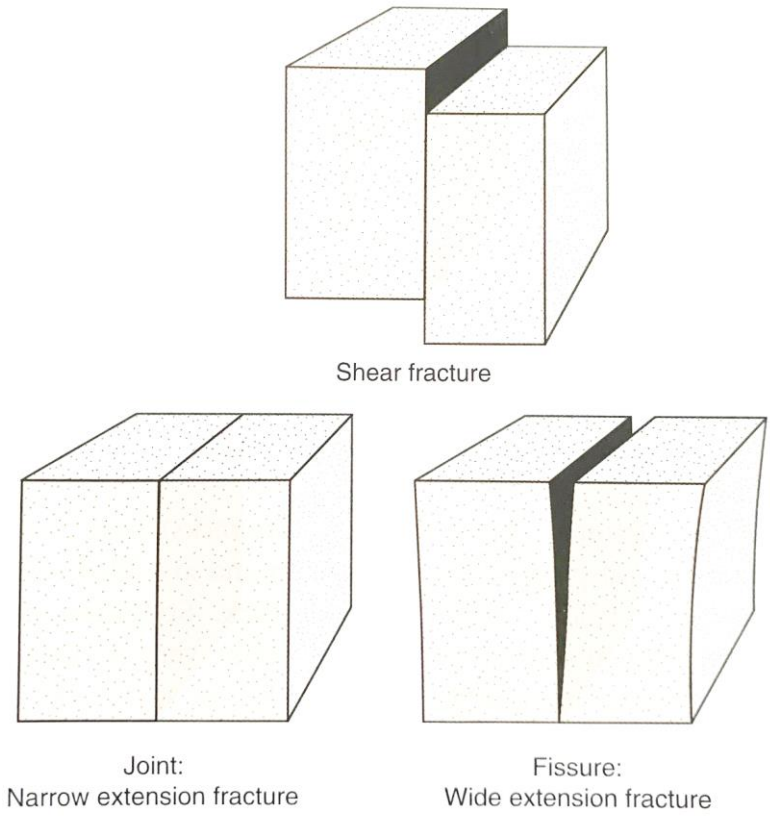

Figure 5: Three different fracture types (Fossen 2016).

Opposite event to brittle fracturing, ductile deformation occurs without any breaking when yield strength of material has been exceeded (Boden 2017). Unlike brittle structures, ductile bending and structures are forming in high temperature and pressure conditions (Boden 2017). Folding is mainly occurring when compressive stress regime occurs at high temperatures or sufficiently weak rocks for example in shales (Boden 2017). Folds can be divided roughly into two different types: anticlines and synclines (Boden 2017). If folds are forming an anticline, rocks are then bowing upwards which means that older rocks are exposed in the core section whereas synclines are bowing downwards, exposing younger rocks in the core section (figure 6; Boden 2017). Anticlines can act as traps if rock layers that are transmitting fluid poorly or hot geothermal water is present in the hinge zone (Boden 2017).

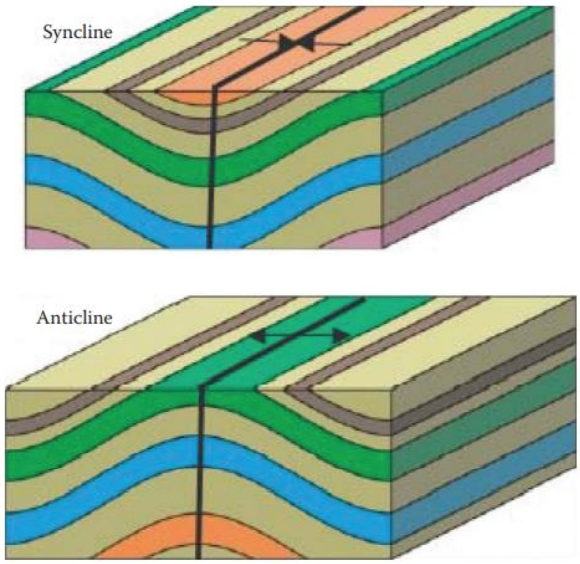

Figure 6: Synclines (top) that have layers bowing down, exposing younger rocks in the cores of synclines and anticlines (bottom) where layers are bowing upwards, exposing older rocks in the cores of anticlines. Black lines are representing the trace of fold axis that is separating folds in half (Boden 2017).

2.6 Borehole Thermal Energy Systems (BTES)

Most rocks have high volumetric heat capacity which means that the ground and flowing groundwater in it can be used as thermal storage (Skarphagen et al. 2019). Usually access to the thermal capacity and huge volume requires drilling and geoengineering which means that underground thermal energy storage (UTES), used commonly in large-slace seasonal heat storage, has some problems in utilization (Skarphagen et al. 2019). UTES can be divided into borehole thermal energy storages (BTES) which includes multiple borehole heat exchangers (BHE) that exchange heat with surrounding material typically by conduction, and to aquifer thermal energy storages (ATES) where paired extraction and reinjection wells are used (Skarphagen et al. 2019).

BTES is especially beneficial in climates that have strong seasonal differences (Figure 7; Skarphagen et al. 2019). BHE is typically located in the drilled borehole between 100-150 mm diameter with common depth between 35-150 meters (Skarphagen et al. 2019). Maximum depth is 350 meters, and typically in crystalline rock terrain of Fennoscandia, depth is about 200 meters (Skarphagen et al. 2019). In Fennoscandia BHE borehole is commonly unlined although surface casing can be used to increase stability (Skarphagen et al. 2019). Due to low

permeability of rocks, water table is commonly quite close to the surface area which fills boreholes with groundwater that creates contact between pipe and surrounding rocks (Skarphagen et al. 2019). In this type of low-permeability rock terrains some “open-coaxial” arrangement can be utilized which includes single pipe inside the borehole that uses surrounding space as outer coaxial conduit (Skarphagen et al. 2019). Therefore, heat exchange fluid has a direct connection with borehole which makes exchange of heat very efficient (Skarphagen et al. 2019). The figure 8 presents the layout view of BTES (Heatstore 2019).

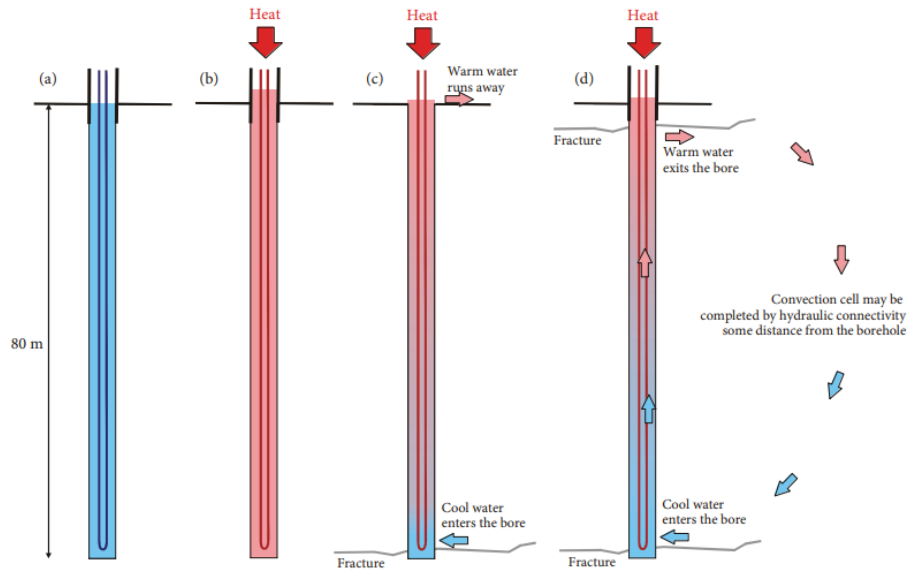

Figure 7: Four different BHE situations where casing and presence of fractures affect to the functionality of borehole (Skarphagen et al. 2019).

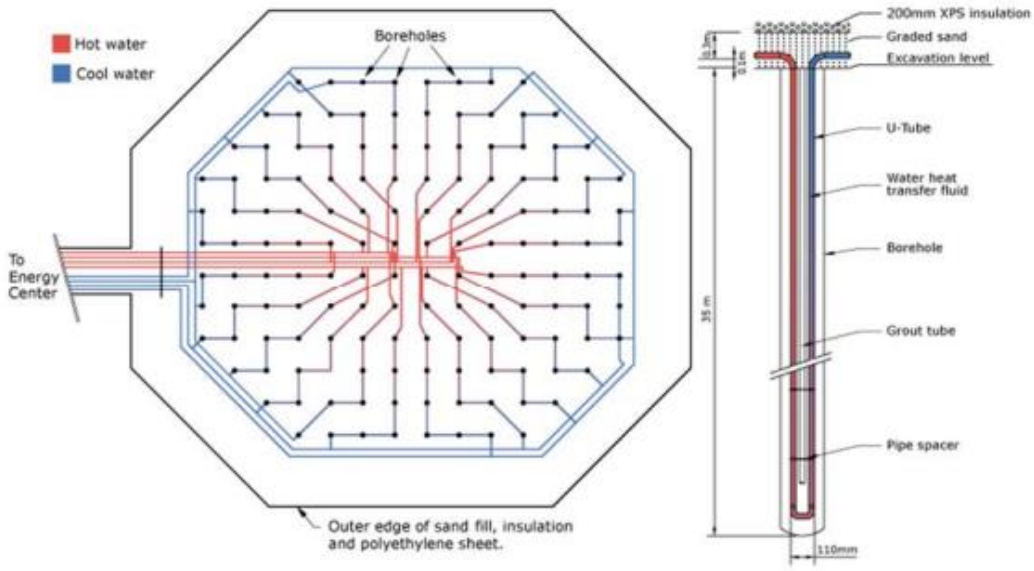

Figure 8: Borehole thermal energy storage as a layout view and cross-section where is single borehole with u-tube (Heatstore 2019).

Borehole thermal energy is typically used in heating and cooling when extraction and injection of heat is directed away from the ground and to the ground (Schulte 2016). This underground thermal energy storage will be only valid when the subsurface is heated on purpose since heat pump source temperature needs to be increased (Schulte 2016). BTES includes variety of boreholes that can be fitted into BHE, which is determining storage size by their radial distance and length (Schulte 2016). Typically, the distance between boreholes is about 2-5 meters and BTES has a limitation which allows the usage in the boreholes that are 20-200 meters deep (Heatstore 2019). The location of BHEs needs to be well considered since BHSs located too far away from each other cannot benefit from heat storage of other ones and BHEs located too close to each other are going to deplete geothermal reservoir too quickly (Schulte 2016). Typical operation scenario includes half-year charging and discharging cycles that can be ideally achieved when radial distance is about 5 meters (Schulte 2016). BTES systems tend to be large and contain multiple BHEs that are located tightly, which creates high storage capacity that is especially fitting for the purpose of seasonal heat storage (Schulte 2016). BTES systems can be expanded if drilling continues to deeper levels and when new boreholes are added (Schulte 2016). BTES is widely used and applicable system although hydrogeological features need to be taken into consideration. Heat storage in porous host rock can be enhanced by groundwater that has high volumetric heat capacity but on the other hand, active groundwater flow can increase BTES performance making it totally ineffective due heat loss (Schulte 2016). BHEs can be classified as underground thermal energy storage systems when annual thermal energy turnover lost to the host rock is less than 25% (Schulte 2016). BTES sites should typically have low permeability and groundwater flow rate to decrease active heat loss which is typically achieved when going on deeper levels where rocks are more compacted (Schulte 2016). Ideally BTES systems are located to shallow depths where reduced lateral temperature gradient is present and to unfaulted crystalline basement rock such as granite and granodiorite in medium depths where content of quartz is high (Schulte 2016). These factors prevent heat dissipation very well and large quartz content has greater thermal conductivity than on average (Schulte 2016).

Medium deep BTES systems have many advantages over shallow systems and the shape and size on them are defining the surface-to-volume ratio, which defines the heat losses and efficiency of the system. Typically, they reach topmost aquifers by penetration which means that thermal impact on shallow aquifers needs to be minimized by thermally insulating medium deep BTES systems (Schulte 2016). This insulation should reach from the topmost part to the

depth of few hundred meters to provide sufficient amount of heat exchange surface without any insulation (Schulte 2016). Deeper BHEs are typically coaxial pipe systems that have outer steel pipe that has high thermal conductivity instead of shallow BHEs that are normally U-pipes or double U-pipes (Schulte 2016). Insulated inner pipe reduces thermal interaction between fluids that are streaming up- and downwards (Schulte 2016). In winter, cold fluids will be injected to annular gap or heat extraction and in summer, warm fluid will be injected to the inner pipe for heat storage purposes (Schulte 2016). It is possible to say by length and spacing between BTEs, that large BTES systems are more efficient than smaller ones (Schulte 2016). Medium deep BTES systems can reach storage efficiency above 80% since those are large enough for storage (Schulte 2016). Storage efficiency also highly depends on the BHE inlet temperature when heat is injected and extracted (Schulte 2016).

2.7 Enhanced Geothermal System (EGS)

The EGS is reaching for the circulation rates that can provide a reservoir that is economically productive (Nadimi et al. 2018). The potential of different EGS areas that include regional stress stains, remains uncertain until investment to the research of the boreholes is made (Finnila et al. 2017). There is also remotely small amount of knowledge about natural fractures and joint systems that are in depth of many kilometers, that are important for the electricity production (Finnila et al. 2017).

Long-term enhanced permeability depends on hydraulic fracturing and/or hydro-shearing (HS) (figure 9). In hydraulic fracturing and hydro-shearing the natural permeability of the rock will be increased while inserting water with high pressure to the bedrock which ultimately leads to the formation of larger fractures (Uski and Piipponen 2019).

Hydraulic fracturing or simulation leads to the generation of new fractures and opening of the existing ones (Nadimi et al. 2018). Fracturing and stimulation will increase the conductivity of the water, leading to the generation of powerful hydraulic paths for heat exchange (Nadimi et al. 2018). Hydraulic fracturing requires the rise of pressure to the level where exceed the magnitude of the minimum principal stress ($\sigma 3$) of the bedrock (Uski and Piipponen 2019). This rise of pressure creates tension fractures that are expanding at first perpendicular to the walls of the fractures and afterwards parallel to it (Uski and Piipponen 2019). The water inserted to the bedrock can include grains of sand or other synthetic substances which will prevent the

closing of the tension fractures afterwards the pressure is not applied anymore (Uski and Piipponen 2019). Several EGS areas need hydraulic simulation to achieve the better connectivity between injection and wells that are produced, and more active pathways from one well to another are being created (Finnila et al. 2017). During hydraulic simulation, factors such as stress conditions, rock properties and fracture orientations should be taken into a consideration (Finnila et al. 2016). If orientation of the natural features and the stress state are known, it is possible to find out the level of pumping pressure that is required to achieve the economic flow rates (Finnila et al. 2016).

Hydro-shearing means that fluid pressure is induced in slip/shear in already existing fractures if driving forces are greater than resistive forces (Nadimi et al. 2018). Hydro-shearing requires that the pressure must exceed the friction of the fracture surface of the rock (Uski and Piipponen 2019). Natural fracture orientation, the surface roughness and in-situ stress field along with other rock mass properties will have a significant effect whether shearing is initiated or not (Nadimi et al. 2018). The change in hydro-shearing is permanent since the unevenness of both surfaces will prevent the closing of the fractures (Uski and Piipponen 2019). One efficient way to investigate is to use hydro-shear natural features where the pore pressure is getting increased to the point where shear failure is possible (Finnilä et al. 2017). The fitting pressure is determined by the stress state function and from the way that the natural fractures are orientated (Finnila et al. 2017).

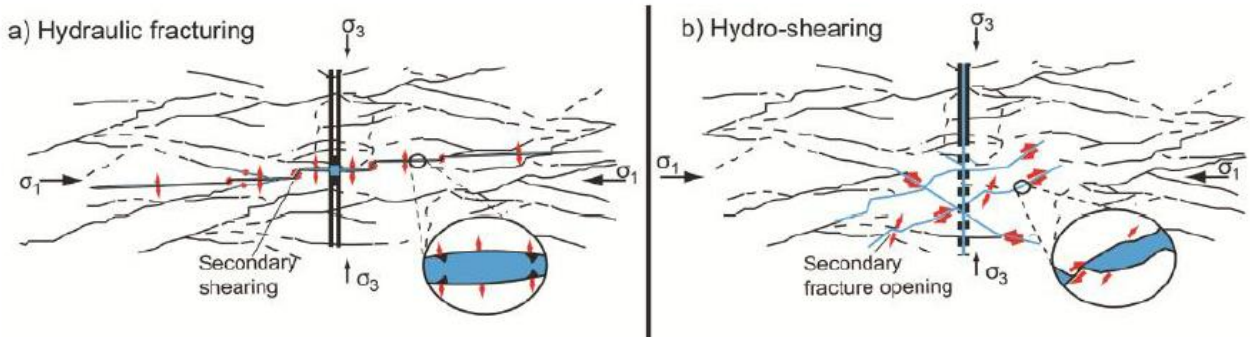

Figure 9: Hydraulic fracturing includes new or already existing fractures that are propagated and initiated (left) and in hydroshearing natural or already existing fractures are getting activated and moved from the influence of fluid pressure and shear failure (right) (Gischig and Preisig 2015/ Uski and Piipponen 2019).

The EGS functioning may be affected by many different properties. Rock properties that affect the performance include thermal conductivity, density, thermal diffusivity, heat capacity, thermal expansion coefficient, compressibility, chemistry, elastic moduli, porosity, crystal size and mineralogy (Finnila et al. 2015). Contributing reservoir properties are permeability, depth, thermal gradient along with heatflow, spacing and orientation, fracture size, formation geometry, stress state, the size and the shape of the blocks and pore pressure (Finnila et al. 2015). Fluid properties include thermal diffusivity, density, heat capacity, chemistry, and thermal conductivity (Finnila et al. 2015).

Mass and heat flow in the EGS rock masses is possible to understand by comprehending the geometry of rock blocks that include fracture networks that pass heated fluids towards production wells by hydraulic properties, thermal geometry, and resource (Doe et al. 2014). Different fracture properties along geometries are giving different results in production, therefore it is important to identify those ones that can be most successful in developing desirable commercial geothermal production (Doe et al. 2014). Figure 10 shows different combinations of factors that provide understanding to a feasible space in EGS. These factors, excluding rock thermal properties, are depending on the induced, natural or stimulated hydraulic properties and geometry that occurs in the rock fractures (Doe et al. 2014).

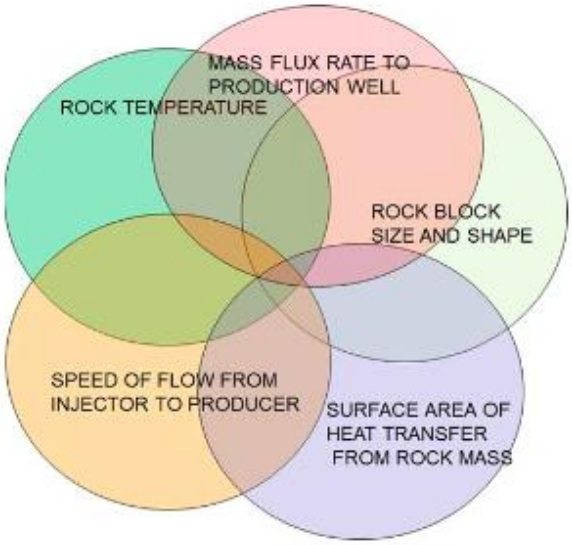

Figure 10: combination of factors that are providing understanding to feasible space of EGS (Doe et al. 2014).

Different stimulation techniques are required to improve the quality of fracture network transmissivity that occurs in rock masses that are fractured. This will give balance to both

convective and conductive heat transport (Finnila et al. 2015). For example, creating EGS areas in large thrust faulting regions in the United States is limited by high minimum stress values and low geothermal gradients (Finnila et al. 2015). Areas that include strike-slip and normal faulting can be traced easily however horizontal drilling may be required in the wells (Finnila et al. 2015). Also, the lithologies effect on constraints which impact to fracture spacing (Finnila et al. 2015). In conclusion it is difficult to design a stimulation program that considers enhancing of the reservoir permeability and at the same time it maintains fracture spacing at an appropriate level (Finnila et al. 2015). A successful EGS production area requires finding out what is the whole range of water fluxes and temperatures that are crucial to beneficial electricity production.

The most suited regions for EGS are areas, that include extensional tectonic settings since the minimum stress state is commonly lower and thermal gradients are higher (Finnila et al. 2015). The EGS sites that include strike-slip tectonics are quite similar to the regions that include normal faults (Finnila et al. 2015). These sites are usually located nearby tectonic boundaries which are increasing the heat flow and decreasing the minimum stresses leading to the possibility where production and simulation can have lower pumping pressures (Finnila et al. 2015). The EGS development is clearly most difficult to execute in the areas which includes thrust faults since lower heat flow is typically associated with lower geothermal gradient (figure 11). It is difficult to achieve the sufficient permeability level to the EGS in the compressional environments due the initial permeability differences that vary from only half an order of magnitude to multiple orders of magnitude (Finnila et al. 2015). Low permeability might increase the impedance of water flow to the point where the flow rates are excessively high which are impossible to maintain by utilizing modern pumping technology (Finnila et al. 2015). Low permeability also affects negatively to the simulation of the thrust-fault regions when higher minimum stress values are observed in the same depths compared to the regions that include strike-slip or normal faults (Finnila et al. 2015). Increasing permeability is possible to achieve by hydraulic simulation, although the pumping pressures must be unreachably high to get to the levels of critical normal or shear stresses (Finnila et al. 2015).

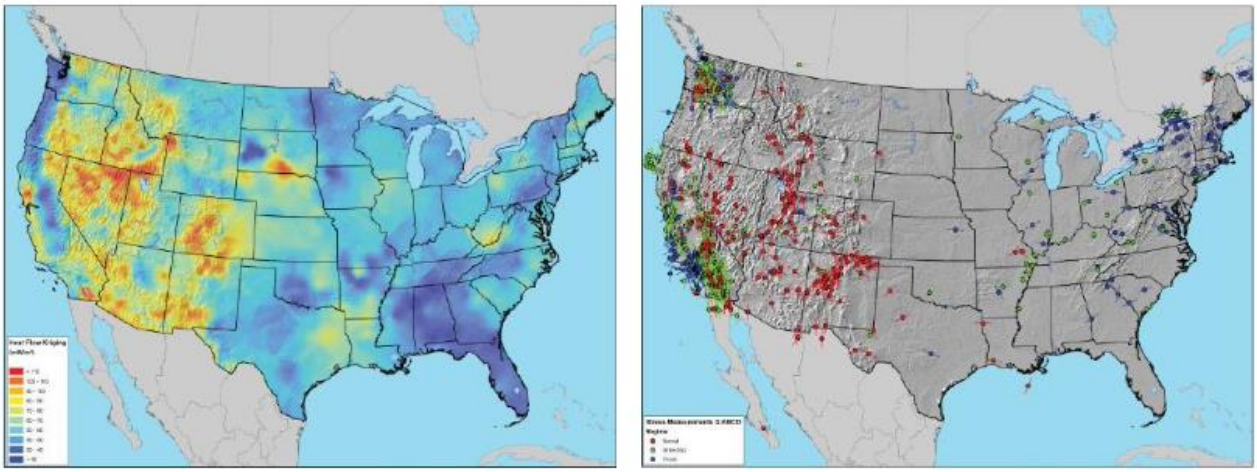

Figure 11: Heat flow and stress maps from the United States. Figure on the left is showing higher heat flows in the red. Figure on the right includes thrust faults (blue), strike-slip faults (green) and normal faults (red) (Finnila et al. 2015).

St1 was the first energy company in the world that executed a pilot project of deep EGS in Otaniemi, Espoo, Finland (St1 2023). The plan was to drill two heat wells that reached over 6 kilometers: other pumps cold water to the bedrock and other delivers the heated water to surface level (St1 2023). The heat would be inserted to the district heating network via heat exchanger (St1 2023). In general, the bedrock of Finland consists mostly of hard granites which means that drilling requires equipment that penetrates through this material, great plan, and time (St1 2023). The other problem was to create connection between these two wells, which would allow the water flow (St1 2023). The project gave important information about the planning of this kind of stations and many uncertainties were cleared however the EGS project itself turned out to be technically and economically very challenging (St1 2023). The water temperature was not sufficient to be useful which means that alternative options to reach the optimal thermal power are still being prospected (St1 2023).

2.8 Approaches in recent EGS investigations

The Frontier Observatory for Research in Geothermal Energy (FORGE) is determined to be a suitable testing and demonstrating site for creating new technologies for the geothermal heat extraction that occurs in host rocks that have naturally low permeability (Nadimi et al. 2018). In Utah, United States of America, FORGE is investigating the possibilities of EGS energy development (Nadimi et al. 2018). There are three deep wells in the area which have crystalline

bedrock where temperatures are more than 197ºC at less than a depth of 3 kilometers (Nadimi et al. 2018). Nadimi et al. (2018) made an investigation where they wanted to clarify what is the ideal completion design in the FORGE project for the Phase 3. This was executed by observing how various parameters are reacting to the fracture network development that occurs between two wells that are drilled horizontally (Nadimi et al. 2018). Representative discrete fracture network (DFN) model was able to be developed since the scientific measurements such as logging, field tests and core tests were able to produce information (Nadimi et al. 2018). Then the DFN was moved to the well and Phase 3 injection site, to clarify how different designs would work (Nadimi et al. 2018). They found out from critically stressed analysis that pumping fluids inside natural fractures will increase pore pressure to the level where shearing occurs, which is typical if factors such as in-situ stress field and natural fracture ordination are present (Nadimi et al. 2018). It is possible to say that the value of the DFN modeling used in the EGS projects is significant. The study improved the understanding of the FORGE natural fractural systems that are already existing, and the optimal pumping schedule was also developed which connects fracture channels (Nadimi et al. 2018). Also, more understanding about injection and production of Phase 3 after stimulation was gathered (Nadimi et al. 2018).

Finnila et al. (2015) investigated possible sites for EGS by examining the changes and effects in different processes that occur in geothermal convection and conduction in North America, where three ideal hydro-sheared and hydraulically fractured terrains are observed. This kind of areas which include fracture area and spacing in depth are creating ideal conditions to the geothermal energy production (Finnila et al. 2015). Finnila et al. (2015 used analytic equations, simulation of multi-stage hydro-shearing fractures, and decrease of transmissivity in the fractures that went through shear failure and rising pore pressure. The focus on this study was to find out how regional stress is possibly going to limit EGS development in the potential areas when impedance and thermal demands are considered (Finnila et al. 2015). Sufficient electric energy production required output temperature limitation to be between 200-180ºC during the 20-year time period, and the flux rates at 0.07 m^3/s (70 1/s) (Finnila et al. 2015). Impedance levels were significantly high, although the level was kept below 1MPa (1/s) by limiting the pumping pressure under 70 MPa (Finnila et al. 2015). This study brought up various challenges that might occur while developing successful EGS (Finnila et al. 2015). The strike-slip model along with the normal faulting model had the similar high thermal gradients, which kept the pumping pressure at the sufficiently shallow level and made hydraulic simulation possible (Finnila et al. 2015). The thrust faulting model had some difficulties with locations that included

low geothermal or normal gradients (Finnila et al. 2015). The reservoir located in this area was more than 8 kilometers deep which increased the pumping pressure to excessively high levels (Finnila et al. 2015). However, this stress orientation is suitable for vertical wells that are accessible to the induced tensile fractures that are horizontal and to the fractures that are hydro-sheared (Finnila et al. 2015).

Finnila et al. (2016) studied the changes of flow paths that were affected by the archetypical DFN models in United States, that have thrust, strike-slip and normal faults. The goal was to find a geothermal system that is economically productive (Finnila et al. 2016). The DFN models combine induced hydraulic fractures with hydro-sheared natural fractures and the models were estimated to different simulation levels in various parts of the simulation (Finnila et al. 2016). Finnila et al. 2016 found out that the strike-slip model, which had natural sets aligned together with the first slipping orientations, was most easily simulated. The impedance of it was under 0.15 MPa/(1/s), when three (10, 100 and 1000) fracture transmissivity enhancement factors were taken into a consideration (Finnila et al. 2016). The compressional stress model in this case went through significantly greater stress conditions, and natural features that were first to fail in shear, were missing (Finnila et al. 2016). Simulation level must be clearly higher so the economic flow rate could be reached (Finnila et al. 2016). The simplification in this study led to the realization that the flow rates are getting overestimated in the deeper parts of the fracture (Finnila et al. 2016). It is possible to say that when natural fractures are not aligned, it requires either greater stimulation level or greater transmissivity enhancement factor (Finnila et al. 2016). They also found out that the minimum block dimensions are, without exception, aligned with the principal stress direction during simulation processing (Finnila et al. 2016).

Finnila et al. (2017) executed an investigation where they used the orientation from two conjugate sets to find out the effectivity of hydraulic simulation, and how it could be used to form desirable EGS areas in regions that include normal, strike-slip and thrust faults. This execution was made using DFN models and simulation that was created using the following effects of increased pore pressure of hydro-shearing (Finnila et al. 2017). They kept different factors such as lithology, geometries of the wells and thermal gradients the same, when they varied the set orientation of the natural fracture and regional stress state (Finnila et al. 2017). They found out that there should be at least one well-aligned set so that sufficient impedance, that makes the system economically beneficial, is achieved (Finnila et al. 2017). In the areas where strike-slip stress is observed, it is possible to utilize horizontal wells whereas in regions

where normal and thrust faults are typical, vertical wells are required (Finnila et al. 2017). Thermal drawdown of 20-year period is reasonable if flow pathways can be connected to wells, although it is difficult to assume the temperature of early stages production water in the vertical wells that have zones with grand fracturing (Finnila et al. 2017).

Doe et al. (2014) made a paper where they addressed how the possible space in the EGS can be identified by the using the key elements such as properties of induced, natural, and reactivated fractures and geometry. These factors are dominating the quality and rate of the heat that derives from the EGS reservoir (Doe et al. 2014). The possible space is determined by the ability to produce rock masses by fracture simulation that leads to the wide area of thermal conduction (Doe et al. 2014). Determination can also be made by the flow rates that are relatively slow so the outlet water temperatures can be sustained (Doe et al. 2014). They used the dimensionless analytical solutions created by Gringarten et al. (1975), that are emphasizing the illustration of relative roles of conductive heat transport from rock matrix to flowing fractures and convective heat transport through fracture network towards producing wells (Doe et al. 2014). This is possible by using spaced parallel fracture networks that are part of the idealized systems (Doe et al. 2014). The results form Gringarten solutions was emphasized by using DFN which made fracture networks more realistic (Doe et al. 2014). Gringarten addressed simple fracture geometries and concluded that dimensionless time leads to the fact that second power dependency on fracture area and flow rate is present in the thermal breakthrough (Doe et al. 2014). Gringarten made also clear that the flow rate distributed over various fractures that include spacing and properties that are uniform, is going to enhance the performance of EGS (Doe et al. 2014). The improvement can be observed also in the networks that are simpler, such as ones including parallel fractures that have irregular flow properties and spacing (Doe et al. 2014).

2.9 Discrete Fracture Network (DFN)

Although EGS systems have been researched for over 40 years and the development of using it as a source of energy production has been rapid, the pace has been still rather slow due different conditions of potential sites and poor understanding of underground simulation and heat exchanger work (Doe and McLaren 2016). Potential of EGS has not been comprehended since analyses made in past from EGS systems have been using models that are simplified (Doe and McLaren 2016). DFN models should be more investigated for their ability to

combine valuable factors such as heterogeneity and anisotropy instead (Doe and McLaren 2016). The generic regional DFN models are crucial tools in the future when the controlling parameters of the EGS development are getting further investigated (Finnila et al. 2015). This means that different parameters and methods can be corresponded to the sensitivity studies and estimations for different factors such as water volume, durations and for pumping rates which can be calculated for well simulations (Finnila et al. 2015). The research has been lately focusing on to the development of methods and effects of DFN systems, in situations where hydraulic fracturing propagation is occurring (Nadimi et al. 2018). For example, in Finland DFN-models have been tested in Olkiluoto by executing prediction-outcome exercises on DFN-model during 2017-2021 (Posiva 2022).

DFN aims to improvement of the well production forecasts through fracture simulation, which can be done by offering excessive complexities that are part of the fractured subsurface, included in the modeling softwares (Nadimi et al. 2018). Complex fracture network includes both temporary and permanent fracture spacing behavior which can occur in different stages (figure 12; Doe and McLaren 2016). When constant temperature is produced the stage is called pre-breakthrough (Doe and McLaren 2016). The stage of thermal depletion of stimulated zone includes temporarily spaced blocks and the stage of stimulated, everlasting zone includes thermal sink by stimulated volume (Doe and McLaren 2016).

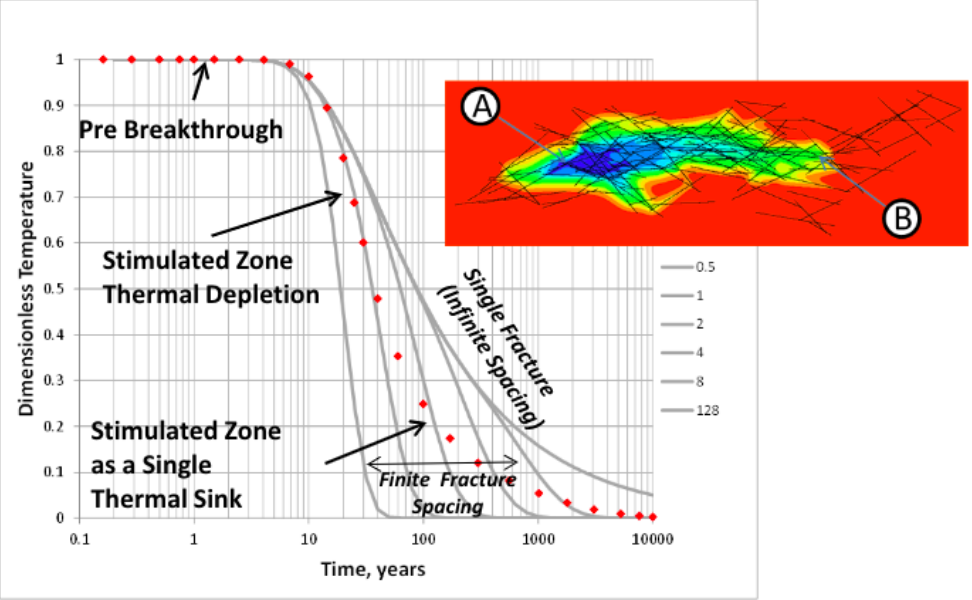

Figure 12: An example of how temperature behaves in EGS reservoir while it produces A and B well pair. It is compared to DFN results (red dots) with analytical solutions made by Gringarten and Witherspoon (1975) (Doe and McLaren 2016).

2.10 Challenges of the boreholes

Successful borehole systems have high efficiency, small environmental impact and most of all, those are economically viable (IEA 2020). These kinds of systems can typically be achieved by distinct disciplines that include high quality designing, engineering, construction methods, and knowledge (IEA 2020). Designing and construction requires proper education, experience and information about the local geological and hydrogeological settings along with high quality construction tools and materials (IEA 2020).

Risks associated with groundwater protection can occur in all different phases of designing and construction of borehole systems (IEA 2020). Typical risks can be for example pollutants from the surface area or water, which can be mixed into the water with better quality, or heat transfer fluids that might leak away from the pipe contaminating the nature (IEA 2020). If the BHE field is under-sized, heating power is not sufficient, heating costs are too high, and failures are typical in the system (IEA 2020). This may lead to the unexpected costs for repairing and replacing different components, for example due freezing in cold Scandinavian countries or due the external pressure that may occur when boreholes are located too close to each other (IEA 2020). Confusion about the geology, ground thermal conductivity and underground temperature can also create problems (IEA 2020). Problems may arise if possible geological variation in large BHE field is not considered or if TRT is producing incorrect measurements when determination of thermal properties has failed (IEA 2020). These problems can be avoided by test drilling and proper evaluation (IEA 2020).

Drilling of borehole is extremely crucial part of the whole process. Chosen drilling method may turn out to be disappointment in operation even though it appeared to be valid option in the designing phase (IEA 2020). There are numerous problems that can be associated with drilling. For example, desired borehole depth may not be reached when other holes are required, pipe may leak water, or the borehole can be clogged and collapsed (IEA 2020).

2.11 Ground heat and geothermal energy production in Finland and Helsinki

The goal of city of Helsinki is to reduce the impact of climate change by being carbon neutral by 2035 (Vähäaho 2021). This goal can be achieved by reducing greenhouse emissions radically, which can be partly done by heating and cooling of buildings with ground heat and geothermal energy (Vähäaho 2021). The amount of usage of ground heat and geothermal energy in the heating of buildings in Helsinki in 2019 was only 1%, however the plan is to increase the amount to 15% by 2032 (Vähäaho 2021). The annual amount of energy produced from ground heat and geothermal resources should be around 1,000,000 MWh starting from the year 2035 (Vähäaho 2021).

Ongoing energy production using ground heat and geothermal energy aims to increase the amount of large energy wells that are vertical and reach deeper (Vähäaho 2021). In Espoo, there are two geothermal energy well stations: In Koskelo, the well is reaching the depth of 1,3 kilometers and the two wells in Otaniemi EGS station, are 6,1 kilometers deep (Vähäaho 2021). The stations using geothermal energy has been planned in numerous other locations in Helsinki, Turku and Tampere, however the confirmation of these stations is waiting the experience from the existing stations (Vähäaho 2021). In Finland, shallow ground heat wells are typically more cost-effective compared to geothermal energy wells, by the value of generated energy (Vähäaho 2021). In the future, mass production of geothermal energy solutions is expected to decrease the construction costs of geothermal energy, and hence increase the cost-effectiveness (Vähäaho 2021). The use of geothermal energy has many benefits compared to ground heat wells. The usage requires much less boreholes, in fewer locations and the usage can be modelled for example for a next 1000 years, whereas usage of ground heat wells is typically calculated for 20-50 years since the lifetime of a system is typically between 17-24 years (Vähäaho 2021). Figure 13 illustrates the energy production of 2 km deep geothermal energy wells in Helsinki. The modelling has been done for the next 1000 years and it is possible to see that the energy production of the wells will initially reach annually 800 MWh and after 1000 years the level still reaches 640 MWh annually (Väliaho 2021).

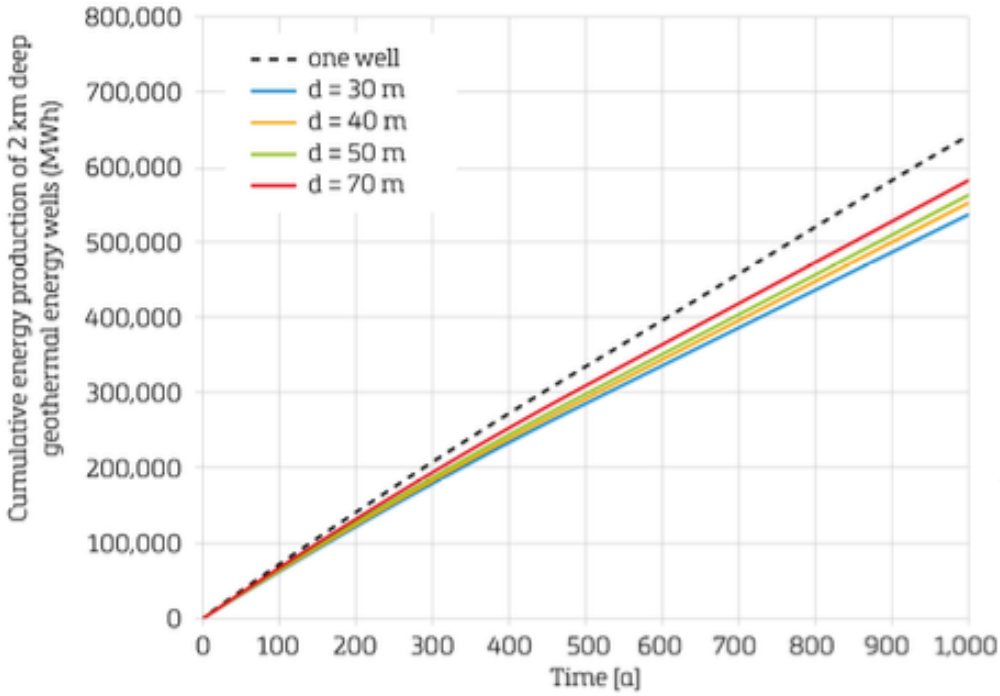

Figure 13: Cumulative energy production in the geothermal energy wells that are 2 kilometers deep. The distance between the wells is marked by d (Vähäaho 2021).

3. Geological setting

3.1 Bedrock of Helsinki

Bedrock of Helsinki has characteristics initially suited for the usage of geoenergy as the bedrock is composed of recrystallized granitoids and light-colored gneisses and schists (GTK 2023). The lithosphere is relatively thick (150-200 m) in Finland (Kukkonen 2000). The heat flow in the bedrock is typically below continental average (< 65 mW m^{-2}; Kukkonen 2000). The temperature of the surface varies in Finland between 0.5-7.6 ºC and in Helsinki it is on 6,8 ºC on average (figure 14; City of Helsinki 2019). Temperatures of 40 ºC are typical in the depths of 2-3 kilometers whereas 100 ºC can be achieved in the depth of 6-8 kilometers (City of Helsinki 2019). This means that the geothermal energy with high temperatures is not available in Finland. The wells of EGS power stations in Helsinki area should be 6-7 kilometers deep to minimize the earthquake risk (Vähäaho 2021).

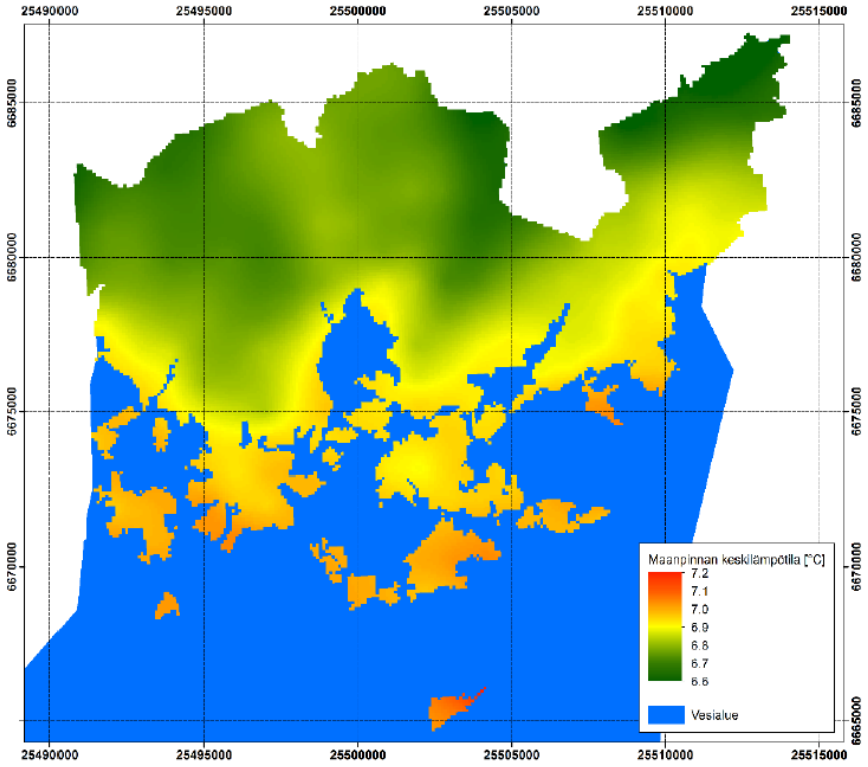

Figure 14: The average temperature of the Earth surface in Helsinki. Coordination system used in a map is ETRS-GK25FIN (City of Helsinki 2019).

The area of Helsinki is part of the Precambrian bedrock of Finland, which is part of Svecokarelian orogeny belt (GTK 1991). The typical rock types of the area are supracrustal and plutonic rocks (GTK 1991). During Svecokarealian orogeny (1,9-1,8 Ga ago) rock types such as sediments and volcanites were altered to gneisses and schists due strong folding and metamorphism of the bedrock (GTK 1991). The intruded magma also altered sedimentary rocks, which led to the formation of migmatites (GTK 1991). The deep roots of the Svecokarelian mountain range are nowadays eroded (GTK 1991).

The rock types observed in Helsinki (figure 15) can be divided into ones that have been formed in the surface level and on a deeper level of the crust. The mica gneisses of the area consist typically of quartz, plagioclase and biotite (GTK 1991). The amphibolites of the Helsinki city area are highly metamorphosed mafic pyroclastic rocks and/or lavas (GTK 1991). The plutonic rocks such as gabbros, quartz diorites and quartz-diorites appear in Helsinki area as intrusions that are concordant with dominant structures of the surroundings (GTK 1991).

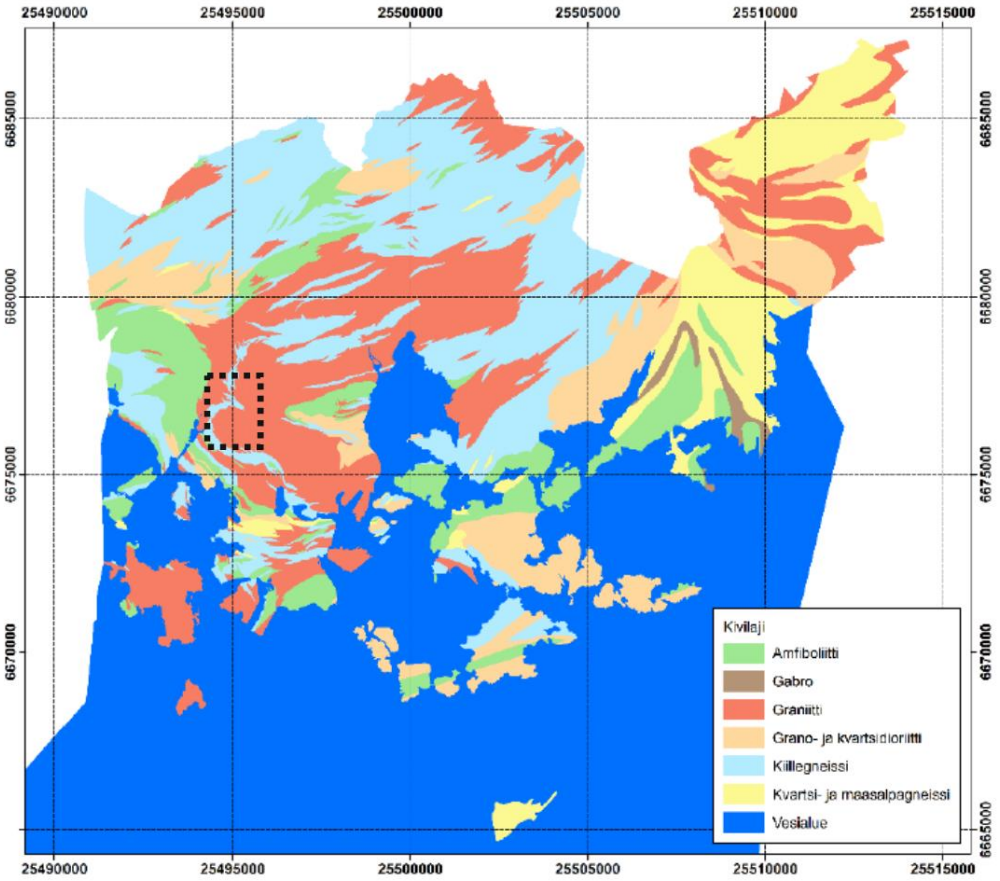

Figure 15: Simplified rock type map of Helsinki. Main rock types are amphibolite (green), gabbro (brown), granite (red), grano- and quartz-diorite (beige), mica gneiss (light blue), quartz and k-feldspar gneiss. The water is marked with dark blue. The study area of Ruskeasuo and the area of Central Park – Laakso hospital is marked with black rectangle. Coordination system used in a map is ETRS-GK25FIN (City of Helsinki 2019).

One of the best thermal conductors in bedrock of Finland which typically defines the thermal conductivity of the rock, is quartz (City of Helsinki 2019). Quartz is a typical mineral within light-colored, granitic rock types and in schists, which typically have great heat conductivity and transfer characteristics (City of Helsinki 2019). The average value of thermal conductivity measured in granites in Finland is 3,55W/(mK) (City of Helsinki 2019). In Helsinki, granites and gabbros tend to have the highest values of thermal conductivity (figure 16). In the darker rock types the content of quartz is lower which leads to lower average value of thermal conductivity, for example average thermal conductivity value of amphibolite measured in Finland is 2,59 W/(mK) (City of Helsinki 2019). In the Helsinki area, the porosity of surface level rocks is very low due to the recrystallized character of the rocks (City of Helsinki 2019). The bedrock in the Helsinki area can be heavily fractured (GTK

2008) in places which make the movement of groundwater easier especially in granitic rocks (City of Helsinki 2019).

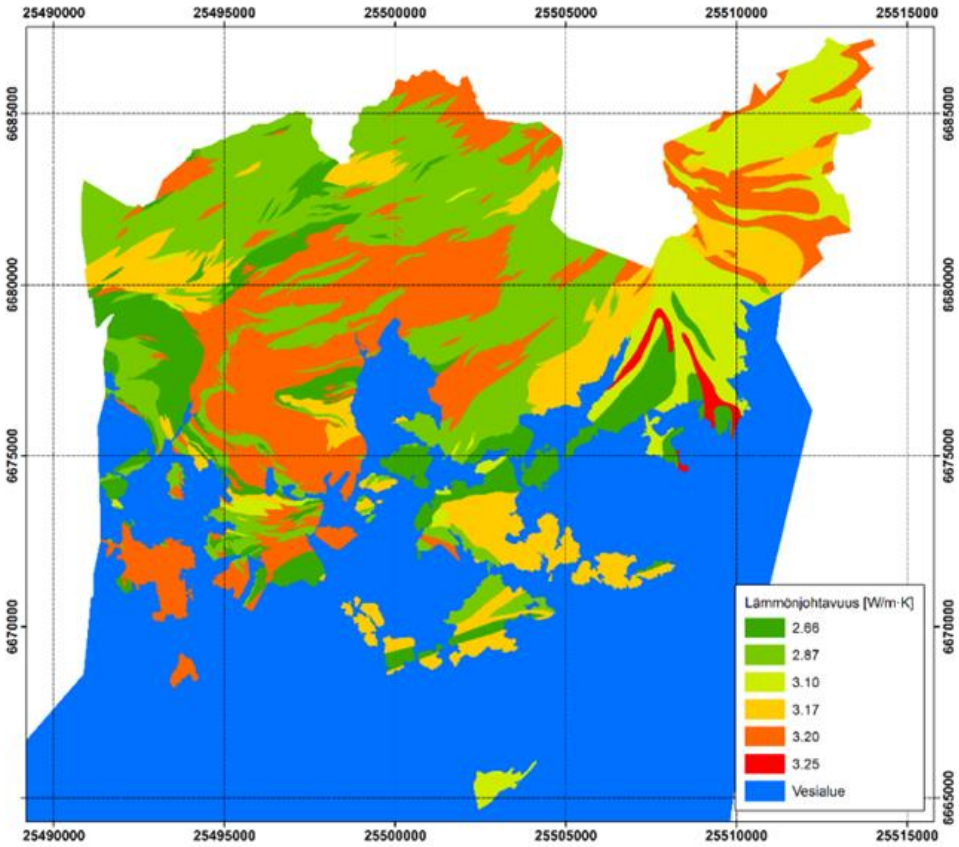

Figure 16: Thermal conductivity of bedrock of Helsinki. Coordination system used in a map is ETRS-GK25FIN (City of Helsinki 2019).

3.2 Geology of the Central Park – Laakso hospital area

The Central-Park-Laakso hospital area is located on the southern side of the study area of Ruskeasuo. On the northern side of Laakso hospital area there is NNW-SSE (figure 17A) directed topographical depression, which is the dominating linear topographical depression in the whole Laakso - Ruskeasuo area. This depression extends to the eastern side of the geothermal well. In the area it is also possible to see depressions that have secondary directions such as WSW-ESE and E-W. Bedrock outcrops on the edges of the depression are dipping on the other or both sides towards the center of the depression. On the bedrock outcrops, it is possible to observe fracturing, which is controlling the topography. This is also possibly related to the main structures of the bedrock. The dips of the structures are typically over 60^{o} (figure 17B).

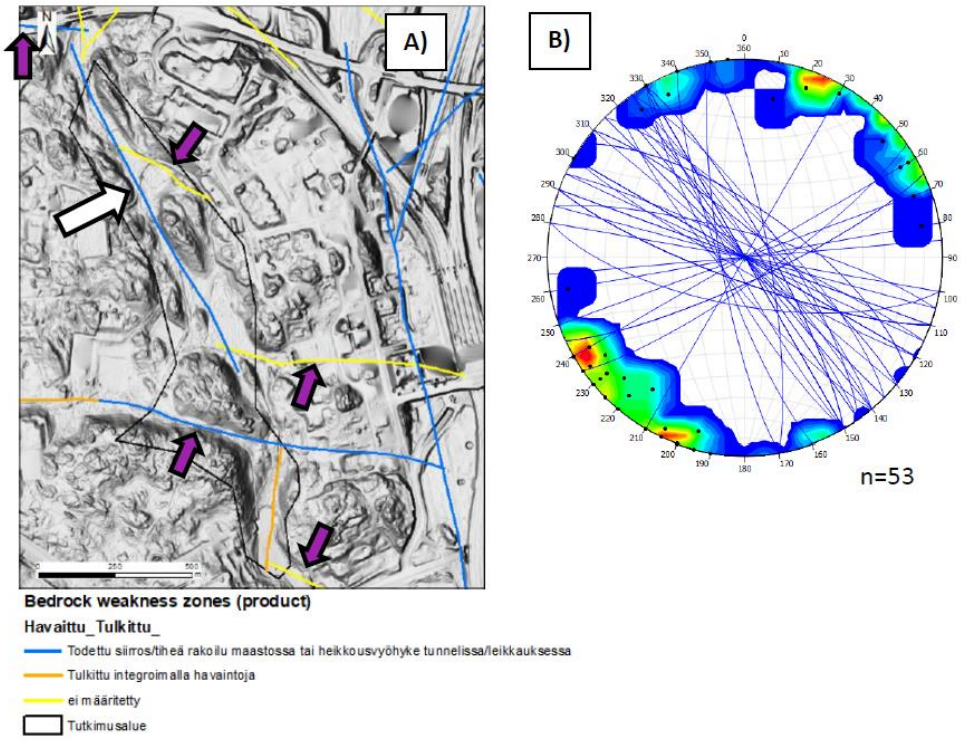

Figure 17: A) Weakness zone map of Laakso and Ruskeasuo where NNW-SSE structure is marked with white-black arrow and WNW-ESE structures are pointed with purple-black arrows. In the background there is oblique hill shaded laser scanning data which represents the topography of surface. B) Diagram of directions of measured foliation observations (GTK 2022b).

3.3 Drilling process of the well in Ruskeasuo

The well was planned to be a half-open system, which means that a pipe is installed in the middle of the drilled hole (GTK 2022c). In this kind of system water flows downwards and upwards on the outside of the pipe (GTK 2022c). This movement of water collects heat from the surrounding rock and transports it to the surface (GTK 2022c).

The drilling process of the geothermal was not easy. In the beginning, mixture of water and rock material filled the borehole and made it appear brownish and unclear. Cleaning process of the water challenging. First fracture/s were encountered in the depth of 648 meters, where the casing of the well ended. This created some challenges to the drilling. The purpose of casing is to protect the borehole from possible fractures that could feed cold water to the system or collapse the system. The drilling continued until the next fractures were encountered at the depth of 804 meters. These fractures continued to the depth of 865 meters. This is the depth, where the drilling ultimately stopped. The depth of 2,5 kilometers was never achieved.

The depth of 865 meters was achieved after 155 days counting from the start (GTK 2022c). Based on the timeline of the drilling process, is possible to say that at the depth of 300 meters the angle of speed of drilling progress is changing from steeper to gentler (figure 18; GTK 2022c). At some points it is also possible to see that the progress of drilling has been very fast which may have been affected by scheduling the work, different phases of the work and logistics (GTK 2022c). Some sort of fracture penetration of the well is observed in the graph at the depth -450 meters and after this depth, the drilling has been slower (GTK 2022c).

Drilling process was ended since continuation of the process would not have been economically profitable anymore. This means that these fractures at the depth of 865 meters were not impossible to penetrate through. It is still possible assume that some other problems with fractures would have appeared when drilling to the deeper levels even though those might not have been that crucial.

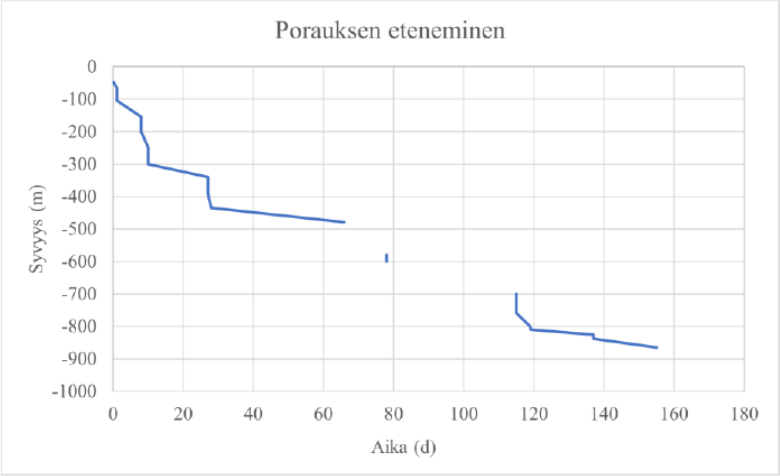

Figure 18: A graph representing the progress of the drilling based on the collection of the samples (GTK 2022c).

4. Materials and methods

4.1 Study area

The study area located in Ruskeasuo, Helsinki, is surrounded by busy roads and settlement (figure 19A). On the southern side of the road, there is the geothermal well drilled by Helen Oy that was supposed to utilize medium-deep geothermal energy in the depth of 2,5 kilometers (figure 19C). The dominant feature of the study area in the large E-W oriented rock cut on the northern side of the road (figure 19C). The outcrop and the geothermal well are located significantly close to each other which emphasizes the interest of studying the effect of the location of the outcrop to the well.

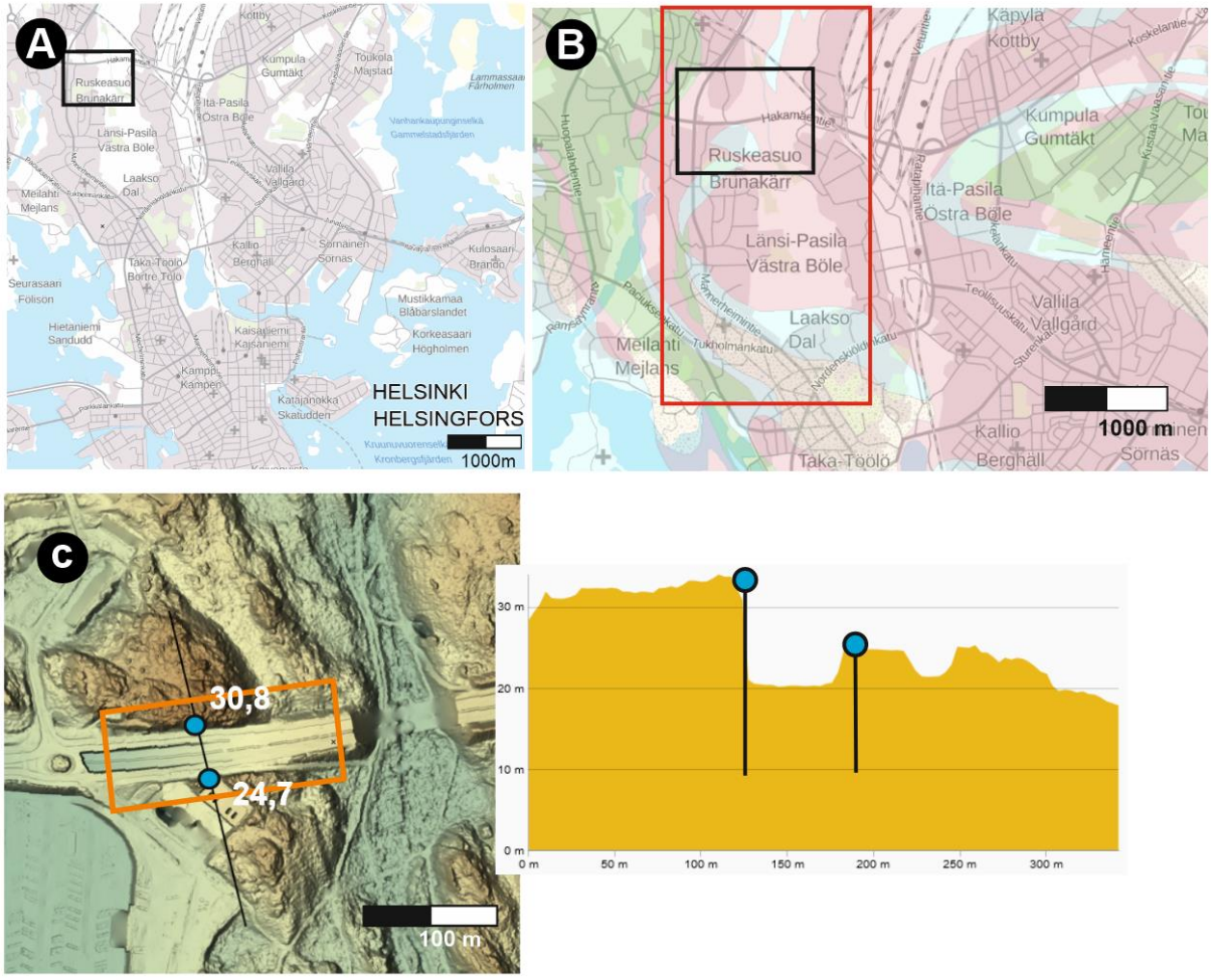

Figure 19: Caption overleaf.

Figure 19: A) The location of the main study area of Ruskeasuo in Helsinki City outlined with a black rectangle. B) 1:200 000 Bedrock map of the study Ruskeasuo area where typical rock types are microcline granite (red) and biotite paragneiss (blue). Other rock types observed near the study area are amphibolite (green), granodiorite (beige with dots) and quartz feldspar paragneiss beige). The study area of Central Park – Laakso hospital is outlined with red rectangle C) Oblique hill-shading map from the study area where two spots are marked and cross-section between those is marked. The E-W directed fault has elevation of 30,8 meters and the location of the well has the elevation of 24,7 meters from sea level. The extent of the bedrock mapping observations is outlined with orange rectangle (Paikkatietoikkuna 2022).

4.2 Surface studies

The data for the subsurface studies was gathered by using multiple different methods. Figure 20 shows an orthophoto of the study area. The focus was on the bedrock mapping of the area. In total 40 observation points were visited from where 114 observations were gathered. These included measurements from faults that were located on both sides of the road (figure 20), (4), fold axial surface measurements (4), lineations (4), foliations (28), fractures (37) and observations of different rock types (37). Also, two samples were gathered from two different observation points (figure 20). From these samples, three thin sections were created. The observations from bedrock mapping were supported by photogrammetry footage, which was collected on both sides of the road, and 2D-fractopo analysis which was done on southern side of the road from group of outcrops.

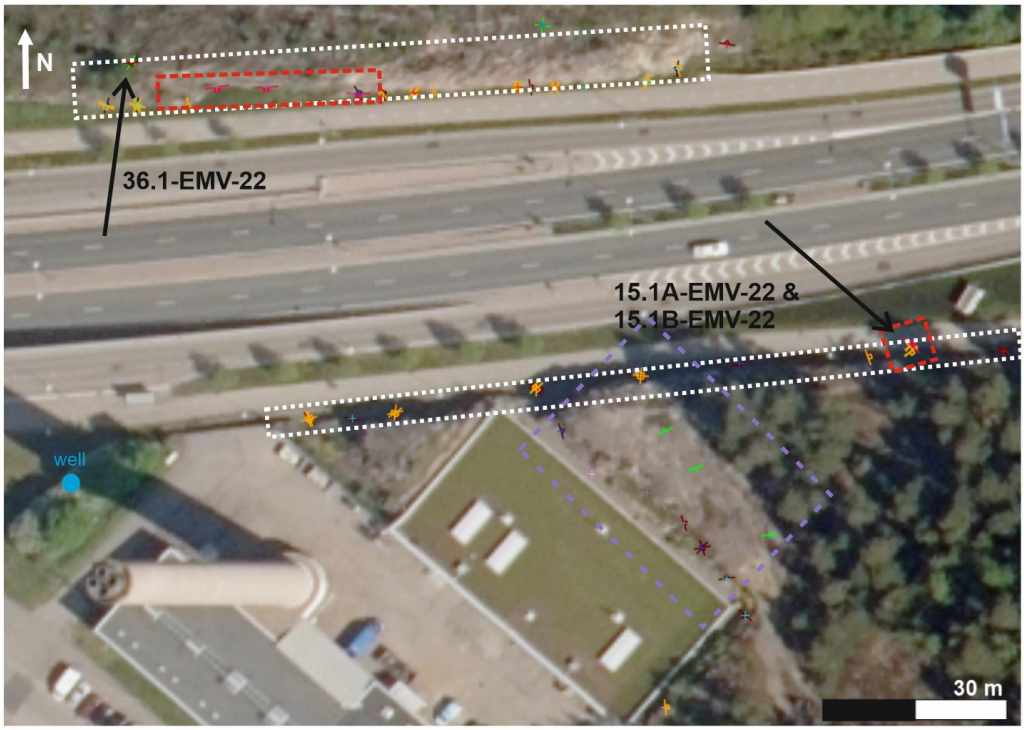

Figure 20: Caption overleaf.

Figure 20: The orthophoto of the Ruskeasuo study area (MML) where location of the well is marked with blue dot. The observation points (40) and the measurements/observations (114) are marked with different symbols. The locations of the two sample sites are marked with black arrows. The photogrammetry footage was collected on both sides of the road (rectangles white dashed outline) and 2D-fractopo analysis was done on the southern side of the road (a rectangle with purple dashed outline). The area includes two faults on both sides of the road (a rectangle with red outlines).

4.2.1 Bedrock mapping of the study area

The mapping of bedrock outcrops is an inexpensive way to get an overview of the study area. This is an efficient way of getting to know the general geological characteristics and features. In this study the focus was mainly on the ductile and brittle structures, and how these are related to another. It was also important to observe different rock types and varying characteristics between same types and different ones. This comprehensive data gave information about the fracture systems and the coherent or incoherent nature of the rocks.

Mapping of the area was executed by walking making careful observations. A rough mapping plan was made beforehand by using maps and map apps, such as Karttaselain, where potential outcrops were marked. In this case potential outcrops are considered as sufficiently large, well-observed and rich in structures. New observation points were created when rock type varied from the adjacent rock type or when something important was found. Each point got their own identification code, and coordinates were added to each point by using the map app. Rock types were named and described to the notebook as accurately as possible. Rock type observations included information about colors, relationship between rock types, type and direction of fractures, grain size and orientation. Each observation point was photographed by using a camera, and few samples were collected by using a hammer. It was important to photograph the placement of the rock sample and directions, that were marked to the rock by using permanent marker. From these samples, thin sections were created to reveal the petrological characteristics of the rocks. Most important part was to get the measurements from faults, folds, foliations, fractures and lineations. These measurements were done by using a geologist compass.

4.2.2 2D-modelling of the bedrock

Bedrock observations were added to a sheet in Excel. Declination was fixed to every dip direction value. This means that 11 degrees was added to every dip direction value. Description of every observation point was also added. Every photo was named by using the name of observation point and a short description was added to the name. Also, the direction of the

photograph was added. Each group of structures were added to different sheet and added to the MOVE. After coordinates were fixed, the 2D-map of bedrock was created. Also, by using orthophotos, fracture network was created by tracing fractures. Based on those fractures, 2D-fractopo (Ovaskainen 2022) analysis was used to produce XYI-ternary plots that revealed the topological properties of the fracture network. The analysis also gave information about the orientations of the fractures by producing a trace azimuth from the measurements.

4.2.3 3D-photogrammetry

Drone imaging was executed to get a coherent photogrammetric footage from the rock cuts. Based on this material, a model which allows interpreting the structural features of the bedrock efficiently after field observations, was created. Before flying, control points for georeferencing were placed in different spots around and on top of the outcrop. These control points were placed to improve the accuracy of the modeling in the program, where the footage was later applied. The program calculated depth variations from the upper surface by detecting variations between subsequent photos. Based on these photogrammetric pictures from the rock cuts and the surrounding group of outcrops, it was possible to create 2D- and 3D-photogarammetric models of the rock cuts. The aim was to map fractures from 3D-photogrammetric models (using CloudCompare software) which revealed dips and dip directions of the fractures and to create fracture systems from 2D-models, which revealed the main topological features and trends in the area.

4.2.4 Thin sections

Three thin sections, 15.1A-EMV-22, 15.1B-EMV-22 and 36.1-EMV-22, were made from two samples that were collected from the different sides of the road. Thin sections 15.1A-EMV and 15.1B-EMV were created from the sample that was collected form the southern side of the road (figure 20). The sample was taken from the fault core, where quartz-k-feldspar gneiss and granite are encountering. Thin section 36.1-EMV-22 was made from the sample that was taken from the ending part of the fault located on the northern side of the road (figure 20). Sample was located on the upper side of the fault where the distance between sample site and the core of the fault is about 2-3 meters.

These thin sections are representing two different kinds of faults. The aim was to find indicators by using polarized light microscopy, that could inform about the geological characteristics of

the faults. For example, possible shearing movement or rotated clasts can inform about kinematics and temperature conditions of the deformation events that the rock went through.

4.3 Subsurface studies used in subsurface-surface correlation

4.3.1 Studies of GTK

GTK made a report about the studies made from Ruskeasuo geothermal well during and after the drilling process. This report includes data from samples that were gathered from the drilling soy during the drilling process (GTK 2022c). These samples revealed the mineralogy of the drilled rock, and the classification of the rock was done (GTK 2022c). Before drilling process started, GTK made some bedrock observations in the surrounding area and when drilling was done, the temperature of the well was measured as a function of the depth (GTK 2022c).

GTK executed multiple different studies from the area of the geothermal well. For example, they made their own interpretation from different rock types of the area and performed multiple studies that were related to the geothermal well. Based on their observations from the seismic profile, rock type on the surface, is granite (figure 21). At the depth of about 800 meters, the rock type is mica gneiss until the depth of 1500 meters is achieved, and the rock type changes to amphibolite. The amphibolite layer is about 200 meters thick. After that, granite is being observed until amphibolite layer would be penetrated on the northern side of the borehole. The location of the amphibolite in the depths is crucial since mafic lithology typically has weaker value of thermal conductivity (GTK 2022c).

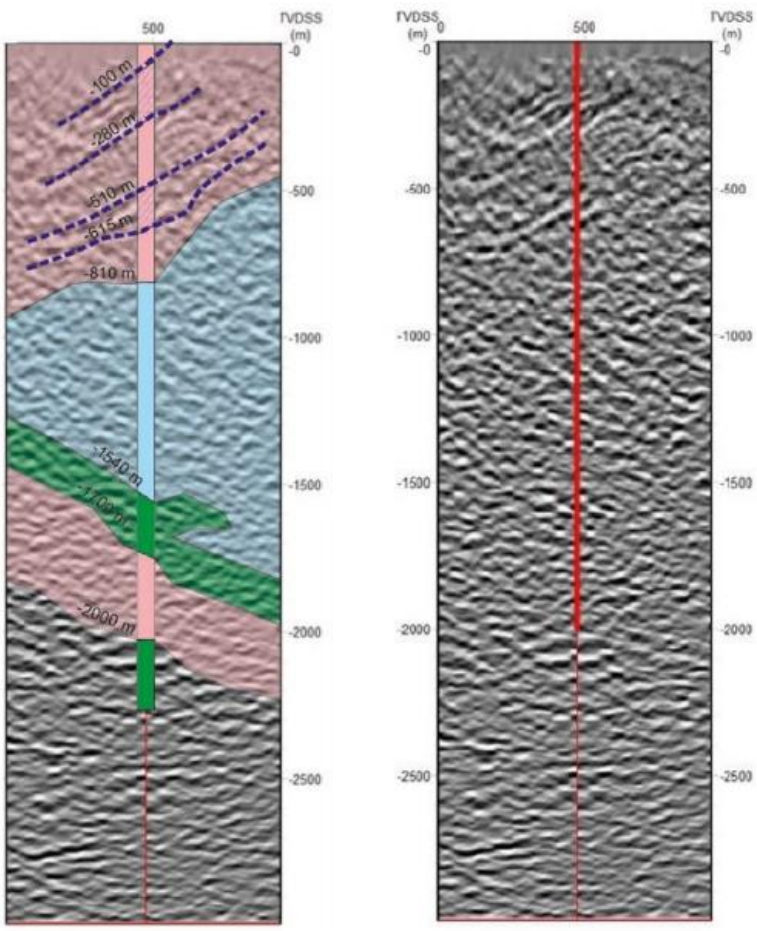

Figure 21: Geological interpretation of seismic profile. Pink is indicating granite, blue mica gneiss and the green amphibolite. The purple dashed lines are representing interpretation of weakness zones on top of the granite lithology (GTK 2022c).

During the drilling process, samples were collected between about 50 meters. The rock observations made from the samples correlated with observations made from the surface level and seismic profile, however the determination was difficult since the material was typically quite fine-grained. Rock types were granitic at the depths of 0-760. In some samples, rock type was changed to gneiss, since the samples were more greyish, and the content of biotite was greater. The variation of grain size of the samples was very extensive, and it continued throughout the depth of the well. The color of the samples was varying from red to grey showing colors that are distinctive to granites. Most typical minerals in the samples are quartz, plagioclase, and k-feldspar along other minerals such as biotite, hornblende, epidote and illite. Illite is characterized as a mineral that can be observed as filling mineral in fracture zones. Therefore, it can be considered as an indication of fracture or weakness zones.

At the depth of 800 meters, the rock type changes from granite to gneiss or mica gneiss. Based on two samples (802 and 820 meters), the color of the rock and content of minerals are

distinctly changing. The color is greyer, and larger rock fragments have visible lineation and orientation. The content of biotite and muscovite along with plagioclase is higher in these rocks.

Petrographic studies were done from three samples that were collected from the depths of 65 meters, 155 meters and 235 meters. These studies indicated that the most typical minerals in all the samples. These minerals are quartz, plagioclase, and feldspar, which are indicating the origin of granitic material. Typical accessory minerals are hornblende, biotite, tourmaline, and epidote. The measured temperature curve did not indicate any abnormalities (figure 21). However, in the end of the curve, at the depth of about 800 meters, the temperature curve deflects, which may be indication of intense fracturing which causes water flow and transport of the heat.

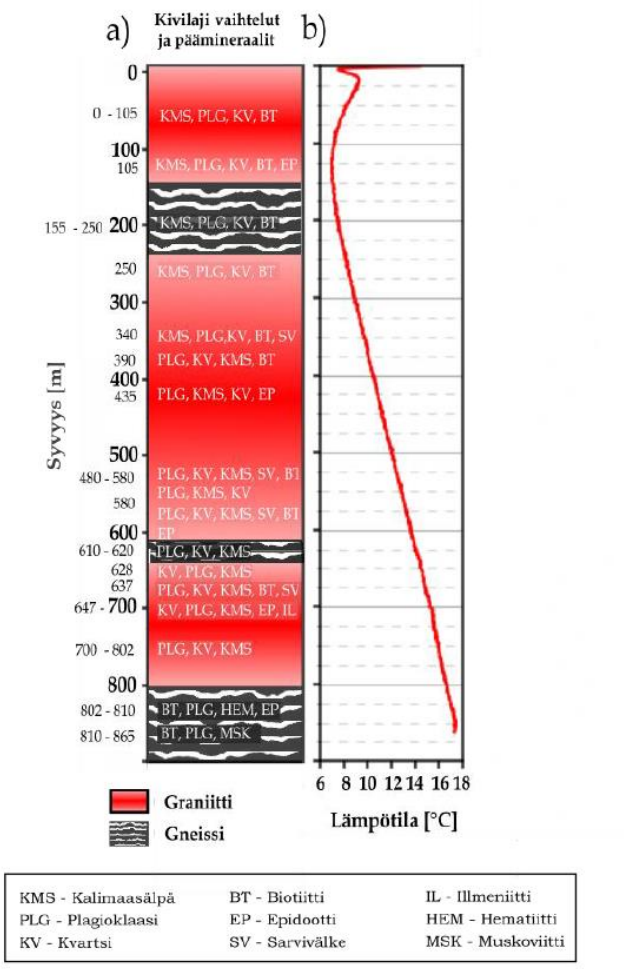

Figure 22: The petrology of the well and the temperature measured from it. Color red is representing granite and variation of black and white is representing gneiss (GTK 2022c).

4.3.2 Geophysical measurements

Geophysical measurements were done by Astrock (2022), when the borehole was 650 meters deep. These measurements included Sonic, OBI (optical) and ABI (acoustic) imaging, slope measurements, magnetic susceptibility, gamma-gamma density, and gamma spectrometry. Optical imaging the first method used in the borehole (Astrock 2022). Before this procedure, the borehole was rinsed well to clear the water (Astrock 2022). Measurements had a tight time limit which meant that only the end part of the borehole was measured (Astrock 2022). Slope measurement equipment enabled trying out ABI measurements, which were executed with normal resolution of about 25 meters and after that, resolution was reduced to maximize the speed of measurement (Astrock 2022).

By optical imaging, some video material was collected from the borehole. Based on the screenshots, it is possible to say that the water in the hole is not clear from the very start of the water interface (figure 23 right). This turbid character of the water appeared during the whole measurement, which was only extended to the depth of about 134 meters (figure 24). The lightning properties of the borehole were sufficient to film footage from the borehole. Because of this, some small fractures were observed (figure 25). Even though the unclear water was disturbing the imaging, some interpretation was done from the OBI material (figure 26).

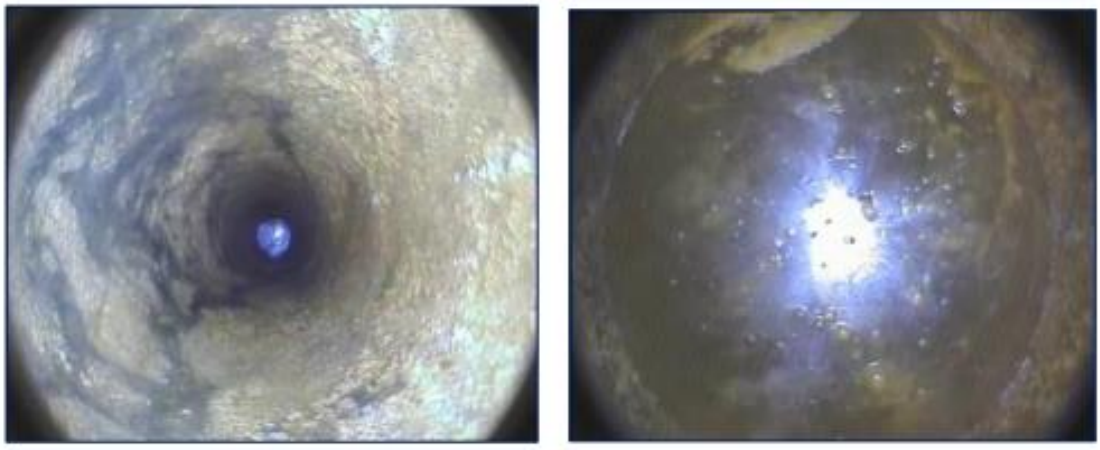

Figure 23: Screenshots from the hole video, where the hole is dryer. The water interface is visible in the right screenshot (Astrock 2022).

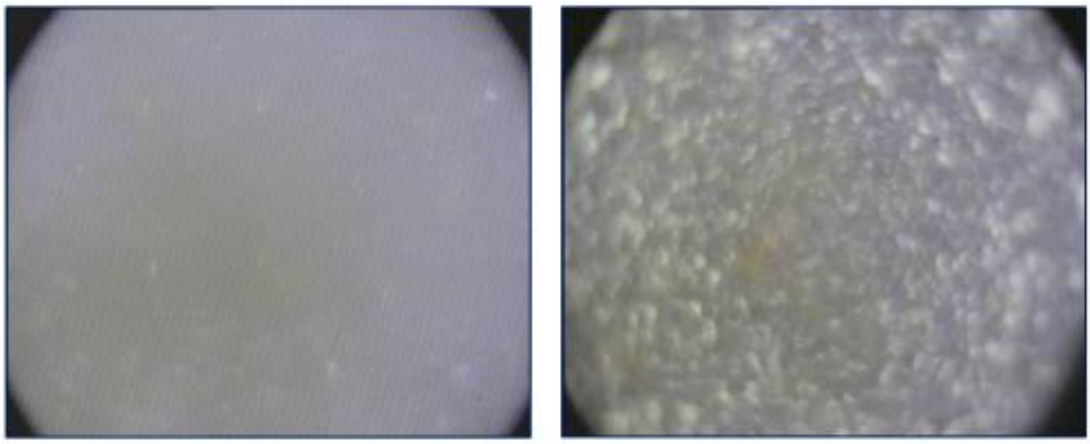

Figure 24: Screenshots from close to the water interface (left) and at the depth of about 134 meters, where it is possible to see that the water inside the hole is very blurry (Astrock 2022).

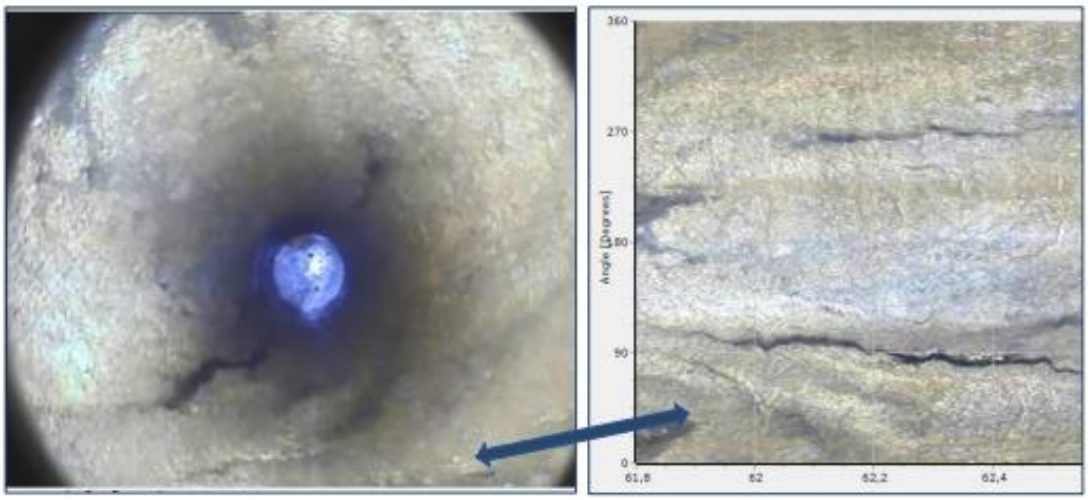

Figure 25: Screenshots from the video where fracture is showing in the lower part of the image (Astrock 2022).

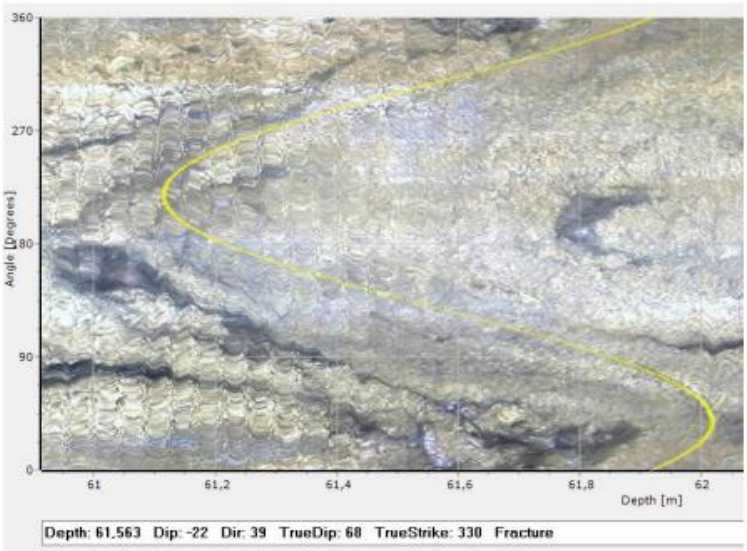

Figure 26: An example interpretation made on top of the OBI-picture (Astrock 2022).

Acousting imaging (ABI) and slope measurements did not produce any reasonable results, which may be due the size of the hole and the rough surface of the wall (figure 27). Based on slope measurements, it is possible to say that at the ending part of the hole (560-600 meters), the declination of the hole is closer to the 88 degrees (figure 28).

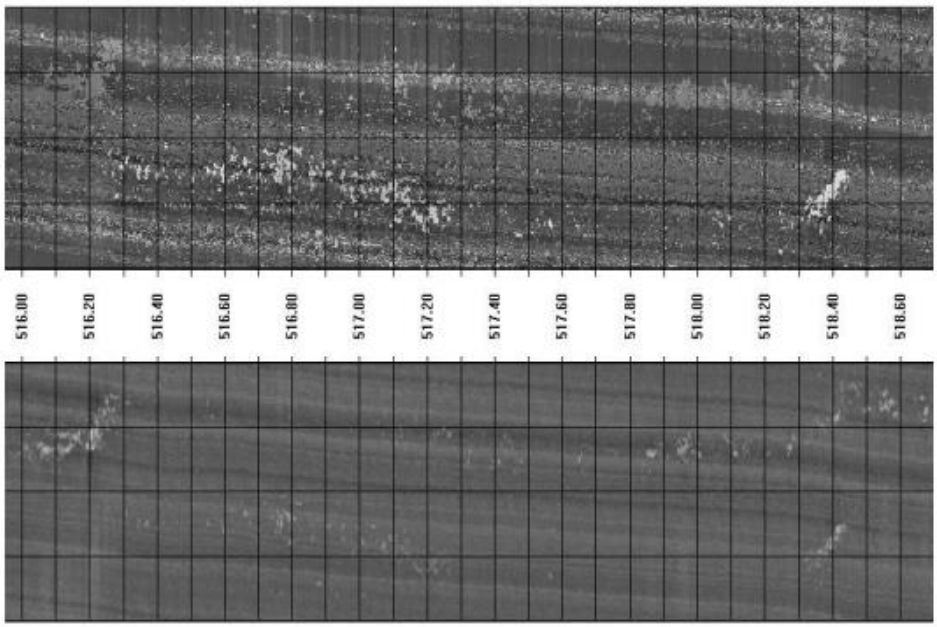

Figure 27: Failed example of the ABI results. Travel time of ABI (upper part) and the amplitude in relation to the depth of the hole (lower part) with resolution of 288 pixels. The depth values are incorrect due to problems travel correlation. (Astrock 2022).

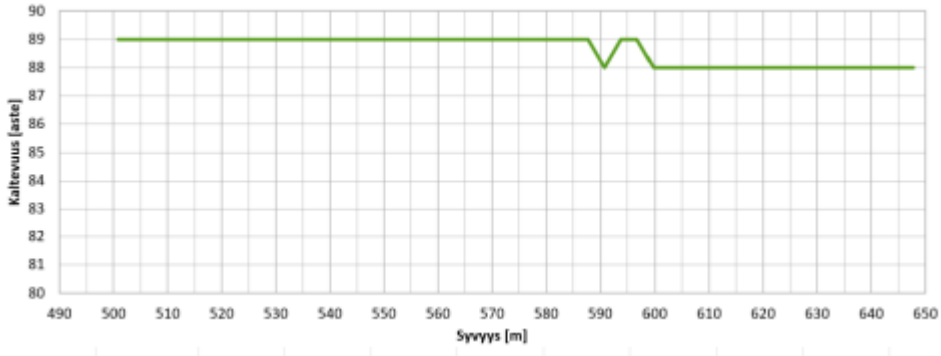

Figure 28: Inclination measurements where minor deviation of the hole is observed in its ending part (Astrock 2022).

Gammaspectrometry was measured in the hole with small hole size calibration (figure 29). Measurement included potassium (top), uranium, thorium, total radiation, and magnetic susceptibility (bottom). Measurements of magnetic susceptibility (figure 30) were also used as a calibration method that was not made for a bigger hole.

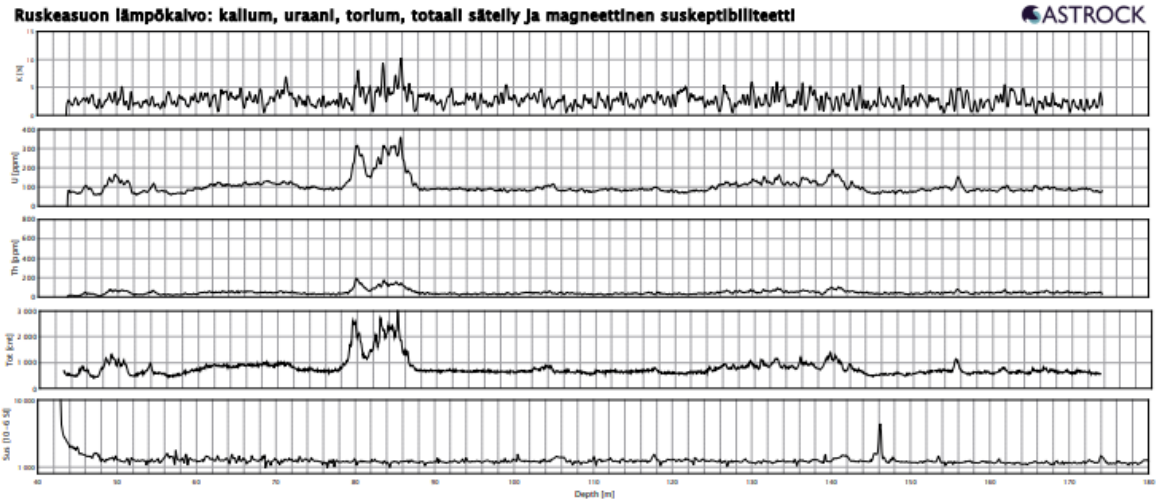

Figure 29: Results from gammaspectrometry (Astrock 2022).

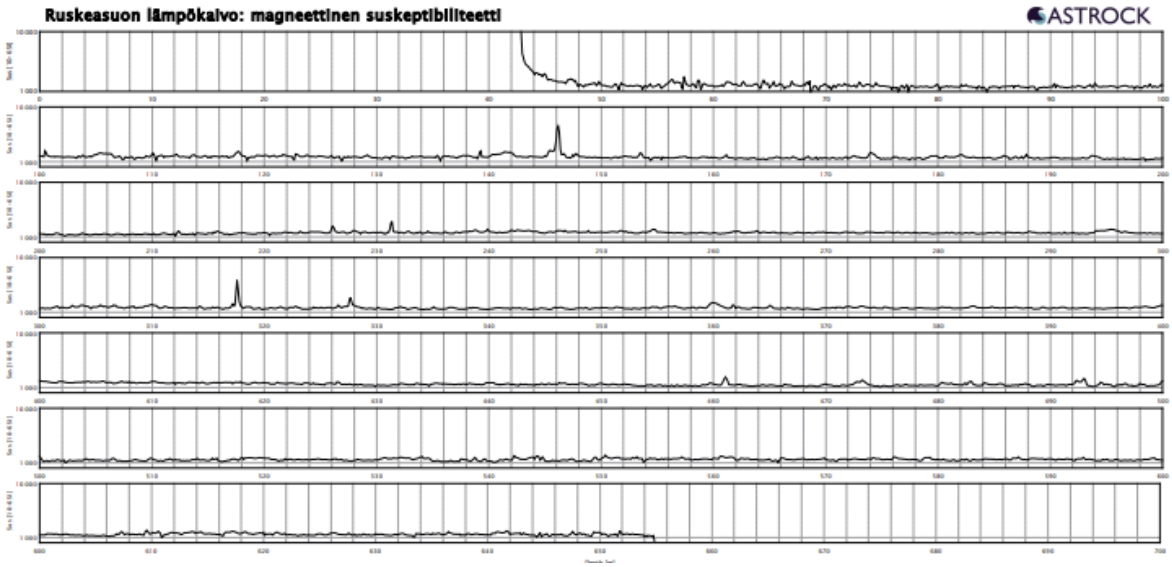

Figure 30: Magnetic susceptibility from the borehole (Astrock 2022).

4.3.3 Distributed Temperature Sensing (DTS), temperature probing and pumping test

DTS-measurements were executed by GTK by using optical fibre method, which is based on scattering of the optical rays of light in optical fibre (GTK 2022a). This method allows measurements to be done throughout the whole depth of the well, and the space between the measurements can be extended to 25 centimeters (GTK 2022a). Scattered photons are returning to the DTS-measurement device, which calculates temperatures to each depth (GTK 2022a). DTS-measurements were calibrated by using ice-water mixture as a reference temperature (GTK 2022a). Optical fibre cable was attached to the well in 14.6.2022, and measurements were started on the following day (GTK 2022a). The depth of the borehole was assumed to be

865 meters, which had casing that reached to the depth of 642 meters (GTK 2022). The cable was not set down all the way to the bottom of the borehole since there was a risk that it would get stuck to the possible drilling soy (GTK 2022a). The pumping test was done on 16.6.2022 by pumping water to the borehole and by observing temperatures (GTK 2022a).

Based on temperature profile created from temperature measurements it is possible to say that the surface of the ground water was -22.60 meters from the top of the borehole (figure 31). On the top part of the groundwater surface there is negative anomaly which is related to the seasonal changes and the air temperature of the well is also observed before the groundwater surface (GTK 2022a). Groundwater temperature was about 9,3 ºC degrees in the depth of 23 meters.

It possible to observe few distinct temperature changes from the temperature profile. The first smaller change can be observed in the depth of about 350 meters. The value remains same in few tens of meters. The other change, relatively larger one, is observed in the 630 meters which lasts to the end of the well. The changes in temperature are varying between positive and negative. These changes are most likely related to the climate change, which is has been intensified by human actions, although streaming of the groundwater on the shear zones of upper bedrock may also amplify the change in temperature (GTK 2022a). These changes may also be caused due varying thermal conductivity of different rock types (GTK 2022a). After the depth of 220 meters is achieved, temperature is rising according to the geothermal gradient. This indicates that the temperature increases 15,9 Cº/km on average (GTK 2022a). Last 500 meters of the temperature measurements include small anomalies compared to the temperature gradient (figure 32). Between depths of 640 and 730 meters, the temperature change, compared to the temperature gradient, is positive whereas between 750 and 860 meters, it is negative. This can be caused by the flowing groundwater or the differences of the thermal conductivity of different rock types. The temperature is 17,4 ºC degrees on the bottom of the borehole.

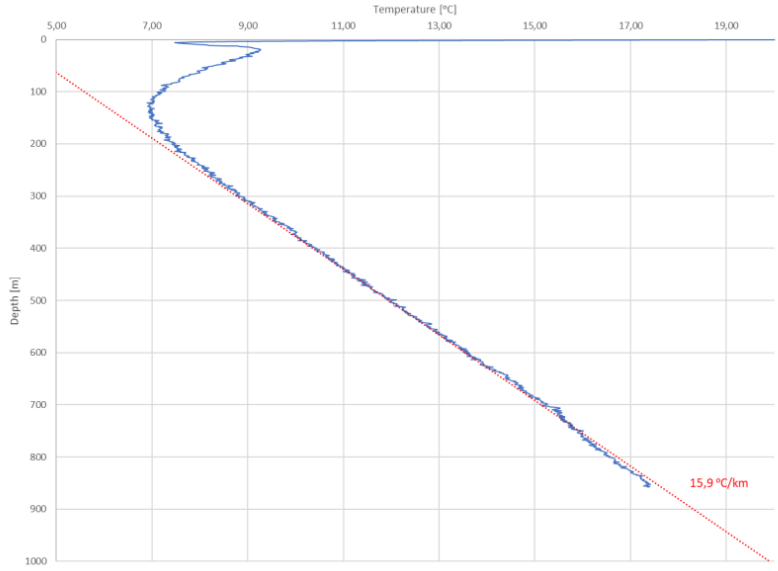

Figure 31: Temperature profile based on the DTS-measurement marked with blue and temperature gradient (°C) with respect to depth (m) of the well (GTK 2022a).

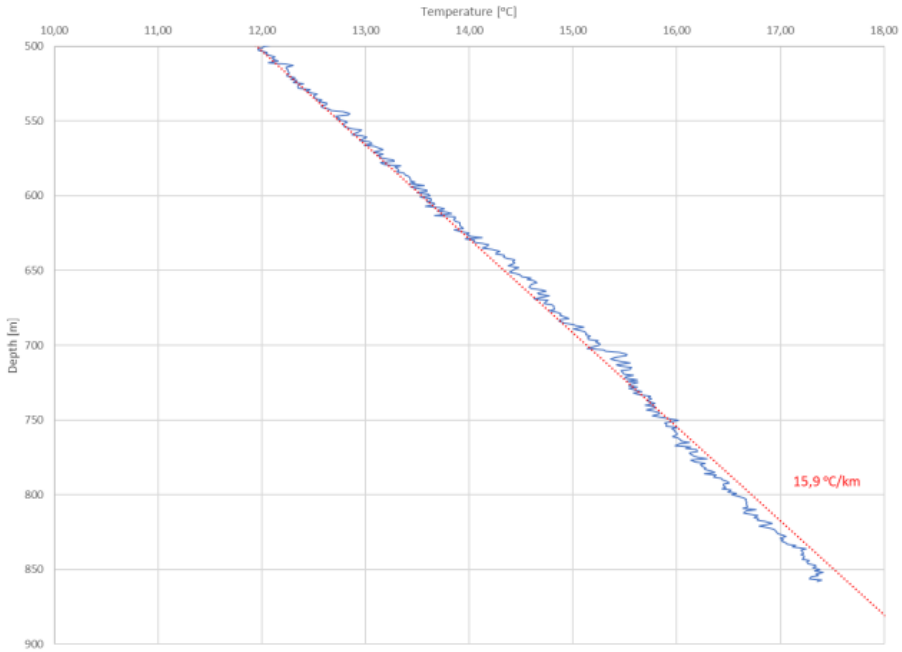

Figure 32: Last 500 meters of temperature measurements compared to the straight temperature gradient (marked with red) (GTK 2022a).

Pumping test was executed by inserting four litres of water to the well per minute for one hour (figure 33). Changes in temperatures were observed by measurement spaces of 2 minutes. It is possible to say that the pumping test did not cause any significant changes to temperature gradient.

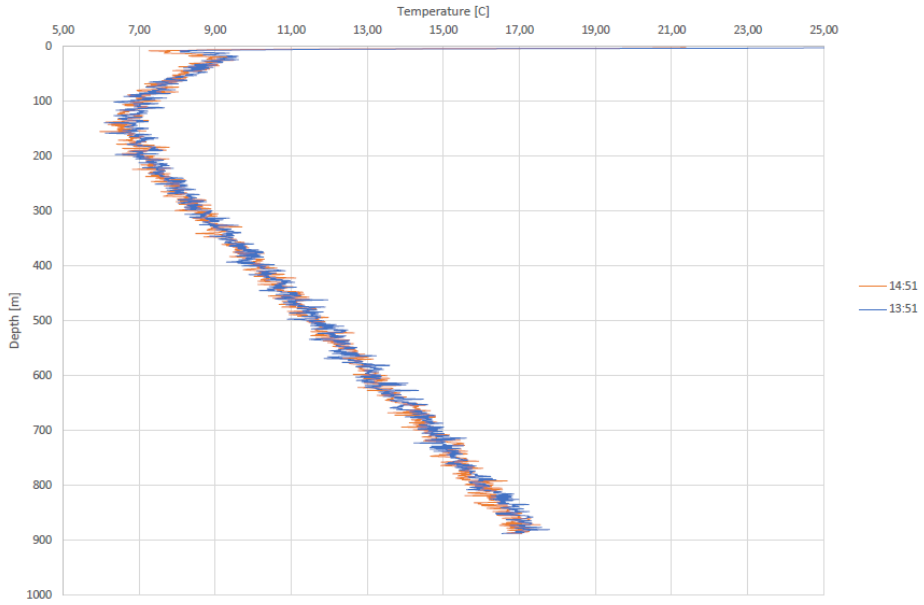

Figure 33: Results of the pumping test where 4 l of water in a minute was pumped to the borehole during one hour (GTK 2022a).

The water conductivity was calculated from values of pumping test, where water was pumped from the well with output of 67 l/s. At the same time, the drop of the water level was measured. A test, where the well was filled with water and recovery of the water was measured, was executed at the same time. This test was repeated later for more reliable results. Calculated water conductivity values are equivalent to the values of fine sand, which means that the water conductivity is weak. By using the water pumping pressure below 1 l/s, the flow of the shear was not effective enough to be evident in the DTS-data. The pumping pressure should be at least 2,5 l/s. The calculations are including uncertainties for example related to the thickness of the groundwater.

4.3.4 Reflection seismic data

In Helsinki city area, data acquisition is relatively difficult since typical factors of urban environment such as power, accessibility, survey design and high noise level, need to be taken into a consideration (Cyz et al. 2022). Despite of all the difficulties related to acquiring of reflection seismic data, 2D/semi-3D seismic data was collected in the Helsinki Central Park in 2019 (Cyz et al. 2022). The measuring line extended from south towards the north, with total length of about 10 kilometers (GTK 2022b). The line crosses the area of Ruskeasuo. This data was gathered to find out structures that may cause risks to the building of the geothermal wells (GTK 2022b). In this case the risks were related to the construction and execution of the wells

and to the economical aspect of the project (GTK 2022b). Structures can also be affecting to productivity of energy and to the efficiency of the geothermal wells (GTK 2022b).

Data was collected by using Vibroseis sources along with wireless acquisition system which included 750 channels (Cyz et al. 2022). The Vibroseis sources included two 9,5 t INOVA UniVibe trucks (Cyz 2022). Main part of the acquisition a profile that was approximately 5 kilometers long (figure 34) (Cyz et al. 2022). This profile had receivers with spacing of 10 meters and two perpendicular lines that were shorter and had a receiver spacing of 20 meters (Cyz et al. 2022). Multiple different approaches were tested to process seismic data (Cyz et al. 2022). Ultimately, the data was processed by using 3D-manner and pre-stack depth migration (PSDM), which used velocity model that was created based on the first-arrival tomography (Cyz et al. 2022). This reflection seismic data of Central Park was processed in 2019-2022 by using program called Globe Claritas whereas visualization and interpretation was done by using GoCAD 3D-modelling program (GTK 2022b). Created seismic profiles were showing reflects, which were interpreted as structures of the bedrock which appear in different depths (GTK 2022b).

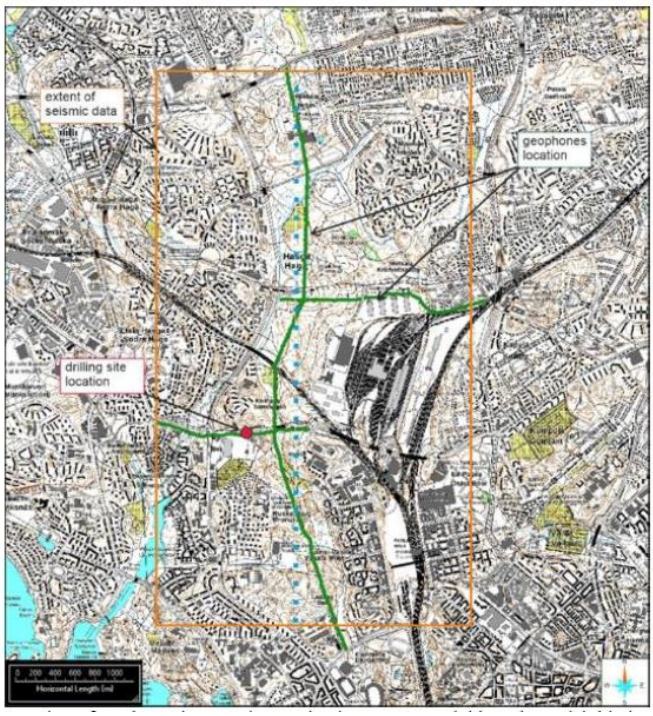

Figure 34: Helsinki city map with the extent Keskuspuisto semi-3D seismic survey. An orange rectangle represents the extent of the seismic data, the green lines are marking the locations of the geophones and the red dot represent the drilling site of the geothermal well. (Cyz et al. 2022).

The main reflection seismic line extends from north (Pirkkola) to south (Laakso, figure 35). It also includes two E-W directed traverse lines. Most of the data has been recorded in the

middle part of the measuring line since vibrating points are lacking on the ends (GTK 2022b). Quality of the data is increasing when same reflection point is detected underground multiple times in different source-receiver distances (GTK 2022b). Therefore, signal from reflecting structure is increasing while disturbances are decreasing (GTK 2022b). Limited amount of data may affect to the reliability of the results in the ends of measuring line (GTK 2022b).

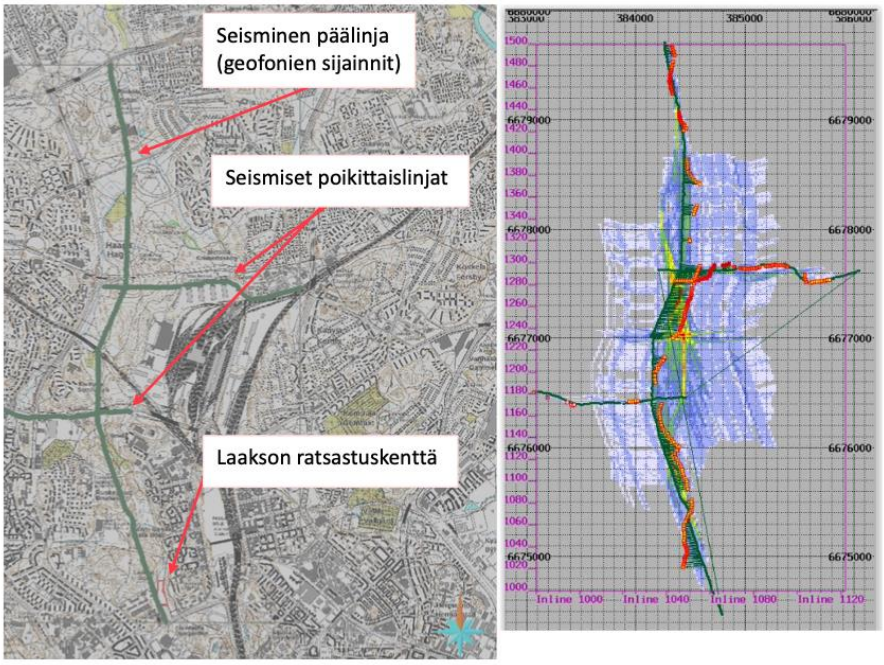

Figure 35: Seismic mainline (N-S), seismic traverse lines (E-W) and riding field of Laakso (lowest arrow) (left) and distribution of theoretical reflection points in seismic data. Geophones are marked in green points and red squares are vibrating points (right) (GTK 2022b).

Based on characteristics of reflections and changes in it, it is possible to see that towards north from riding field of Laakso, two E-W directed structures extend close to the surface (figure 36). These were also discovered during field observations (figure 37). At the surface level structures of the bedrock are correlating with topographical depression which indicates that those can be assumed to be some sort of weakness zones in the bedrock.

Beneath the study area one larger structure was observed in the depth of about one kilometer, which possibly reaches surface in the southern side of the study area (figure 36). This feature will probably be punctured during well drilling, since changes in reflection may be caused by rock contacts that have different physical features compared to each other or some sort of a damage zone (GTK 2022b). Based on seismic studies, all the observed structures are dipping in S-W direction more gently than field observations and local structures are indicating.

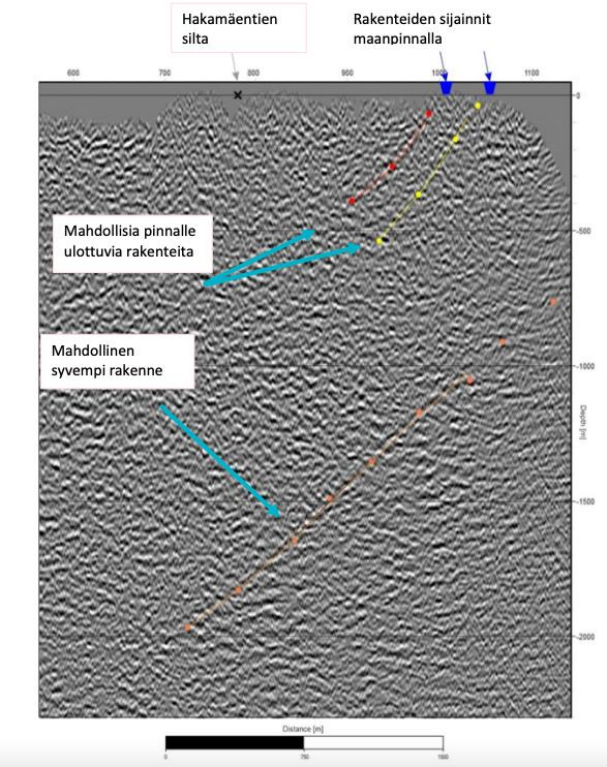

Figure 36: Characteristics of reflections and changes in it observed from reflection seismic probing line. Red and yellow lines are representing some structures that are possibly extending to the surface level. The orange line is representing some sort of possible deeper structure (GTK 2022b).

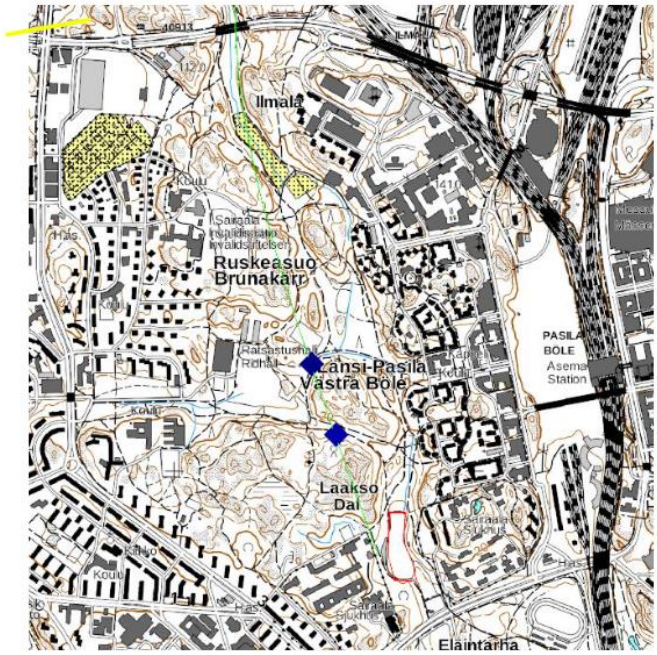

Figure 37: Locations of structures that are extending to the surface level that are presented on figure 36 (GTK 2022b.

Depth-migrated 3D-seismic volume measures geometrical attributes, highlight faults and gains stratigraphic recognition, which is related for instance to semblance, curvature, dip and azimuth and to detect possible faults based on similarity (Cyz et al. 2022). Attributes used

alone are not giving reliable and reasonable results therefore those should be combined. However, some attributes such as fault likelihood can possibly display steeply dipping structures such as faults (Cyz et al. 2022). Seismic attributes used in this study pointed the fault which is located near the drilled well (Cyz et al. 2022).

5. Results

5.1 Bedrock mapping and 2D- and 3D-visualization study area

The dominant rock type in the area is quartz-k-feldspar gneiss, which has some migmatizing or intrusive granitic and pegmatitic parts (figure 38). The area also has gneisses, mica gneisses, and minor occurrences of darker supracrustal rocks that are aligned along ductile foliation (figure 38). The foliation is subvertical in the area. Ductile foliation is defining open asymmetrical s-shaped folds, that have steeply east-plunging statistical fold axes. Structural geological features such as fractures and folds can be observed both on northern and southern sides of the road (figure 38).

The most interesting part of the study area are the faults, that can be also observed in both sides of the road. On the northern side, there is about 170-200 m wide, E-W directed rock cut, which has a fault in the middle part of it. The core of the fault is well observed (figure 38). The other fault is located on the southern side of the road (figure 38).

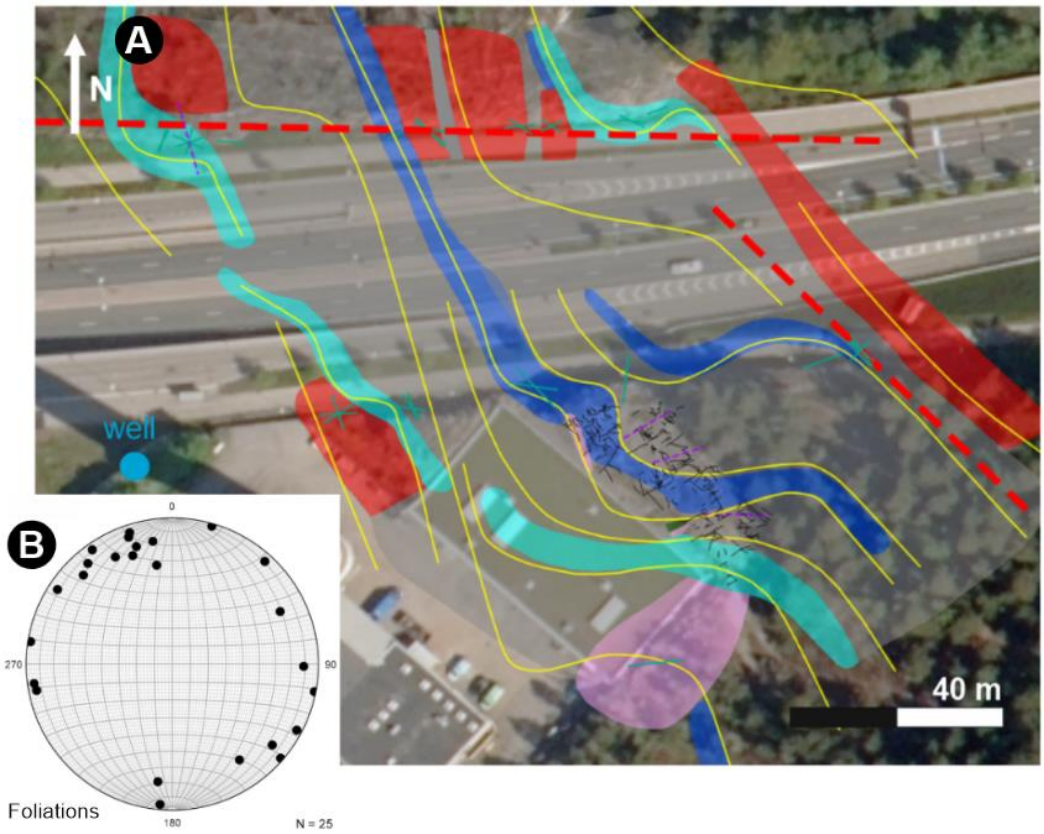

Figure 38: Bedrock map from the study area which includes the main rock types: quartz-k-feldspar-gneiss (grey), granite (red), pegmatite (pink), dark surface rock (dark green), gneiss (light blue) and mica gneiss (dark blue). Tracelines of subvertical foliation of the area is marked with yellow lines, and it is based on 25 measurements which poles are also shown in the stereogram in left. Locations of fracture measurements are marked with light green lines and fold measurements with purple dashed lines. Faults are marked with large red dashed lines and the location of the well is marked with blue dot.

5.2 Lithology

The most typical rock type of the area is quartz-k-feldspar-gneiss (figure 39). It typically appears to the fine-grained or equigranular. The color of this rock type varies from lighter gray to darker gray. It typically has some mixing with mica gneiss and granite especially on northern side of the road. The granite in the area is medium-grained and equigranular (figure 39). The color of the granite is grayish on southern side of the road, whereas on the northern side, the color is more reddish. The granite is typically occurring as migmatizing or intruding veins along the foliation surfaces of other rock types such as gneiss. The granite is also cutting the main lithology of quartz-k-feldspar-gneiss. Granite also contains quite large quartz-k-feldspar phenocrysts of quartz and k-feldspar. The color of pegmatite in the area varies from lighter pink to more pinkish (figure 39). It is typically observed as veins between other lithologies. Pegmatite is mainly observed on the southern side of the street. Gneisses of

the area are without exception quite stripy and show some orientation (figure 39). Gneisses are relatively light in color. The mica gneiss has always a contact with quarts-k-feldspar-gneiss, which makes these two rock types to appear mixed. Mica gneiss has also some leucosomes and can be oriented.

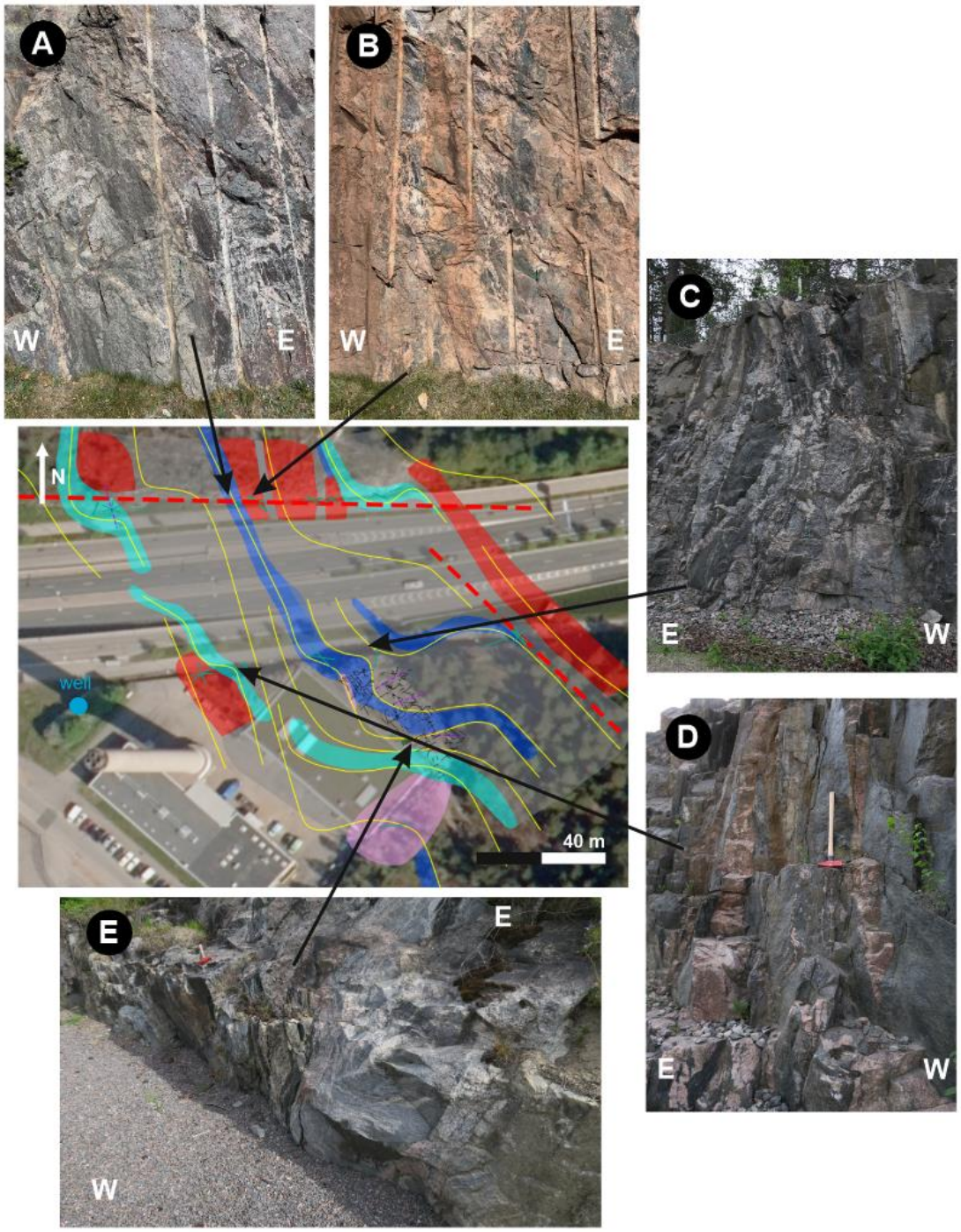

Figure 39: Photographs and locations of the rock types of the study area. A) mica gneiss that has strong foliation, B) granite with mica schist veins and quartz-k-feldspar-gneiss phorphyroblasts, C) quartz-k-feldspar-gneiss that has boudinage and broken parts, local anomaly in dominant direction, D) gneiss, that has migmatite/granite veins directed along the foliation and E) pegmatite vein on the right with dark surface rock in the middle and mica gneiss on the northern side.

5.3 Folds

A few folds are observed in the study area (figure 40). Folding is more typical in northern side rock cut, on the western part of it, where the gneissic/ quartz-k-feldspar-gneissic parts are bent (figure 40A). Some sort of folding/bending is also observed on the top of the northern side rock cut in gneissic granite (figure 40B). On the large rock cut are on eastern side of the geothermal well, there are a few small folds observed (figure 40C and D).

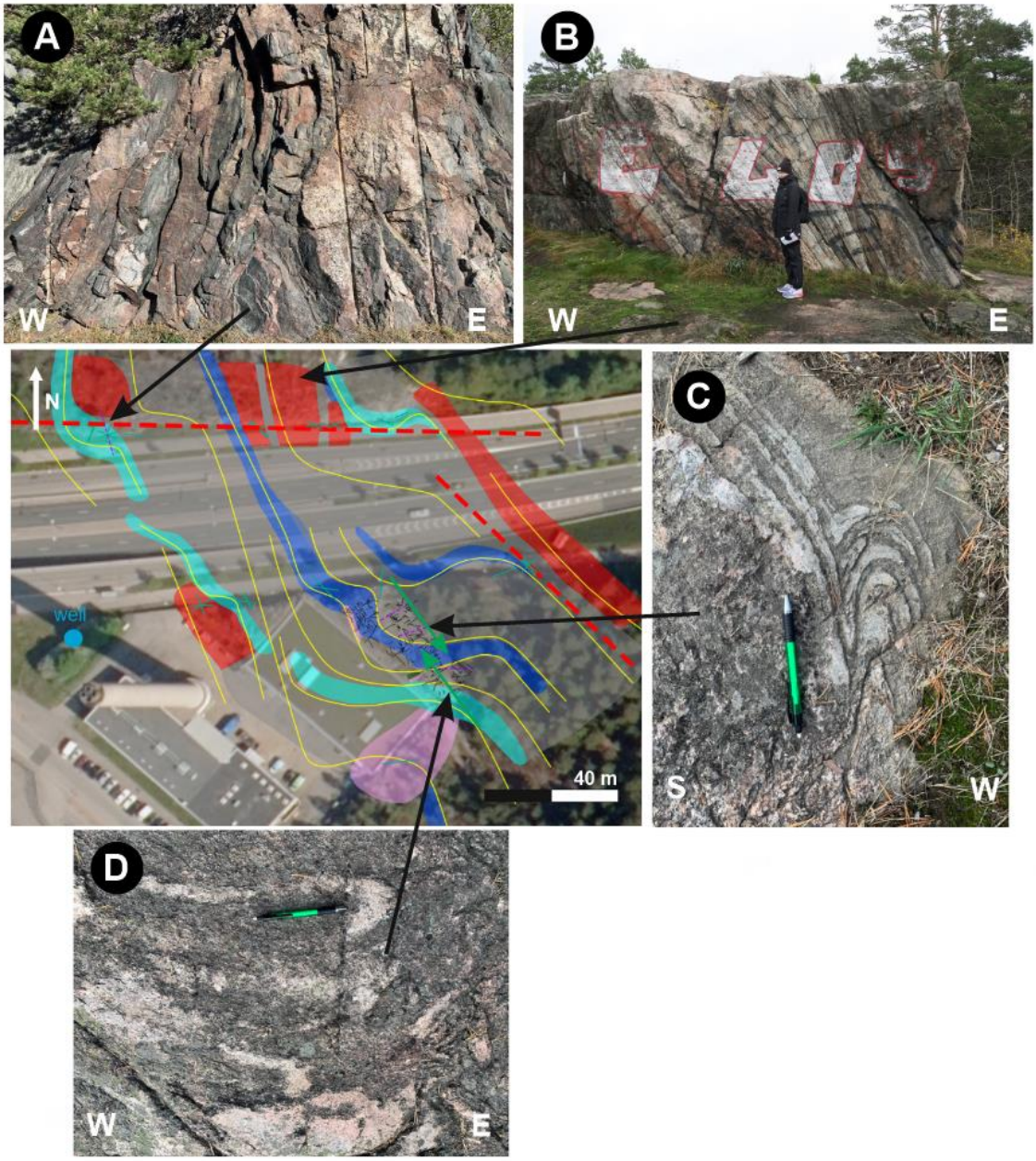

Figure 40: Photographs and locations of the folds of the area. A) Overview of folded gneiss with axel surface measurements of 258/88, B) Folded/bended gneissic granite with measurements of 001/88, C) and D) Small folds on the eastern side of the geothermal well (orientation marked with green arrows) where measurements are 162/88 (C) and 329/82 (D).

5.4 Faults

There are two faults that can be observed in the study area. On the northern side of the road there is E-W trending, about 100 meters wide rock cut, where E-W directed fault is observed in its central part. The dip of the fault wall is about 85° and the dip direction about 176°. The core of the 22 cm and the fault has an approximately 190 cm wide damage zone on the southern side (figure 41), while extent of the northern damage zone is difficult to constrain. It is possible to say that the core of the fault is severely damaged (figure 42A and B). The host rock of the fault is homogeneous quartz-feldspar-gneiss which has granitic intrusive parts. The rock type on the footwall (N-side) of the fault is more granitic or mylonitic which has granitic origin (figure 42C). The fault wall has some strong horizontal lineation which indicates some sinistral strike-slip character (figure 42D). The indication of sinistral movement is presented more in detail in 2D-view the chapter 5.5.1 (figure 49). On the southern side of the street there is this relatively small SE-NE directed fault that dips about 77° towards 219° (figure 42E). The host rock of the fault consists of quartz-k-feldspar-gneiss and granite. The core of the fault is about 6 centimeters, and the damage zone is about 45 centimeters wide. The fault has slickenslide with direction of 022/83° on the western side and some wing cracks on the eastern side of the fault core.

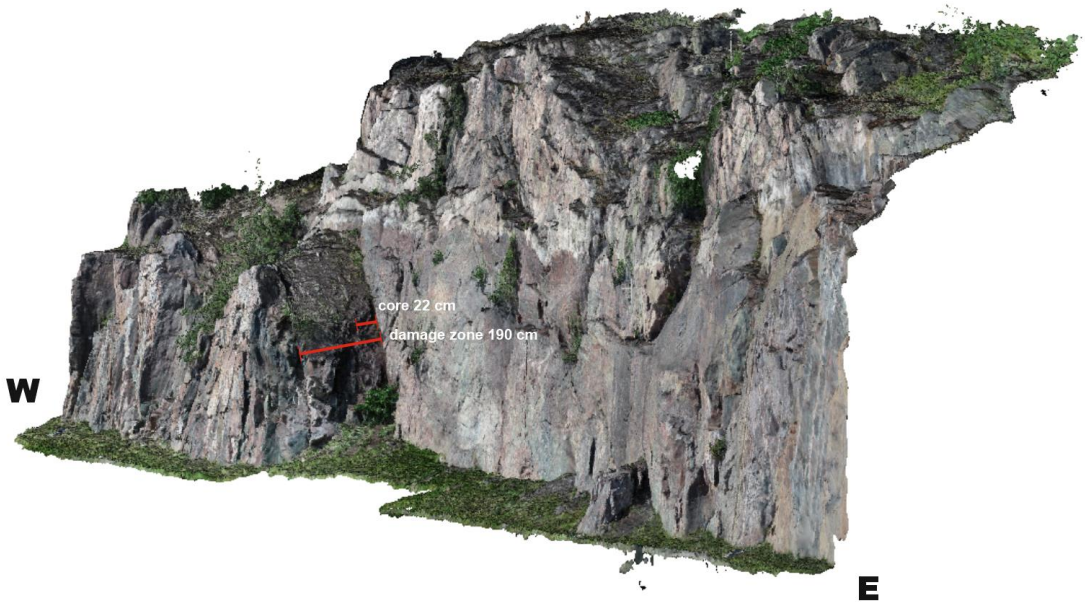

Figure 41: The fault core from the side view. The core of the fault is about 22 centimeters wide and the damage zone is about 190 centimeters wide.

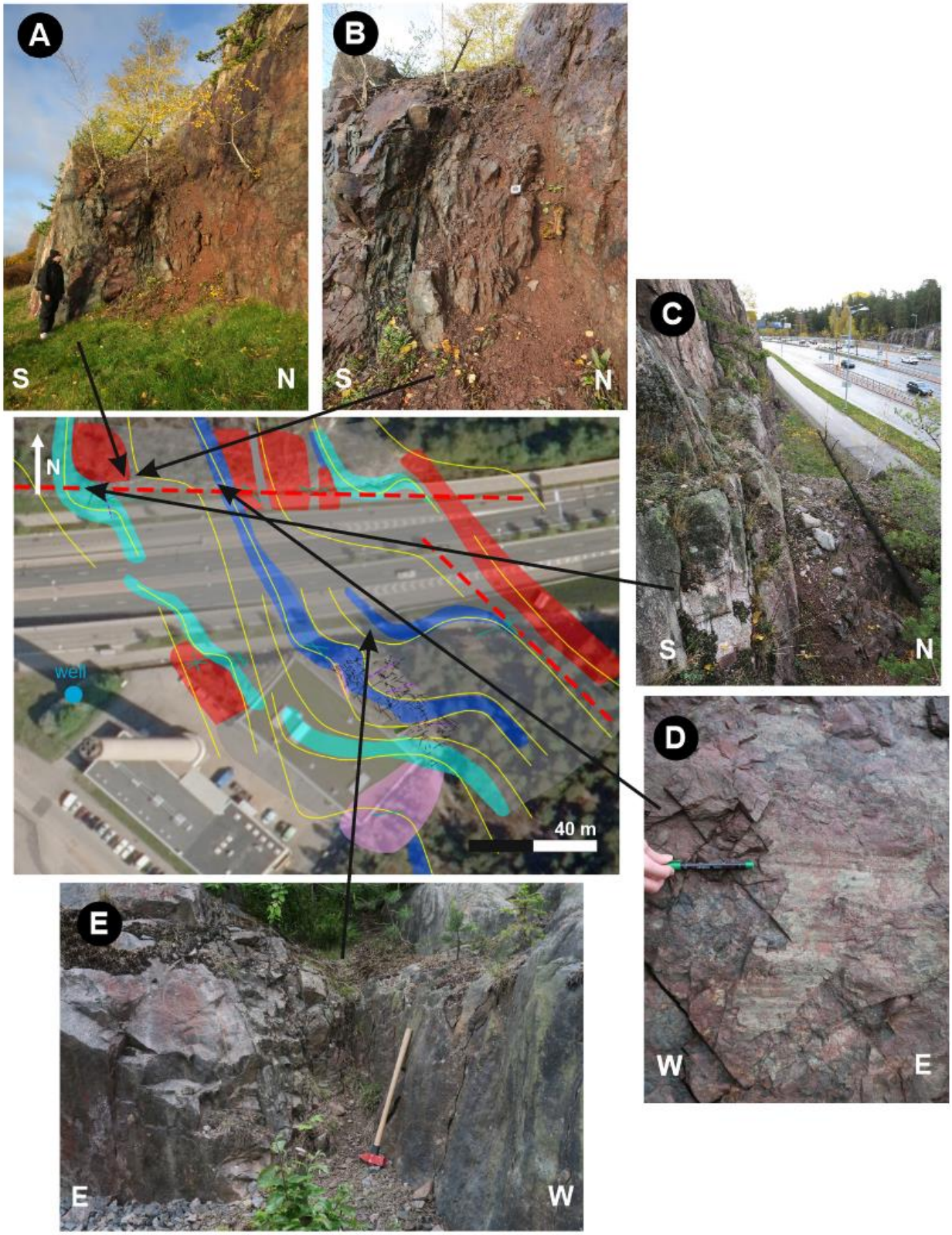

Figure 42: Photographs and locations of the two faults of the area. A) Overall picture of the core of the fault, B) Destroyed fault core with loose material, C) Upper side view from 1-2 meters from the fault core D) Strong horizontal lineation on the middle part of the northern side fault wall and E) core of the southern side SE-NE trending fault core.

5.5 Fractures

Fracturing can be observed in the study area in all the bedrock outcrops and different rock types. At first, all the material and orientation distribution of fractures is presented by photographs and stereogram in figure 43. Afterwards the fractures are divided into direction sets and the relationship between fractures, lithology and ductile fractures is displayed. Overall, the fracturing is better observed in the southern side of the road since the rocks have not been faulted (figure 43 and 44B). Fractures are not that well observed in the rock cuts located in the northern side of the street since large part of the outcrop has been faulting. Although, the N-side rock cut contains still a lot of fractures which can mainly be observed on top of the outcrop and mapped from the photogrammetric models (figure 49 and appendixes 2 and 3).

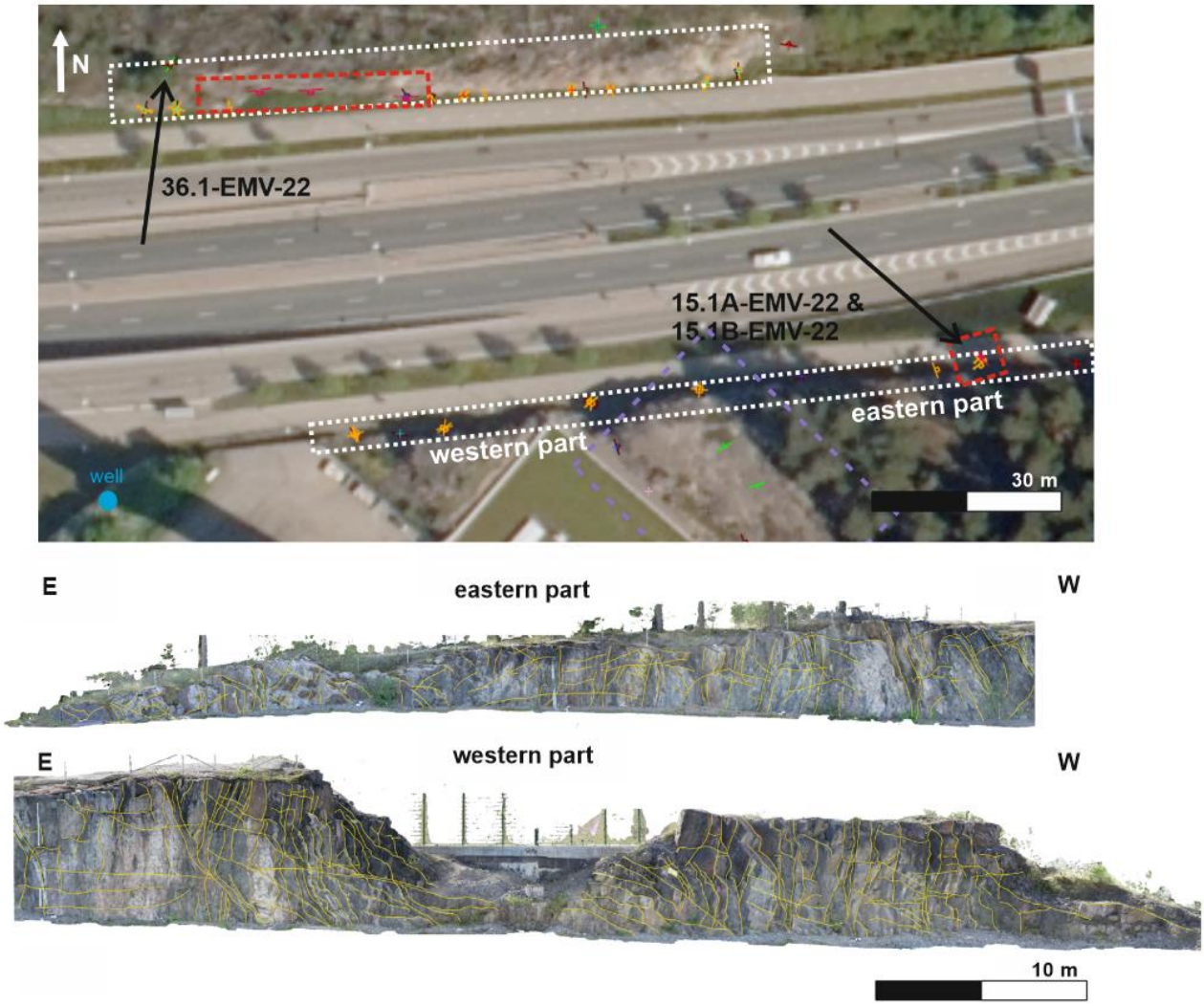

Figure 43: Fracture network of the rock cut located on the southern side of the road.

The fractures of the area can be divided into ones that are following the ductile foliation and to ones that have fractures that have gently dips, dominantly towards orientations between 050-100º (figure 44). Especially quartz-k-feldspar-gneiss (figure 44E) granite (figure 44C) and pegmatite (figure 44D) have strong and dense fracturing that are typically directed along the dominant foliation of the area. The fracturing of the mica gneiss and gneiss (figure 44A) is not that apparent since the rock type is not that dominant in the area.

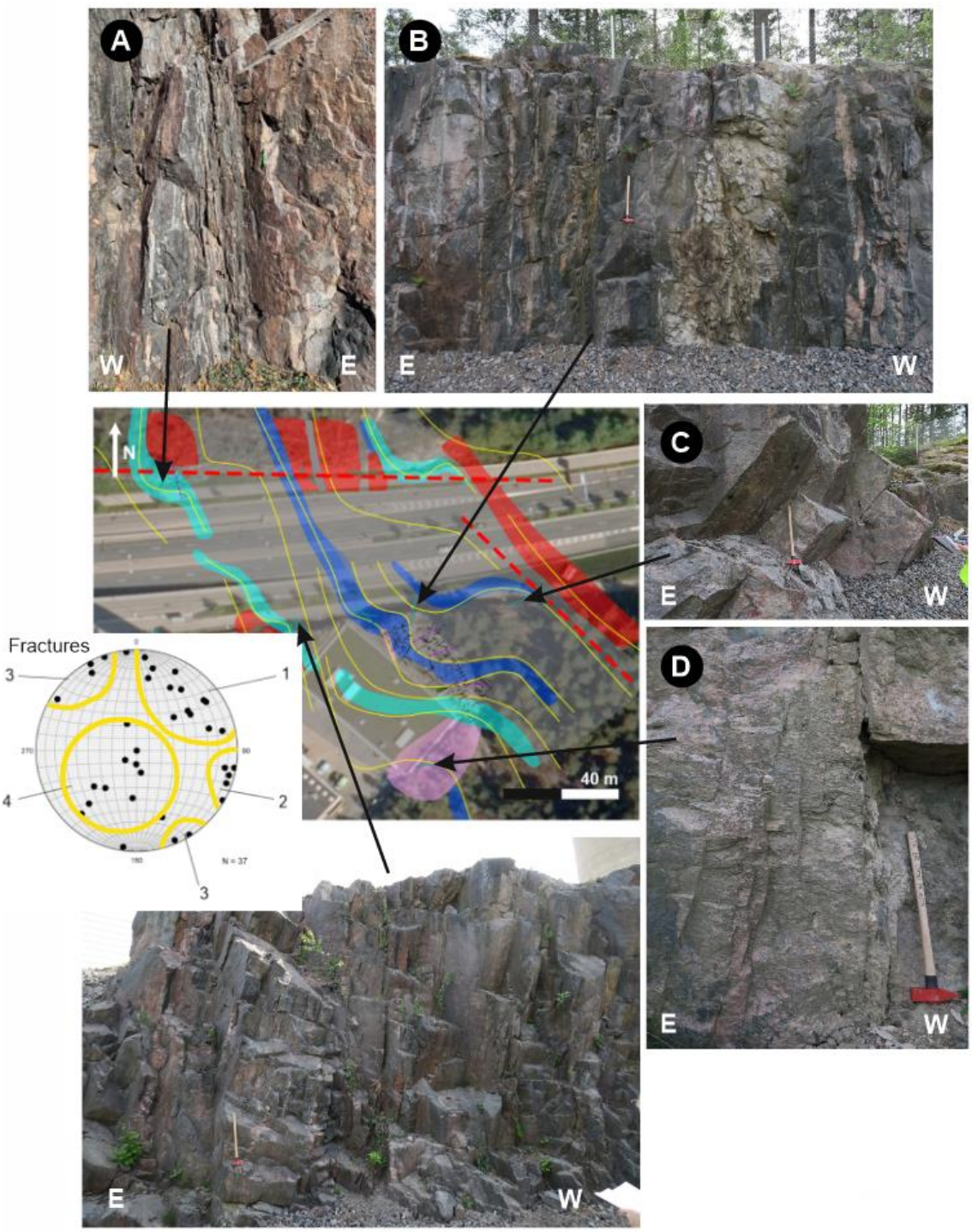

Figure 44: Capture overleaf.

Figure 44: Photographs and locations of the example fractures with a stereogram where the fractures can be divided in to ones that are following the ductile foliation (clusters 1-3), and the to the one that has fractures with dominantly 50-10° gently dipping orientations (cluster 4). A) Vertical fracturing on gneiss that has strong striping and thin pegmatite veins, B) Overview of gently sloping fractures of multiple rock types, C) Planar and continuous fractures in granite, where the direction of the fractures and foliation is parallel, D) Set of parallel vertical fractures in the pegmatite and E) Overview of fracturing of quartz-k-feldspar-gneiss.

5.5.1 2D-fracture network

On the eastern side of the drilled geothermal well, a wide bedrock outcrop area shows multiple fractures (figure 45A). These fractures are forming a network which consists mainly of an orthogonal patter of NE-SW and NW-SE trending fractures (figure 45B). It also includes fractures that have more mixed arrangement. The total amount of traced fractures was 635. Based on XYI-ternary plot (Ovaskainen 2022), it is possible to see that these fractures are dominated by I-nodes (497 fractures; figure 45C). I-nodes are forming, when fractures are totally ending on and are not connected to any other fractures (figure 45). The amount of X-nodes in fractures is 46, and the amount of Y-nodes is 92. X-nodes are forming between fractures that are crossing each other and Y-nodes forming when fracture is connected to other fracture from only one end (figure 46).

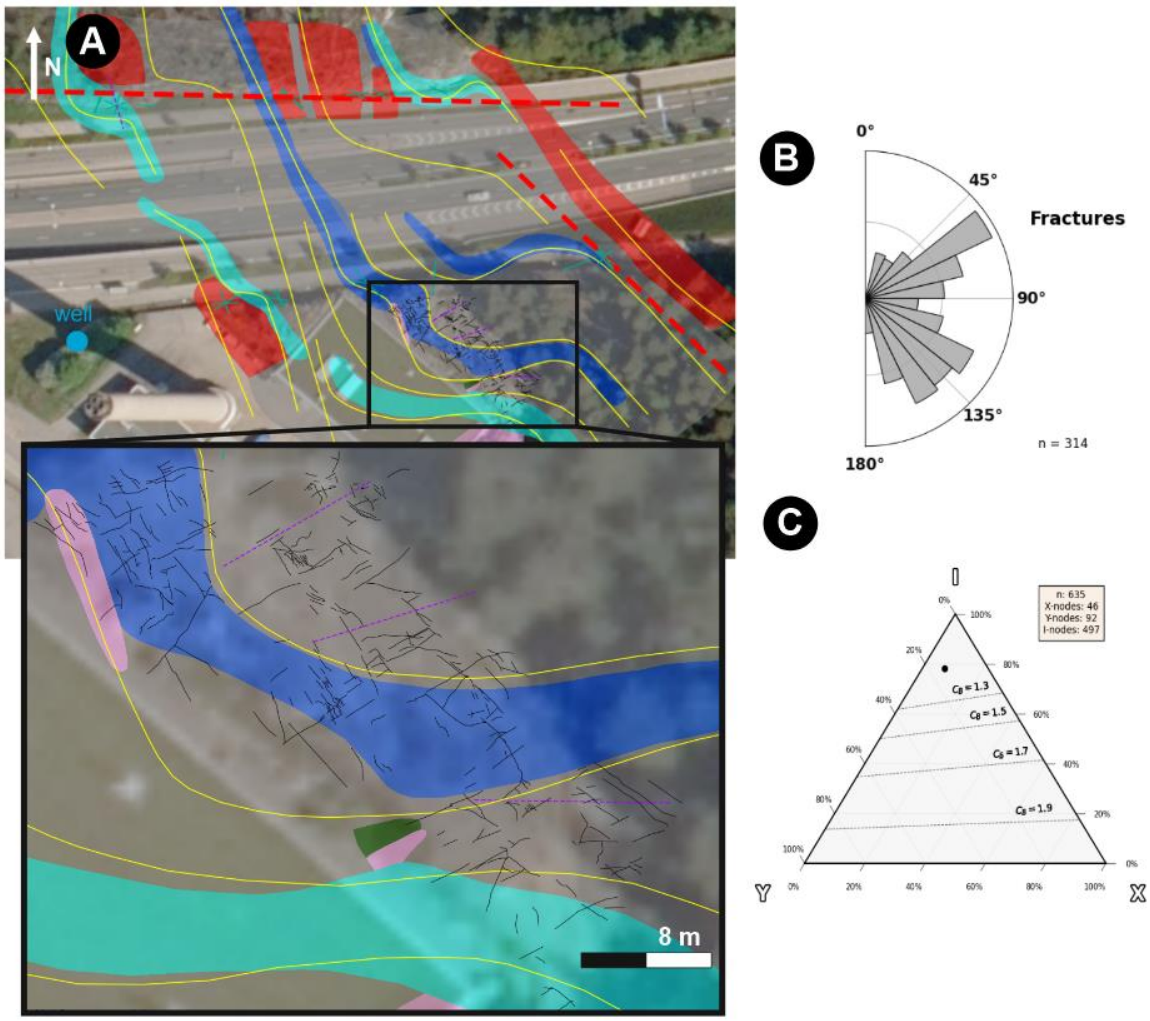

Figure 45: 2D-fracture network. A) Bedrock outcrop area on eastern side of the geothermal well, where fracture trace system was created, B) Trace azimuth which reveals that most of these 635 fractures have directions between 50-60- and 120-150-degrees and C) XYI-ternary plot which where the black dot is indicating the most typical node type of 635 drawn fractures (I-node).

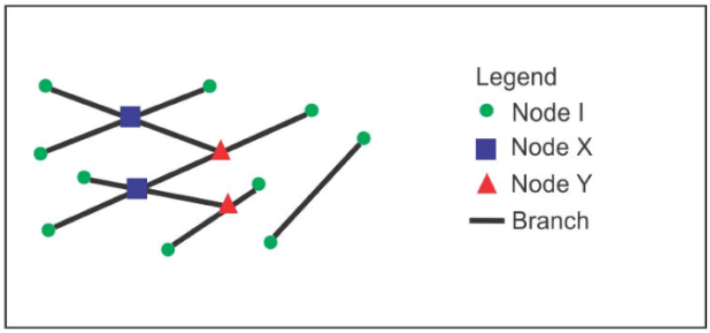

Figure 46: Explanation of X, I and Y-nodes (Sanderson and Nixon 2015).

5.5.2 2D- and 3D-photogrammetric models of the E-W trending fault

The most interesting part of the study area is the E-W directed rock cut where the fault is the most dominant feature of it (figure 47). When faulting movement took place in the bedrock, damage zone was formed (figure 48). This created fractures that have similar direction as the main fault (figure 49) Based on 30 measurements, the average dip of the fault and fractures with the same direction, is 83°. The average dip direction is 186°. This faulting movement also formed Riedel-fractures that are oblique to the fault (figure 50). Based on 14 Riedel-fracture measurements, the average dip of those is 77° and dip direction 176°. During the formation of Riedel-fractures, alternative direction of stress δ_1, was present. Along with these faulting related fractures, there are background fractures that have mixed arrangement. From the variation of the orientations of fault related fractures and Riedel-fractures, it is possible to say that the faulting movement was sinistral.

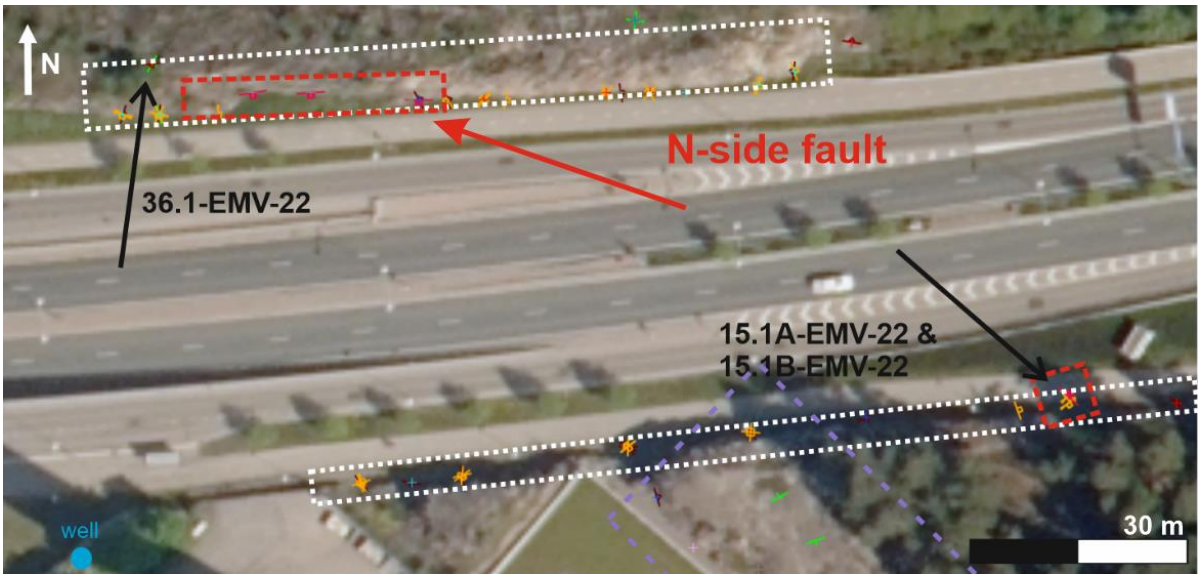

Figure 47: Location of the N-side fault.

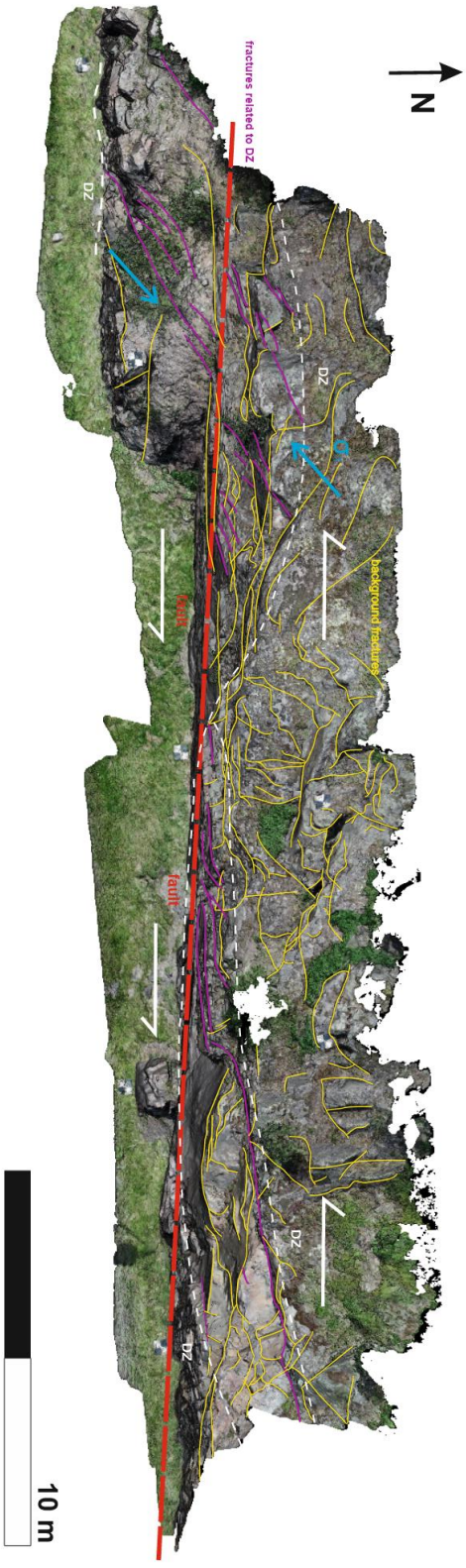

Figure 48: A top view (2D) of E-W trending, steeply S-dipping fault (red dashed line) on the northern side of the street in 2D-view. Sinistral movement of the fault has been marked with white arrows. Fractures related to the damage zone created due shearing movement have been marked with purple lines. Stress related to the formation of those is marked with blue arrows. The whole damage zone is outlined with white dashed lines. Background fractures are marked with yellow lines.

Figure 49: 30 measurements from the fault and fractures, that have the same direction. Average dip is 83 and dip direction 186.

Figure 50: 14 Riedel-fracture measurements. Average dip is 77 and dip direction 176.

5.6 Thin sections

Thin section 36.1-EMV (figure 51) has some oriented minerals on the right side which may give information about the movement direction. Also, some folding can be observed on the left side of the thin section. The color of the minerals is quite light to brownish. The mineral orientation on the thin sections 15.1A-EMV (vertical cut) and 15.1B-EMV (horizontal cut) is more miscellaneous, and only minerals with more coherent arrangement on the left edges of the thin sections, may give indication of direction of shearing movement (figure 51). The overall color of the minerals is greenish to brownish.

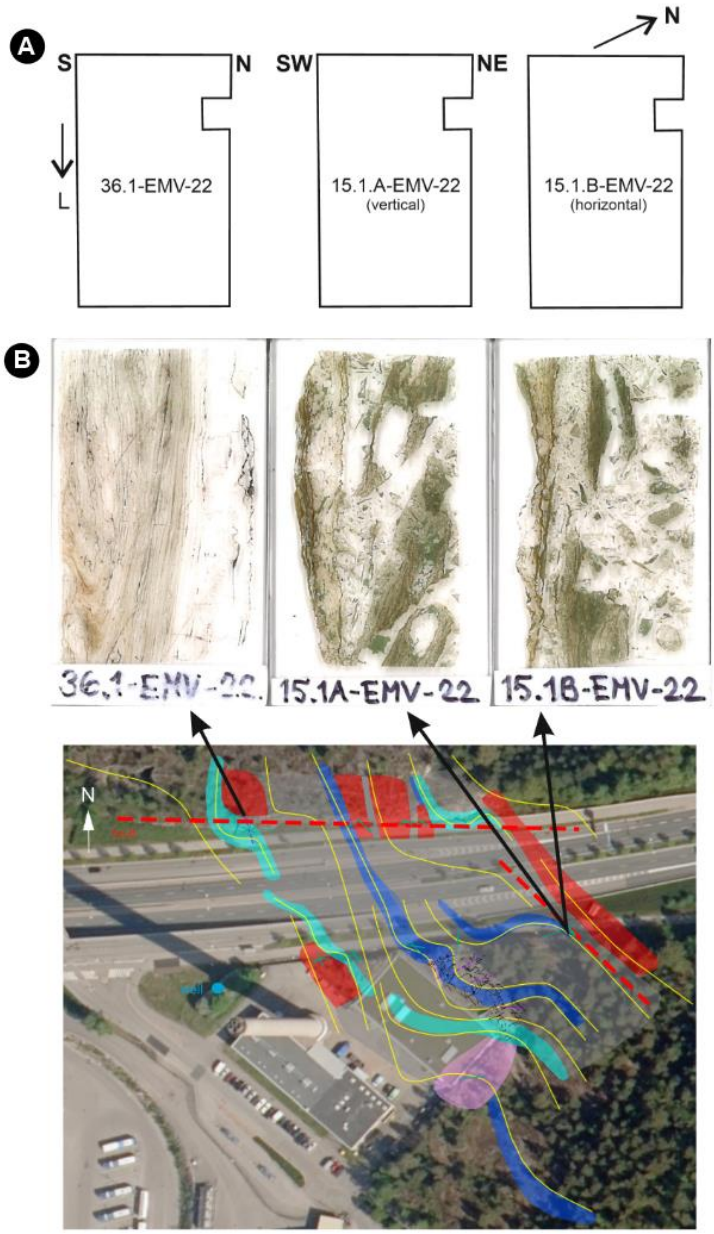

Figure 51: Caption overleaf.

Figure 51: Thin sections from the study area. A) A sketch which represents the direction of where the thin sections were cut. The direction of the arrow on thin section 36.1-EMV-22 is pointing towards the direction of lineation. B) Two locations of the samples where three thin sections 36.1-EMV (northern side of the street), 15.1A-EMV and 15.1B-EMV (southern side of the street) were collected.

5.6.1 Thin sections 15.1A-EMV-22 & 15.1B-EMV-22

The rock sample was cut into two thin sections: vertically cut 15.1A-EMV-22 and horizontally cut 15.1B-EMV-22. Typical minerals of this rock are quartz, muscovite, amphibole, and chlorite. This rock also contains a substantial amount of opaque minerals. Overall, the rock is has gone through strong hydrothermal alteration, which is shown by the overall greenish appearance (figure 53B). Large portions of the sample are composed of a mixture of coarse-grained quartz and greenish silicate minerals (likely amphibolite). However, some small parts of the mineral mass do have some sort of direction, but the mass is missing shear indicating clasts, which makes recognition of the shearing movement impossible (figure 53A). The edge domains of the thin sections represent a more coherent part, where the kinematics is observed. The edge of thin section 15.1A-EMV-22 includes C-type shear bands that are indicating dextral movement (figure 52A and 53C-F), whereas the edge of 15.1B-EMV-22 contains C'-type shear bands that are indicating sinistral movement (figure 52B and 54A-D). The rock has first experienced mylonitization which is post-dated by brecciation. Brecciation is present as the angular textures of coarse-grained material. This explains the highly varying size of quartz grains.

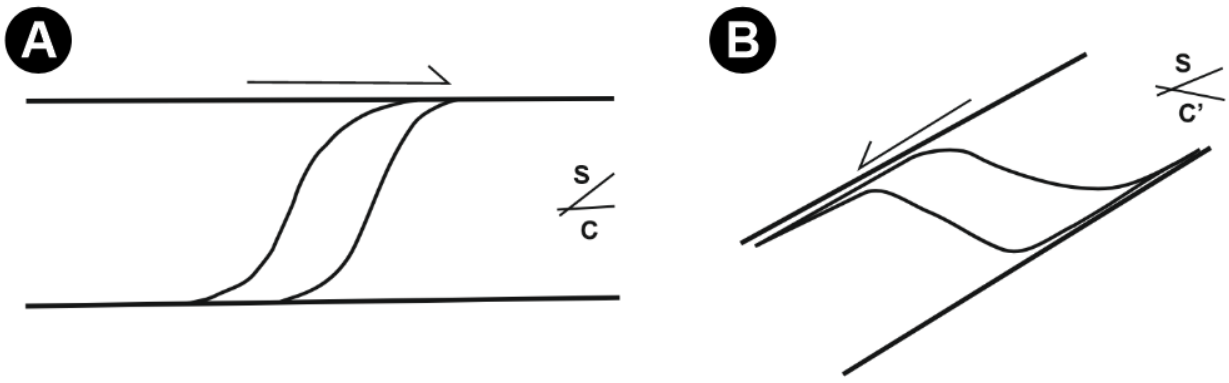

Figure 52: A sketch of two types of shear bands that were observed from the 15.1A-EMV-22 and 15.1B-EMV-22. C-type of shear band A) indicates dextral movement and that was typical in 15.1A and C'-type shear band B) indicates sinistral movement which was typical in 15.1B.

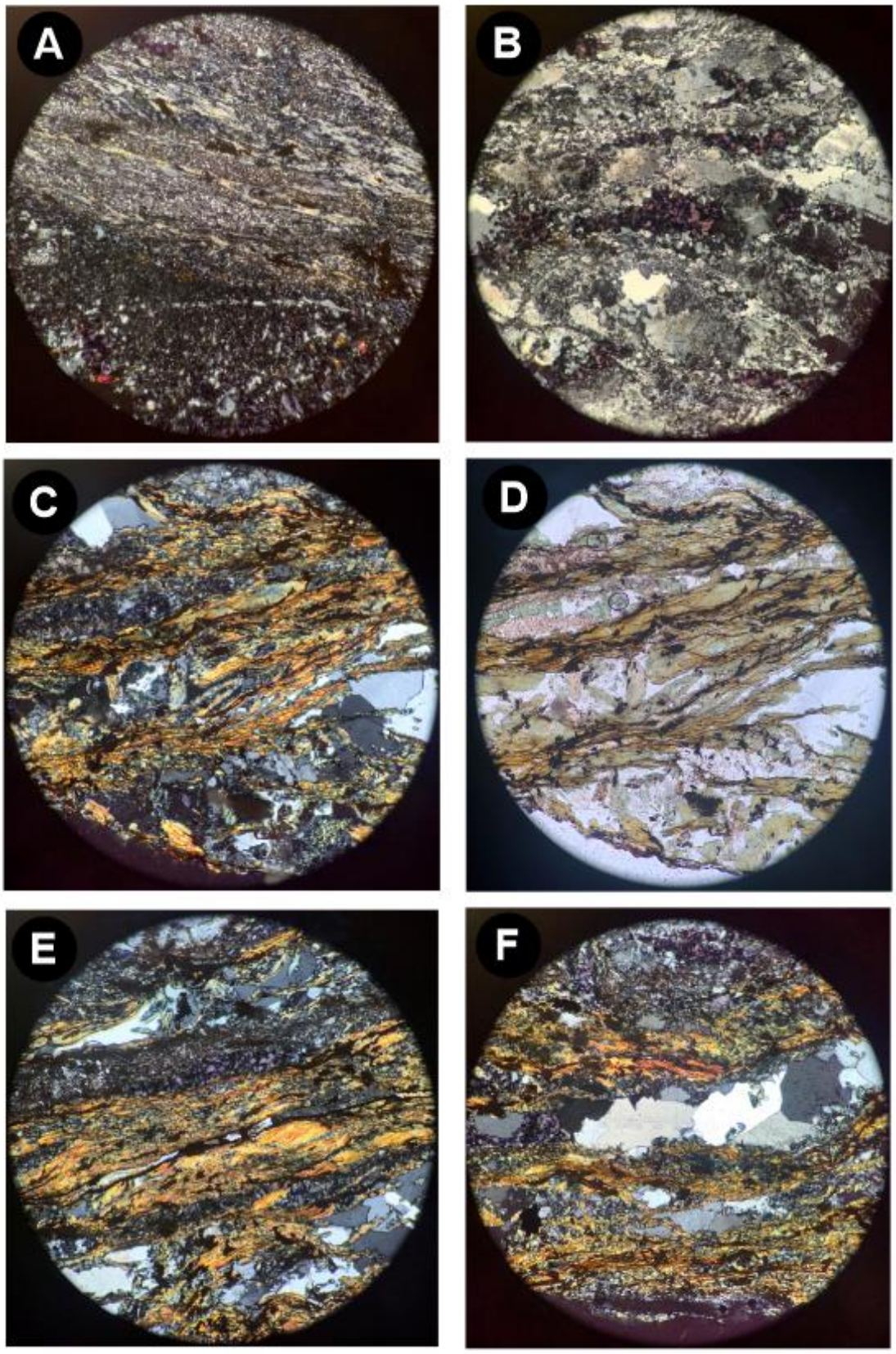

Figure 53: Thin section 15.1A-EMV-22. A) Overall picture of a mineral mass that has some orientation of minerals, B) Miscellaneous orientation of minerals, C-F) Pictures from the left edge of the thin section where C-type shear bands are observed.

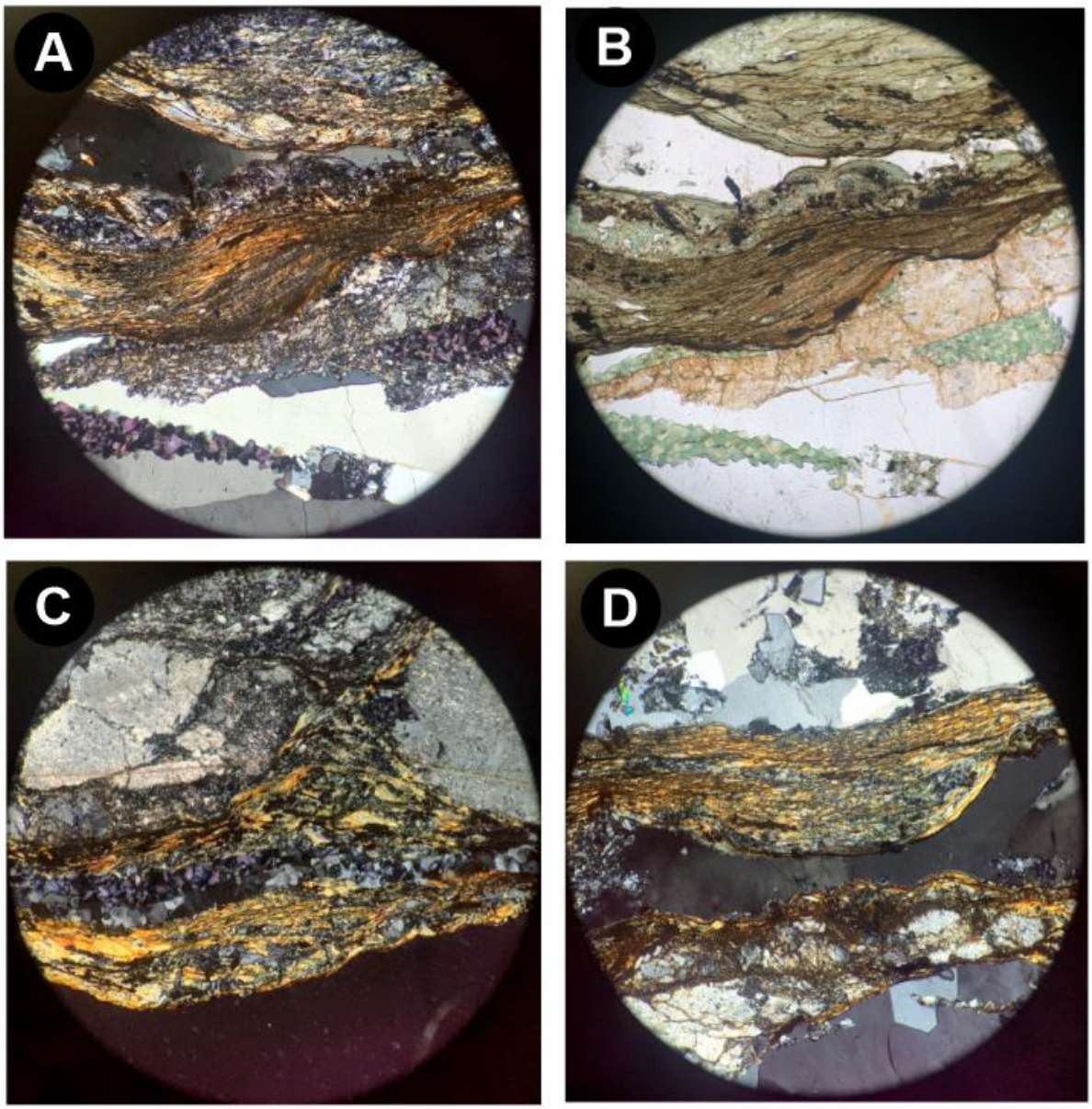

Figure 54: Thin section 15.1B-EMV-22. Pictures A-D from the left edge of the thin section where mineral orientation is visible and C'-type shear bands are observed.

5.6.2 Thin sections 36.1-EMV-22

This sample is an intensely sheared mylonite with a granitic protolith. It consists mainly of minerals such as quartz, plagioclase, feldspar/microcline, muscovite, biotite and opaque minerals. Based on the grain size and the appearance of the rock, it is possible to say that this rock is an ultramylonite, which means that the material is very fine-grained (figure 56A and B). However, the main mineral, quartz, has multiple different characteristics in this thin section as it is banded, and also occurs as large clasts that are rotated in places (figure 55). The rock is not hydrothermally altered which means that the impact of fluid has not affected the rock during the deformation. The rock includes winged sigma σ-type clasts, that are typically quartz and

feldspar/microcline (figure 56A, B and F). These clasts are indicating dextral movement. There is also a small fold observed, however, it is not indicating any sense of movement (figure 56D).

The rock has been going through dynamic recrystallization. This means that grain boundaries are forming and/or transforming which can typically replace older grains by creating totally new ones (Urai et al. 1986). Dynamic recrystallization deformation is synchronized with deformation (Urai et al. 1986). Dynamic recrystallization within this rock occurred due to dextral shearing, which has created these elongated quartz and muscovite into bands that have different sizes (figure 55A-C and 56E). This process also created the rotation of the clasts. When shearing ended, static recrystallization took place in the process of rock formation. Static recrystallization occurs when deformation is absent at the same time (Urai et al. 1986). During static recrystallization the grains become strain-free (Niimi 2002). This event has not been active for that long. During this event, some of the quartz grains have formed into foamy texture (figure 55D, figure 56C). The growth of quartz grains is limited by micas such as biotite and muscovite.

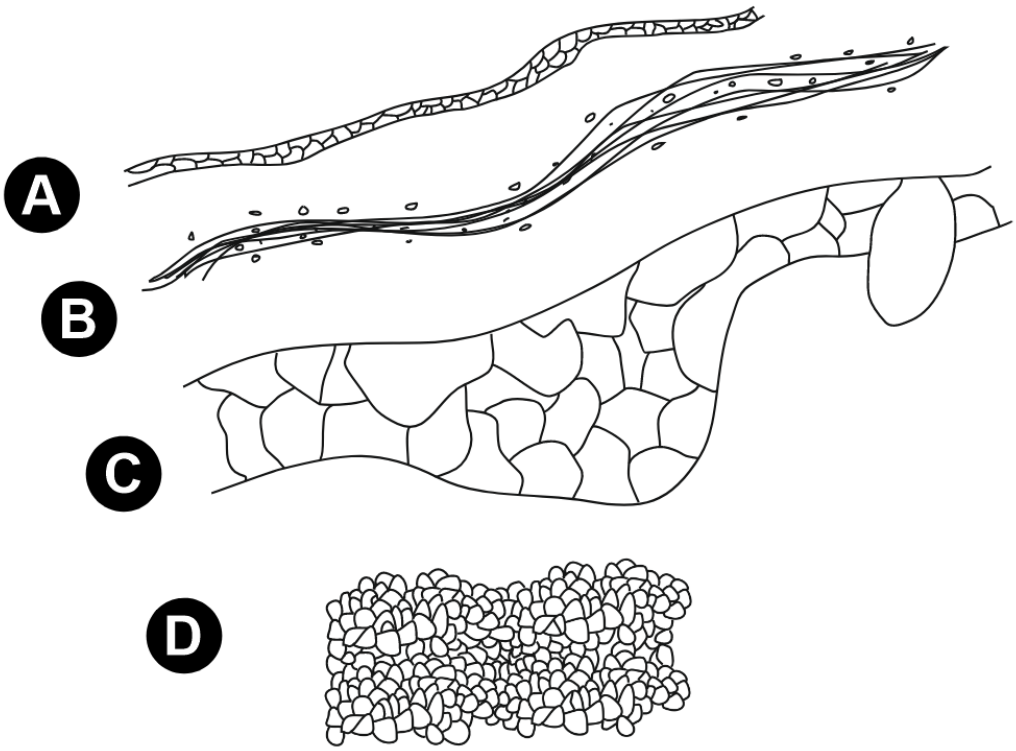

Figure 55: A sketch of different forms of quartz: A) Small quartz grains elongated by shearing and limited by micas. Elongated and very fine-grained quarts and muscovite, C) Expanded quartz which is ultimately limited by micas and D) Foamy texture of quartz which is created due static recrystallization.

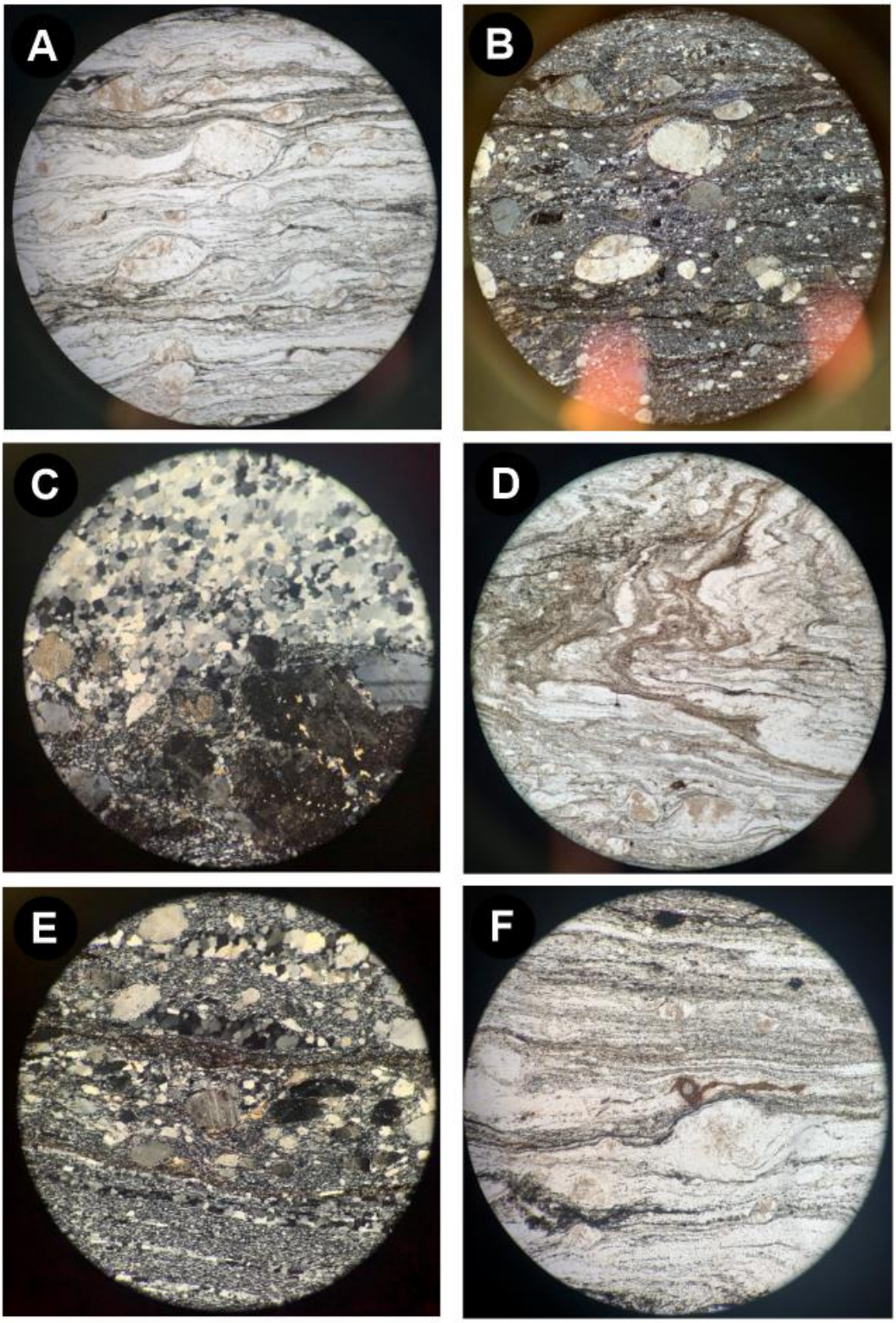

Figure 56: Thin section 36.1-EMV. A) and B): overall pictures of rotated clasts under plane polarized light (A) and under crossed nicol (B). C) Foamy texture of the quartz and D) Small fold in the thin section. E) Bands of quartz that have different thicknesses between larger quartz grains. F) δ-type clast in the thin section which indicates dextral movement.

6. Discussion

6.1 Importance of surface datasets

Bedrock mapping revealed that the large fault of the E-W trending rock cut on the northern side of the street, is caused most likely the greatest challenges of the drilling process. Based on the measurements of the fault, it is possible to say that this fault is dipping steeply in about 80° towards south (figure 57). This means that the downwards projection, and likely depth-continuation of the fault intersects the well between the depths of 804-865 meters (depth of the well). The other fault located on the southern side of the street, is dipping about 77° towards west, where the geothermal well is located. The structural geological observations were not that comprehensive with that fault since only the small core of it is observed and because of that, only few measurements were done. Therefore, it is difficult to evaluate the impact of the fault to the geothermal well.

Based on the comprehensive bedrock observations, it is possible to say that the rock types of the study area display an overall strong fracturing, which was typically quite dense. The traced fracture systems from different bedrock areas did not indicate any direct risks related to the functioning of the geothermal well, however the strong density of the fracturing indicates the incoherent nature of the area. The incoherent nature of the rock was also observed for example in the E-W trending fault. The fault core was destroyed, and rock was strongly fractured. Folds of the study area did not have any distinct control over the fracturing with the area in this study. However, they are important features to observe when making comprehensive bedrock mapping.

By using different surface study methods, the accuracy of results differed. The 2D-fracture mapping from the northern side fault, done by tracing the fractures, is giving a rough estimation and fives a general idea of the character and orientation of the fractures. However, these traced fractures are indicating for example more dramatic difference in orientation (about 25°) between fault related fractures and Riedel-fractures. By making exact fracture measurements in CloudCompare, the difference between the orientations of these two different types of fractures is smaller (about 10°).

The two rock samples and three thin sections, gave important information about the petrology of the rock types and directions of movement. For example, the understanding of the faulting

event of the northern side fault, is better understood by finding oriented clasts in thin sections, where the movement direction is detected. However, on the northern side fault, there was no direct indication about the sinistral movement that was detected on the 2D- and 3D-materials, as based on the relationship between slip surfaces and secondary fracturing. The clasts indicated dextral movement, and the conflicting shear senses may be explained by more ductile dextral stage, followed by a more brittle, younger sinistral stage.

The bedrock mapping of the Central Park – Laakso hospital area gave more regional understanding of the surrounding areas of the Ruskeasuo study area. Based on bedrock observations, it is possible to say that the strong fracturing controls both Central Park-Laakso hospital and Ruskeasuo study areas. Also, the fractures have mainly same directions of NNW-SSE and WSW-EEW.

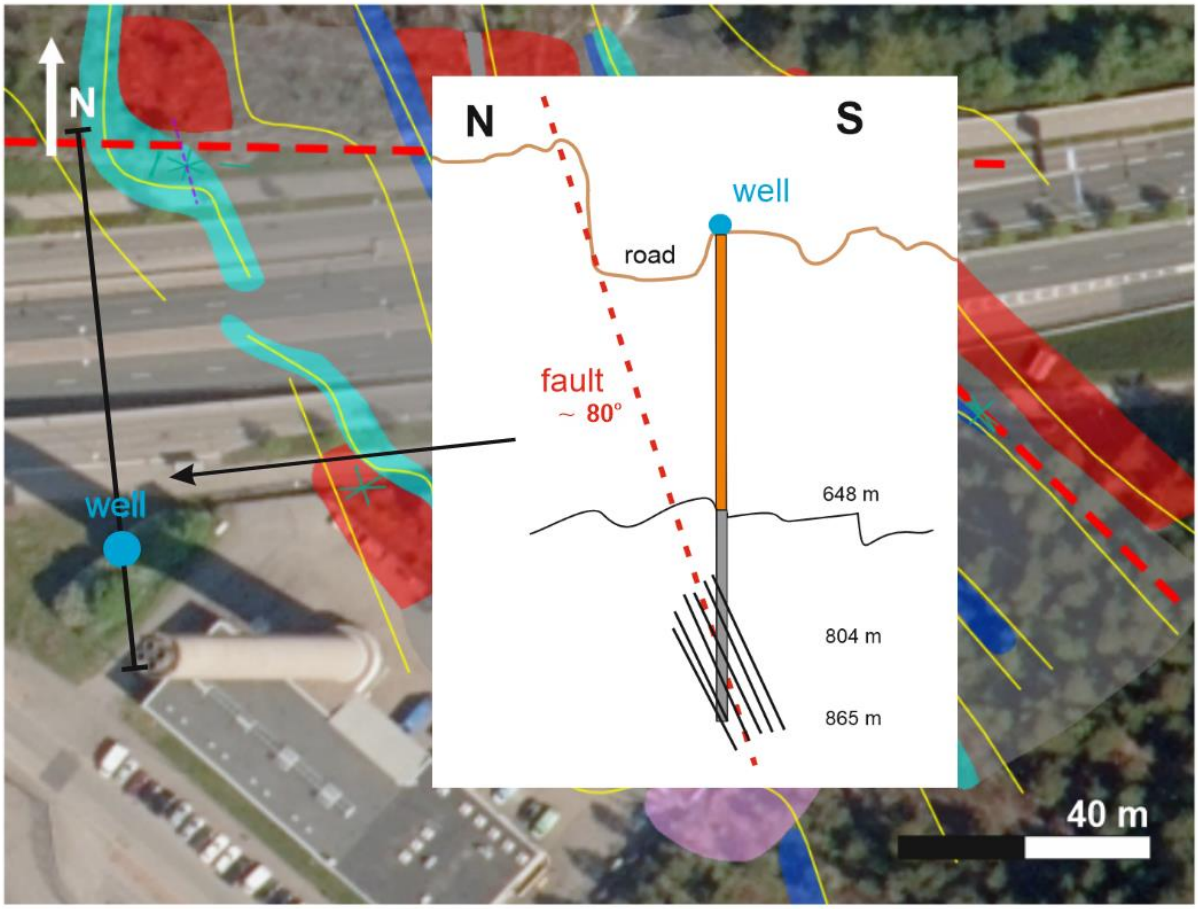

Figure 57: Map of the study area and a sketch, where the cross-cut is describing the situation where the fault related or Riedel-fractures of E-W trending fault are dipping about 80º towards the geothermal well. The orange part of the well represents the casing which reaches to the depth of 648 meters, where the first problematic fractures were encountered. Between 804-865 meters the fractures (black lines) are penetrating through the well. The drilling of the well stopped at 865 meters.

6.2 Correlation of surface and subsurface datasets

The studies of the geothermal well of GTK revealed important information about the properties of the nature of the subsurface. The study included similar rock types that were also observed in the surface level, during this more comprehensive study based on bedrock mapping. Based on the temperature curve produced by GTK, at the depth of about 800 meters, there was an increase of temperature and a decrease of geothermal gradient. This may be indication of fractures, which may be related to the fault, that penetrated through the well at the same depth. This means that correlation between surface observations of the fault and the subsurface observations of the geothermal well, is somehow possible.

Geophysical measurements of the geothermal well failed. Optical imaging did not produce any valuable material due unclear water. Acoustic imaging failed also completely. Other measurements of the slope, gammaspectrometry and magnetic susceptibility did not give any crucial information. This means that the correlation between surface data and geophysical data cannot be proven in this case. Based on DTS-measurements of the geothermal well, there was some changes in temperature throughout the measuring profile. However, these changes are most likely not related to fractures, which makes the correlation of surface observations to this, impossible.

The reflection seismic study produced data where E-W trending structure is clearly visible as a traverse line, in the Ruskeasuo study area (figure 58). The data also presents some vibration points that have the same direction and points, that have alternative direction of NE-SE. This vibration data may be considered as some sort of a structure, since reflection is occurring at those points that are creating a continuous line. At least the E-W trending traverse line can be considered as the E-W trending fault, that was effortlessly observed from the surface level. The correlation between surface and this reflection seismic data can therefore is proven. The correlation between surface observations and these NE-SE vibration points is unclear.

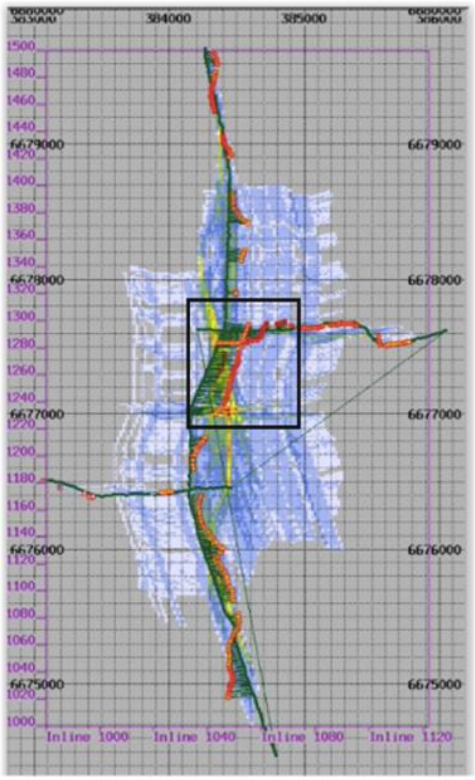

Figure 58: Seismic traverse lines (green) and vibration points (red) of the study area (black outline) (GTK 2022b).

7. Conclusions – A guideline to the future

Based on this study, a few correlations were found between surface and subsurface datasets. For example, large structures can be found solely on the surface by bedrock observations and measurements, that are also observed on subsurface, by reflection seismic data. However, detailed correlation between surface and subsurface datasets cannot be proven in this case as well as wanted, since the geophysical and optical measurements failed from the geothermal well.

Even though the selection of the location of geothermal well/s cannot solely rely on results of structural geological mapping of the bedrocks it the study area yet, these kinds of features should be taken into a consideration. Geological characterization of the planned area for geothermal wells gives important information of local ductile and brittle structures and lithologies.

A comprehensive bedrock mapping of the area should be executed before the site selection of the geothermal well/s. This kind of mapping can find crucial structures such as fault and fractures, which can cause problems to drilling process and ultimately end the process. Based

on the measurements of the faults of Ruskeasuo, the selected location of the well was a risk. The differences between lithologies and fractures in them that can be observed on surface, can give some indication of the conditions that are faced during drilling process. This is proven by this study, since incoherent nature and strong fracturing of the rock observed on surface, likely continued to have the same character within the subsurface.

Comprehensive bedrock mapping of structural geological features may therefore give valuable hints, that should be taken into a consideration, when the location of the well is being selected. Detection of continuous structures such as faults, fractures and folds can suggest the change of location to the direction which is not affected by these features. This detection can also give information which is important when angle of the drilling, used tools and the usage of casing is used. Overall, these features give more reliable estimation of occurrence and variations of structural systems in the area.

Acknowledgements

I would kindly like to thank:

- Professor Pietari Skyttä for great supervising and teaching during this process.
- Teemu Lindqvist (GTK) for great support during the project by being a co-supervisor, and by producing the high-quality 3D-photogrammetry material for the study.
- Helen Oy and GTK for the fruitful co-operation.
- Teppo Arola, Meri Wiberg, other members of the GTK's Geoenergy-team and Marta Cyz (GTK) for being helpful during this process and my internship.
- Petroleum Experts Ltd for letting me to use MOVE under academic license.
- Nikolas Ovaskainen for producing the 2D-fractopo analysis.
- Arto Peltola for preparing the thin sections.
- My family and friends for being as supportive as always.

References

Astrock (2022): Ruskeasuon lämpökaivo – Geofysikaaliset reikämittaukset, Helmikuu 2022, p. 9.

Boden, D. (2017) Geologic fundamentals of geothermal energy. Energy and the Environment, Abbas Ghassemi, Series Editor. CRC Press p, 400.

City of Helsinki (2019): Urban Environment Division, Helsingin geoenergiapotentiaali, kaupunkiympäristön julkaisuja 2019:25, p. 96. https://www.hel.fi/static/liitteet/kaupunkiymparisto/julkaisut/julkaisut/julkaisu-25-19.pdf

Cyz, M., Malinowski, M., Lindqvist, T., Virta, E., Heinonen, S., Arola, T., Riissanen, J., Mustonen, S., Hietava, J. and Skyttä, P. (2022): Seismic recognition of the faults for geothermal exploration in crystalline rocks: results from the pilot survey in Helsinki. Abstract, Lithosphere 2022 symposium, p. 4.

Doe, T., McLaren, R. and Dershowitz, W., (2014): Discrete Fracture Network Simulations of Enhanced Geothermal Systems. Thirty-Ninth Workshop on Geothermal Reservoir Engineering Stanford University, p. 11.

Doe, T and McLaren, R., (2016): Discrete Fracture Network Analysis of Controlling Factors for EGS Performance. 41st Workshop on Geothermal Reservoir Engineering Stanford University, p 10.

Energiforsk (2021): Tools for design of high temperature borehole storage in district heating production. Report 2021:770, p. 206.

Epperbaum, L., Kutasov, I. and Pilchin, A. (2014): Applied Geothermics, Springer, p. 757.

Finnila, A., Dershowitz, W., Doe, T. and McLaren, R., 2015: Hydro-shearing and Hydraulic Fracturing for Enhanced Geothermal Systems in Archetypical Normal, Strike-Slip and Thrust Faulting Terrains. GRC Transactions, Vol. 39, p. 19.

Finnila, A., Dershowitz, W. and McLaren, R., 2016: Geomechanical Analysis of EGS Reservoir Development in Normal, Strike-Slip and Thrust Faulting Terrains. 41st Workshop of Geothermal Reservoir Engineering, Stanford University, Stanford California, p. 11.

Finnila, A., Doe, T. and McLaren, R., 2017: Dependency of EGS Development on the Alignment between Natural Fracture Set Orientations and Regional Stress State. 42nd Workshop of Geothermal Reservoir Engineering, Stanford University, Stanford California, p. 6.

Fossen, H. (2016): Structural geology (second edition). Cambridge University Press, p. 503).

GTK (1991): Helsingin kartta-alueen kallioperä, Lehti 2023, s, 49.

GTK (2008): Tectonic evolution of the Svecofennian crust in southern Finland – a basis for characterizing bedrock technical properties. Special paper 47, p. 329.

GTK (2022a): Kallion lämpötila- ja vedenjohtavuusmittaukset Helen Oy:n Ruskeasuon geotermisestä energiakaivosta, p. 9.

GTK (2022b): Keskuspuiston seismisen heijastusluotaisaineiston tulkinta Laakson yhteissairaalan alueelle. GTK. Customer report, p. 12.

GTK (2022c): Ruskeasuon geotermisen energiakaivon geologiset havainnot, p. 15.

GTK (2023): Kallioperäkartta 1:200 000, https://gtkdata.gtk.fi/Kalliopera/index.html.

Hakala, P., Vallin, S., Arola, T. and Martinkauppi, I. (2021): Novel use of the enhanced thermal response test in crystalline bedrock. Renewable Energy 182 (2022) p. 467–482

Heatstore (2019): Underground Thermal Energy Storage (UTES) – state-of-the-art, example cases and lessons learned, p. 208.

IEA (2020): Quality management in Design, Construction and Operation of Borehole Systems. Technology Collaboration Programme, Final report, p. 272.

Nadimi, S., Forbes, B., Finnila, A., Podgorney, R., Moore, J. and McLennan, J.D., 2018: Hydraulic Fracture/Shear Stimulation in and EGS Reservoir: Utah FORGE Program. ARMA (American Rock Mechanics Association), p. 10.

Niimi. N. (2002): Static recrystallization of the deformed quartz in the granite from Mt. Takamiyama. Journal of Geosciences, Osaka City University. Vol. 45, Art. 7, p. 89-100.

Kallio, L. and Julkunen, A. (2022): Techical report: Ruskeasuon Lämpökaivo, geofysikaaliset reikämittaukset. Astrock OY.

Kukkonen, I. (2000): Geothermal Energy in Finland. Proceedings World Geothermal Congress 2000, p. 6.

Ovaskainen, N. (2022): 2D-fractopo analysis, https://github.com/nialov/fractopo.

Paikkatietoikkuna: Vinovalovarjoste Helsinki 2017 & kallioperäkartta 1:200 000. https://kartta.paikkatietoikkuna.fi (visited 8.3.2022).

Peacock, D., Nixon, C., Rotevatn, A., Sanderson, D. and Zuluaga L. (2016): Glossary of fault and other fracture network. Journal of Structural Geology 92, p. 12-29.

Posiva (2022): Summary of Prediction-Outcome Exercises (2017-2021) on the Discrete Fracture Network (DFN) Model for the Olkiluoto Bedrock, p. 58.

Robertson, E. (1988): Thermal properties of rocks. Open-File Report 88-441, p.110.

Schulte, O. (2016): Simulation and Optimization of Medium Deep Borehole Thermal Energy Storage Systems. Dissertation, p. 160.

Schön, J. (2011): Handbook of Petroleun Exploration and Production, p. 494.

Skarphagen, H., Banks, D., Frengstad, B. S. and Gether, H. (2019) - Design Considerations for Borehole Thermal Energy Storage (BTES): A Review with Emphasis on Convective Heat Transfer. Hindawi, Geofluids, Volume 2019, p. 26.

St1 Geolämpö: https://www.st1.fi/geolampo (visited 5.1.2023).

Urai, J., Means, W. and Lister, G. (1986): Dynamic recrystallization of minerals. Reprinted from Mineral and Rock Deformation: Laboratory Studies – The Paterson Volume. Geophysical Monograph 36, p. 40.

Uski, M. and Piipponen, K. (2019): Selvitys geotermisen energian syväreikäporaamisesta, siihen liittyvistä ympäristönäkökohdista ja riskienhallinnasta. Institute of Seismology, University of Helsinki, p. 58. https://helda.helsinki.fi/handle/10138/301878

Vähäaho, I. (2021): Could ground heat and geothermal energy be the answer to climate change prevention and energy demand? IOP Conference Series: Earth and Environmental Science, p. 9.

Appendices

Appendix 1. 2D-view looking down from the northern side E-W trending rock cut and a stereogram which includes 44 measurements the fault, fractures that have the same direction that the fault and Riedel-fractures.

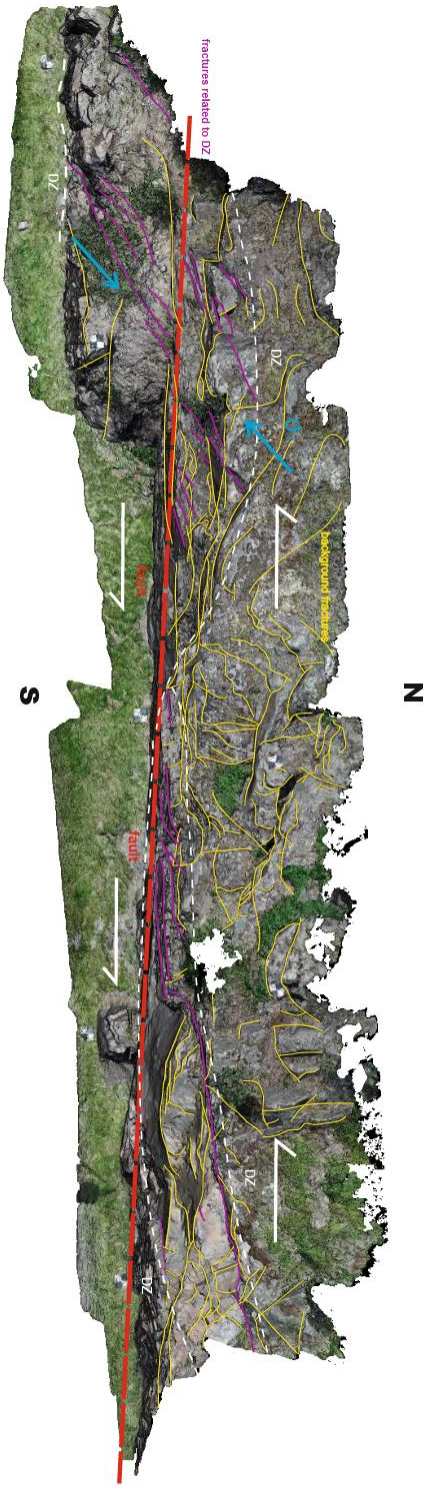

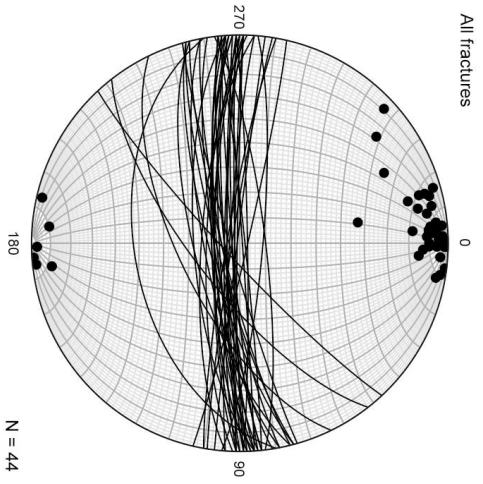

Appendix 2. Part 1 of the E-W trending rock cut with locations of 25 fracture measurements and stereogram.

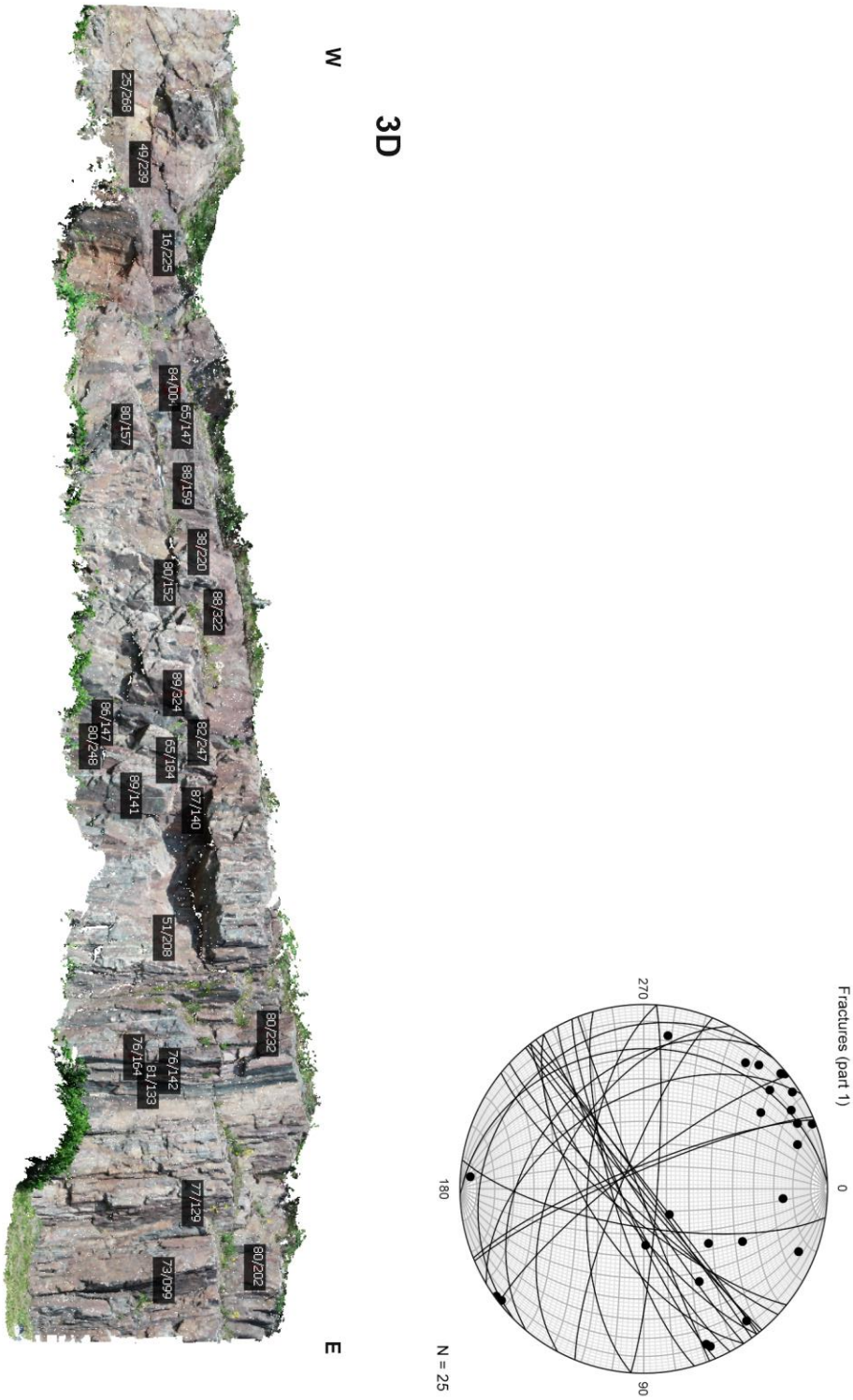

Appendix 3. Part 4 and 5 of the E-W trending rock cut with locations of 20 fracture measurements and stereogram.